Summer 2019

Using LiDAR to measure subsurface movement of slow-moving landslides and study the interaction between the soil and LiDAR scanning targets

Chengxun Lu

Department: Geosciences and Geological and Petroleum Engineering

USING LIDAR TO MEASURE SUBSURFACE MOVEMENT OF SLOW-MOVING LANDSLIDES AND STUDY THE INTERACTION BETWEEN THE SOIL AND LIDAR SCANNING TARGETS

by

CHENGXUN LU

A DISSERTATION

Presented to the Faculty of the Graduate School of the

MISSOURI UNIVERSITY OF SCIENCE AND TECHNOLOGY

In Partial Fulfillment of the Requirements for the Degree

DOCTOR OF PHILOSOPHY

in

GEOLOGICAL ENGINEERING

2019

Approved by:

Norbert H. Maerz, Advisor
David J. Rogers
Leslie S. Gertsch
Jeffrey D. Cawlfield
Bate Bate

ABSTRACT

Terrestrial Laser Scanning (TLS) technology has been used for predicting and researching geological hazards for two decades. This research focuses on using LiDAR (Light Detection And Ranging) to measure the slow-moving displacement of both surface and subsurface soil of landslides. Two kinds of computer simulation software, FLAC3D® and PFC3D® were used to simulate the landslide process to compare with the LiDAR scanning results.

The primary contributions from this research are as follows:

1. Several error tests were done to prove that the three-dimensional LiDAR scanner used in this research can precisely obtain the three-dimensional position, the displacement and the rotational angle of artificial scanning targets.

2. Two kinds of special scanning targets were used for the laser scanner to measure the displacement of surface and subsurface of soil.

3. A series of shear box tests and computer simulation programs were designed to study the interaction between the target rod and the soil so as to prove if the target rods can accurately reflect the subsurface movement of the soil.

4. A large-scale bench model test was designed to prove the applicability of the new LiDAR monitoring method.

This research is innovative and important because it proves the designed scanning targets verifies the function of the LiDAR, and several experiments were used to prove the precision and principle of this new monitor method.

ACKNOWLEDGMENTS

I would like to express my sincere gratitude to Dr. Norbert H. Maerz, my advisor and the chairman of the dissertation committee, for his support, guidance, advice and encouragement throughout my academic life at Missouri University of Science and Technology. Also, I would like to thank him for his constructive suggestion and modification of this dissertation. My dissertation would not have been possible without his help. The other person who has made a great contribution to this paper is Mr. Kenneth J. Boyko, who has developed the LiDAR scanning data processing software used in this dissertation. This dissertation would not have been possible without his help as well.

I would like to thank Dr. David J. Rogers, Dr. Leslie S. Gertsch, Dr. Jeffrey D. Cawlfield, and Dr. Bate Bate, for agreeing to be my dissertation committee members, and also for their suggestion on my research. I would like to thank Dr. Joe D. Guggenberger for his advice and help for the water injection system and Dr. Guxian Lv for the computer simulation programs. In addition, I would like to thank the faculty and staff of the Rock Mechanics and Explosives Research Center, especially Jay R. Schafler and Jeffrey P. Heniff who helped me to finish the sandbox and the bench model tests. I would also like to thank all friends and colleagues at Missouri University of Science and Technology.

Lastly, I would like to thank my entire family, especially my parents, for their dedication and support. I would like to thank my son, Devin Lyu-Cheng for his moral encouragement. I will give a special thanks to my wife and best friend, Yunfei Cheng without her support, love, patience and inspiration, this dissertation would never be finished.

TABLE OF CONTENTS

Page

LIST OF ILLUSTRATIONS

Page

LIST OF TABLES

Page

NOMENCLATURE

Symbol	Description
θ	Rotational Angle of Scanning Target Rod

1. INTRODUCTION

1.1. LANDSLIDE

The term “landslide” describes a wide variety of processes that result in the downward and outward movement of slope-forming materials including rock, soil, artificial fill, or a combination of these. The landslide may move by falling, toppling, sliding, spreading, or flowing (USGS, 2017). There are numerous factors, such as rain, ground vibrations, and freeze/thaw that can lead to landsliding. To research the likelihood of landslides, the factor of safety analysis was developed. The factor of safety is an important measurement of the likeliness of the landslide and when the factor of safety is less than one, failure is predicted to occur because the driving forces are greater than resisting forces. Human factors triggering of landslide include removal of the toe of the landslide, loading of the head of the landslide, and artificial ground vibration. Natural factors triggering include toe removal through erosion, changes in water pressure, freeze/thaw and earthquakes. Any of these triggers can also combine to cause landslides (Waltham, T., 1994).

Landsliding is a kind of geological hazard which is hard to predicted because the triggers of landslide are too difficult to measure accurately even if most landslides do not happen instantly. Many geotechnical engineers have researched landslides using various methods, such as remote sensing and computer simulation. They found that to predict the consequence of landslides depends on knowing the geometry of the slip surface as well as the triggers of landslide, because most of displacement of landslide starts along the failure surface of rock or soil (Maerz, N.H. et al., 2016). But most landslides start with

creep phenomenon which is hard to detect. To monitor the slight movements or deformation in the beginning stage of landslide is important to predict future catastrophic landsliding because the early stage displacement often predicts massive landslide at some points in the future (Figure 1.1). The beginning movement of most landslide starts with the slide material slowly slipping downhill along the surface of rupture. This movement is often small but measurable. The word "slow" means 5 $x10^{-3}$ mm/sec (17" per day) or less (Cruden, D.M. and Varnes, D.J., 1996).

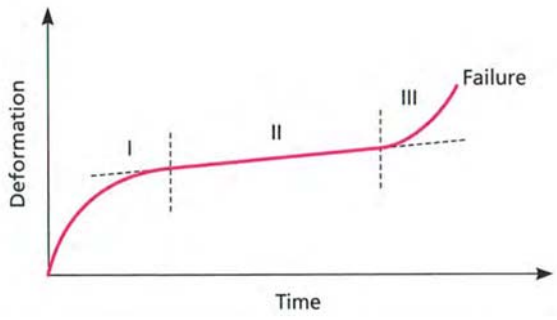

Figure 1.1 Time dependent deformation curve (Gonzales de Vallejo et al., 2011).

Phase (I): Primary or transient creep; Phase (II): secondary or steady state creep; Phase (III) the tertiary of accelerating creep phase. Deformation appear from Phase (I) and the value becomes stable in Phase (II), until material gets damaged over time and catastrophic failure happens in Phase (III). The duration time of Phase (II) can be very short or very long.

To make accurate measurements for a landslide in the early stages, (Phase (I) and (II) in Figure 1.1), the understanding of the type of landslide and its type of motion is necessary. Previous researchers had concluded the types of landslide movement (USGS,

2017). There are many kinds of mass movement included under the term “landslide”, but the more restrictive use of the term refers only to mass movements, where there is a distinct zone of weakness or slip surface, that separates the slide material from more stable underlying material (Varnes, D.J., 1978). The massive material movements which define as “slides” have two major types: rotational slides and translational slides and they are named because of their slip surface shape (Figure 1.2).

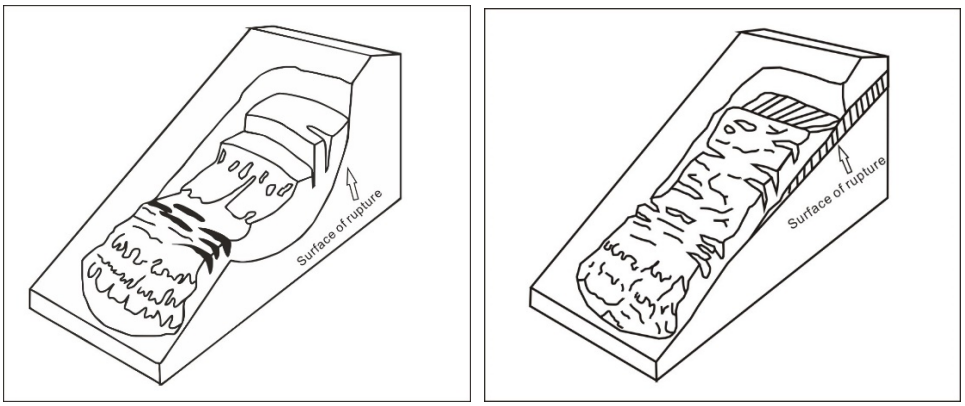

Figure 1.2 Two major kinds of landslide, left: rotational slides; right: translational slides (adapted from USGS, 2017)

The surface of rupture of rotational slide is curved concavely upward and the slide movement is roughly rotational about an axis that is parallel to the ground surface and transverse across the slide. The translational landslide mass moves along a roughly planar surface with little rotation or backward tilting. Both of two kinds of landslide have obvious failure surfaces and distinct zones of weakness.

As discussed above, engineers and scientists invent numerous methods to measure the small displacement or deformation of landslide in the beginning stage, such as

extensometers, interferometric synthetic aperture radar and Light Detection and Ranging (LiDAR) (Jaboyedoff, M. et al., 2012).

1.2. LIGHT DETECTION AND RANGING TECHNOLOGY

Remote sensing techniques are becoming increasingly popular and useful in geological engineering (Shan, J. and Toth, C.K., 2008), because it has several advantages when compared with traditional survey methods: They are fast and time saving, they result in reduced risk, increase in data quality and reliability and the images and scans can be stored for future reference.

In recent decades, remote sensing techniques are undergoing rapid developments. Recent advances in scanning sensor electronics and scanning data manipulation make these techniques more useful than before. The two major remote sensing techniques that are exponentially developing in landslides and rock fall investigation are interferometric synthetic aperture radar (InSAR) (Fruneau, B. et al., 1996; Colesanti, C. et al., 2003; Squarzoni, C. et al., 2003; Mazzanti, P., et al. 2015), and Light Detection And Ranging (LiDAR) (Carter, W. et al., 2001; Haugerud, R.A. et al., 2003; Slob, S. and Hack, R., 2004; Jaboyedoff, M. et al., 2007; Duan, Y. et al., 2011; Abellán, A., et al. 2014; Carrea, D. et al., 2015; Franz, M. et al., 2016). InSAR is a radar technique used in geodesy and remote sensing. This geodetic method uses two or more synthetic aperture radar (SAR) images to generate maps of surface deformation or digital elevation, using differences in the phase of the waves returning to the satellite. LiDAR is a surveying method which measures distance to a target by illuminating the target with pulsed laser light and measuring the time of flight of the reflected pulses with a sensor. Both of these two

technologies are very useful in geological hazard research and prevention (Jaboyedoff, M. et al., 2012). There are two kinds of LiDAR: Airborne Laser Scanning (ALS) and Terrestrial Laser Scanning (TLS) (Shan, J. and Toth, C.K., 2008). This classification of LiDAR depends on the location of laser scanner sensor.

Compared with traditional devices, LiDAR technology uses either time of laser flight of or phase shift sensors to generate a three-dimensional point cloud of a target surface (Figure 1.3). The principle of time of flight LiDAR basically uses the travel time of emission of light pulse from a source onto a target to measure the distance between the laser source and scanning targets. Another principle of LiDAR technology is phase shift which means modulated light is sent out, and its reflection wave phase shift is measured by scanner. The laser scanner then translates the shift to the distance between the scanning target and the scanner (Woodbury et al., 1993).

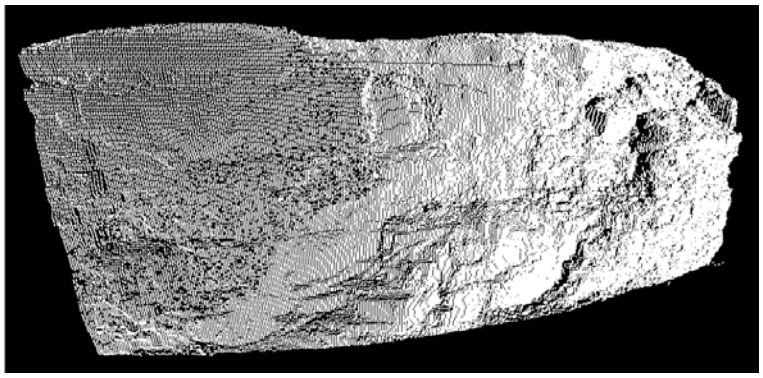

Figure 1.3 Example of LiDAR scan point cloud (adopt from Kassebaum, T.J., 2012)

As a long-distance measure device, LiDAR has higher precision than traditional devices. When the scanning range is over several hundred meters, a sampling resolution can be around 1 mm, and a single measurement accuracy of 6 mm. In scan process, the

laser can make up to 1,000,000 pts/sec measurement speed and return a scan point cloud which include millions of data points can be used to represent the surface of scanning targets (Figure 1.3).

1.3. COMPUTER SIMULATION

Computer science had been used in Geological and Geological Engineering research for a long history and numerous software have been developed. According the function, the software can be divided into three types: (1) Investigate the location and footprint of slope failures, such as Arc GIS or Global Mapper; (2) Calculate the factor of safety, such as Geo-slope and Slide; (3) Model rock and soil mechanics, such as Praxis and FLAC. Besides the commercially available software above, there are lots of free open source software packages to help engineers and scientists to research landslides. For example, the software "THRESH" is for tracking rainfall thresholds for landslide and debris-flow occurrence; the "Scoops3D" is software to analyze three-dimensional slope stability throughout a digital landscape; the "PTCOUNT" is a Fortran-77 computer program to calculate the areal distribution of mapped data points using count-circle methodology (USGS, 2017).

1.3.1. FLAC3D. FLAC3D is used in this paper to support the research. The full name of FLAC3D is Fast Lagrangian Analysis of Continua and it developed by Itasca Consulting Group, Inc. FLAC has two versions: FLAC2D and FLAC3D. FLAC3D is numerical modeling software for geotechnical analyses of soil, rock, groundwater, constructs, and ground support. Such analyses include engineering design, factor of safety prediction, research and testing, and back-analysis of failure (Itasca Consulting

Group, Inc., 2018). FLAC3D is the expansion of FLAC2D which uses the two-dimensional finite difference method and it can do three-dimensional structural stress simulation and plastic flow analysis (Naji, A. et al., 2018). The software matches the actual structure and model by adjusting the polyhedral element unit. The material units in the program can use various linear or nonlinear constitutive models. Under the external forces, these units can accordingly deform and move after the deformation or movement occurs. In mathematics, FLAC3D uses the explicit Lagrange's algorithm. Based on explicit difference, all equations of motion and the step solutions of constitutive equations of the model can be calculated and obtained. In the FLAC3D simulation processes, the constitutive equations are defined by basic stress and strain and derived from Hooke's Law and the equilibrium equation of motion directly uses the Cauchy equation of motion which derived from Newton's laws of motion.

Calculation models in FLAC generally are made up by three-dimensional cells in different shapes which means the space is subdivided to unit networks. When the software does calculations, every unit in space is subdivided to a tetrahedron which is made up by four nodes and all stress and strain in the tetrahedron is transferred by these nodes to other tetrahedron units. For a very short time after load application in a node, the load only can only impact the adjacent nodes. Using equation of motion and according to the move speed and time of nodes, the displacement can be calculated and then the strain can be obtained. At last the stress on units can be calculated by the constitutive equations after the strain and displacement is known. In the calculation processes, FLAC uses Gauss integral theory to simplify the three-dimensional question to two-dimensional (Figure 1.4).

The computer scripting language used in FLAC is FISH. FISH is a built-in language that gives the FLAC3D user powerful control over most every aspect of program operation. FISH is short for “FLAC-ISH” (or the programming language of FLAC), the code for which it was first developed. Now, in addition to FLAC and FLAC3D, FISH is also integrated into UDEC, 3DEC and PFC. FISH is embedded deeply into FLAC3D at nearly every level. It can be used to parameterize data files so that a number of varying cases can be built into the same basic model. Every data type that makes up a FLAC3D model is also available for FISH to manipulate directly-before, after, and during the solution. This means that not only can FISH be used to create custom complex models and customized results, it can also be used to add custom physics to the solution process that is not part of the standard package (Itasca Consulting Group, Inc., 2018).

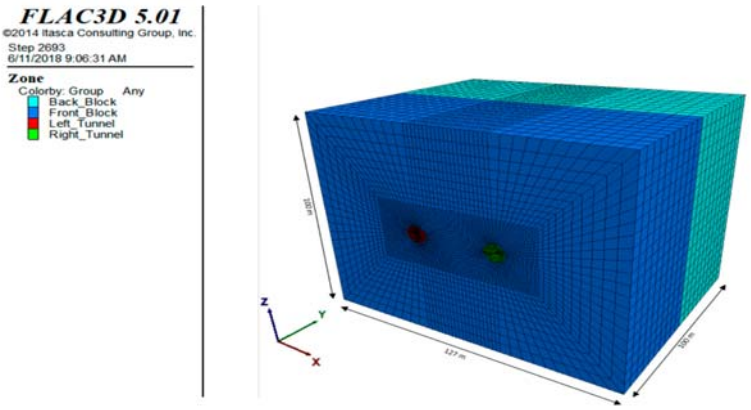

Figure 1.4 The example of FLAC3D simulation result (adopt from Naji, A. et al., 2018).

1.3.2. PFC3D. PFC2D/3D is DEM (Distinct Element Method) software developed by Itasca Consulting Group, Inc. and its full name is Particle Flow Code. The

main objective of PFC is used to research the particles assembly's behavior, such as rupture in soil bodies, and the large displacement of particles. This software is very effective to simulate complex solid mechanics and particle flow problems. The basic research target of PFC3D is particles and contact relation between particles. PFC3D can directly simulate the interaction and movement between spherical particles to solve physical problems; also, it can attach two or more small particles to create an agglomeration of particles in arbitrary shapes and sizes and this agglomeration of particles also can be an independent research target.

As the description above, PFC3D is mainly used to solve the particles and contact between particles. The software can simulate random size of particles and the dynamic behavior of each particle group. It can also automatic statistically generate the specific positional distribution of particle group and the diameter of the particle can follow a uniform distribution or follow a Gaussian distribution. At any time, the diameter of particles can expand with any value of coefficient and thereby change the value of porosity. PFC3D attributes the physical properties to individual particles or contact relation between the particles. Therefore, the physical properties and diameter of particle can be gradually changed by a designed simulation program. The color in the plot is also used to represent certain physical properties and the user can design the contact relationship in diversity mode (Figure 1.5).

The blue zone is the background of landslide; the red zone simulates the failure surface and the original position of the simulation particles; the gray particles are the simulation particles.

The contact relation is another research feature of PFC3D, and it comes with several contact models to calculate the contact relationship between the particles:

1. Linear Spring-Damper model;
2. Simplified Hetz-Mindlin model;
3. Coulomb Sliding model;
4. Contact bonding model and Parallel bonding model;
5. Customize model.

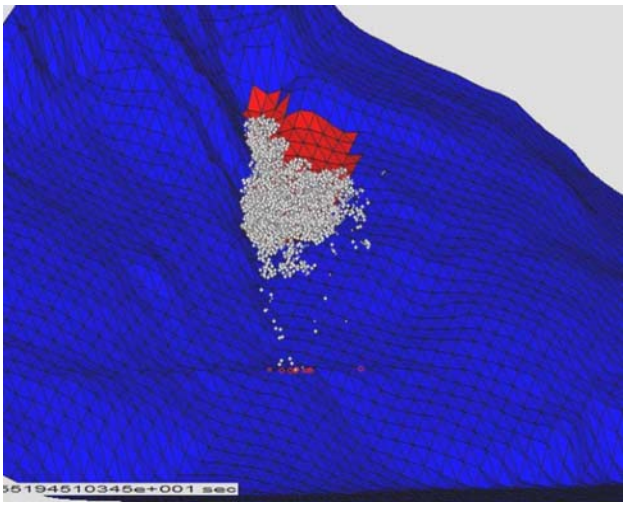

Figure 1.5 An example of PFC3D used to simulate a landslide (Poisel, R. and Preh, A., 2008).

1.4. STATEMENT OF RESEARCH

In past decades, research has developed numerous methods and devices to study landslides, such as discussed above the LiDAR technology and simulation software. But both of the monitoring technology and software have obvious deficiencies. The laser scanner has high-quality and precision scanning ability but can only detect the surface

change of scanning target. The computer simulation methods can analyze the internal situation of landslide, but the unreliable input parameters mean the simulation results are of limited use. To combine the high precision LiDAR technology with computer simulation methods to study the landslide is a better choice.

To develop the new method to research slow landslides, the choice of equipment is very important. The use of laser scanners is necessary to overcome the problems and disadvantages of the manual or traditional method. The difficulty is that laser scanner can nominally only detect the surface of target but landslides always start underground. Therefore, a new tool or method to extend the function of laser scanner is necessary. Additionally, to prove the reliability of the laser scanning technology computer simulation software will be used to compare the scanning results and help to determine if the new research method is suitable for landslide research.

This research is in three parts, the first is to measure the error of the laser scanner and the research method. The second part is to test the new research method in different soil types in shear box and compare the laser scanning results with computer simulation results to prove LiDAR technology can be used to research the subsurface motion of landslide. The final part of research is to build a bench model to test if the new method can be used in natural environment.

1.5. OBJECTIVE AND SCOPE

This research mainly seeks to prove the LiDAR technology can be used to measure the subsurface and surface movement of landslide. Therefore, there are four main objectives in this research:

1. Several error tests had been designed to prove if the FARO Focus3D, the laser scanner used in this thesis, has enough precision (compare with former research results) to obtain the three-dimensional position, displacement and rotational angle of artificial scanning targets;

2. Two kinds of special scanning targets have been designed to extend the function of laser scanner to research the displacement of surface and subsurface of slow moving landslide;

3. A series of experiments have been designed to use the LiDAR technology and the artificial scanning targets in sand and top-soil to detect the motion of sand and soil.

4. The software “FLAC3D” and “PFC3D” had been used to simulate sandbox test processes and compared with the scanning results to prove if could detect the displacement information of landslide efficiently.

5. A large-scale bench model test has been designed to prove if the special artificial targets can help the LiDAR scanning technology to obtain the surface and subsurface displacement of landslide in real environment.

1.6. STRUCTURE OF DISSERTATION

Section 2 presents the research background and comprehensive literature review on using LiDAR technology and computer simulation to research landslides. Section 3 contains the description of the research equipment and methodology. Section 4 contains several designed error tests for LiDAR scanner and the scanning targets. Section 5 uses a series of sandbox tests and computer simulations to verify that LiDAR technology can detect the displacement information of landslide efficiently. Section 6 uses the bench

model prove the LiDAR technology can be used in the real environment to obtain the surface and subsurface displacement of slow-moving landslide. Section 7 contains the conclusion and recommendations for future work, followed by appendices and references.

2. BACKGROUND AND PREVIOUS WORK

This section covers a review of the landside research applications of LiDAR technology and the computer simulation methods in landslide study.

2.1. USING LIDAR IN LANDSLIDE RESEARCH

LiDAR technology are becoming increasingly popular and useful in geological engineering. Not only the Airborne Laser Scanning (ALS), but also the Terrestrial Laser Scanning (TLS) is becoming an efficient survey tool (Shan, J. and Toth, C.K., 2008). The terrestrial laser scanning technology appeared at the end of the 1990s (Heritage, G. and Large, A. eds., 2009), and the function was an evolution of the Electronic Distance Meter (EDM) and of the Total Station Surveying Instrument. After decades of technology and mechanical development, the terrestrial LiDAR scanning technology has become much more mature.

LiDAR can be used in numerous of fields of research, but the first time it was used for environmental research was in 1998, and in that project the best estimate of LiDAR scanning precision was ±3–5cm, with repeatability at the level of ±1.5–2.5cm (Lichti, D. et al., 2000). The precision of the scanning result has direct relation with the brand and type of scanner (Buckley, S.J., 2008) and the precision of laser scanner has great influence on the study aims. Major manufacturers of 3-D laser scanners include Leica, Faro, Trimble, Optech, Riegl, Isite, Zoller+Frohlich, and InteliSum.

Terrestrial Laser Scanning (TLS) can be used in a lot of applications, such as architecture, construction, forensics, heritage, hydro power, mining, geological mapping,

and hazard surveying. There are some pioneers who had already used this technology to do some research about landslides in three different areas: (1) Scanning movements or volume change of landslide; (2) Hazard assessment, susceptibility mapping and modeling; (3) Methods of forecasting and monitoring; (4) Combining LiDAR technology with computer simulation methods (Jaboyedoff, M. et al., 2012).

2.1.1. Scanning Deformation of Landslide and Rock Fall. Some research projects by using LiDAR to characterize landslides in last decades are given by several research teams (Rowlands, K.A. et al., 2003; Jaboyedoff, M. et al., 2007; Aryal, A. et al., 2012; Barbarella, M. and Fiani, M., 2013; Carrea, D. et al., 2015; Franz, M. et al., 2016). These authors show that LiDAR technology is a very useful tool to interpret the landslide mechanism, delineate limits and estimate volume change (Corsini, A. et al., 2009; Dunning, S.A. et al., 2009). Most of the research focuses on the study the surface deformation of landslide because of the characteristics of LiDAR technology which can only ostensibly detect the surface measurement.

Jaboyedoff, M. (2009) described a case study of circular landslides in silty sediments in river banks (Switzerland). This result shows the LiDAR technology has huge potential to be used in landslide research field. The author said in this paper that the landslide volume change and scanning points cloud vectors of displacements can be obtained very accurately and can contribute to a detailed understanding of the failure mechanisms (Oppikofer, T. et al., 2009).

Miller, P.E. et al. (2008) used the HDS2500 scanner, with a precision of ± 6 mm, and found it offered an excellent opportunity for detecting low-magnitude surface change of a slope (the enabled detection of low-magnitude < 8cm changes over a six-week

period). The research result indicated that TLS is well-suited to the evaluation of embankment stability at local scales. The high spatial and temporal resolutions achievable suggest that TLS would provide a valuable complement to techniques such as LiDAR and photogrammetry, as part of an integrated risk assessment strategy (Miller, P.E. et al., 2008). The research results of this paper presented here have been useful in evaluating potential early characteristics of slope deformation. To monitor the displacement and volume change, the author set up several scanning targets to let the scanning result to be reliable.

Akca, D. et al. (2011) had built a reality model and then put some scanning targets on the model area which can be used several IDS uEye UI-6240 C gigabit internet video cameras to monitor the movement of slope. The author found that the surface deformation was quantified by tracking the small tennis balls which were pegged into the ground and achieving an average 3D point positioning precision of ±1.8 cm. The results of the photogrammetric work provide a better understanding of the surface dynamics of landslides. It was proven that the artificial targets could be used in detecting surface change of landslides (Akca, D. et al., 2011).

Barbarella, M. and Fiani, M. (2013) proposed to use Terrestrial Laser Scanners (TLS) and Global Positioning System (GPS) receivers to do scanning work. The equipment used in the research was Optech Ilris 3D, Leica Scan station C10 and Riegl VZ400. The software which used for editing scanning data was Cyclone, Leica and RiscanPro tool and all surveys have been framed in the same absolute reference system. The scanning process lasted 4 months and the research group determined the volume

change result of the landslide in Pisciotta, in the Campania Region in Italy (Barbarella, M. and Fiani, M., 2013).

Maerz, N.H. et al. (2013) and his research team have used LiDAR to do several research projects with Leica Scan Station II and FARO Focus3D. The research results showed the LiDAR scanning technology is an efficient tool to detect deformation and volume changes of the outcrop over time (Maerz, N.H. et al., 2013).

Franz, M. et al. (2016) proposed the result of his research about using LiDAR to monitor landslides. The research area is the Peney landslide in Geneva, Switzerland, which is covered by bushes and trees. The author used LiDAR techniques with some scanning targets made of polystyrene placed at different locations inside and outside the landslide area. Outside targets were control points and inside targets were floating points. The volume change is difficult to calculate because of the vegetation change and the author used IMAlign modules of the InnovMetric PolyWorks v.12.1 software to process data and MATLAB to remove the influence of vegetation (Franz, M. et al., 2016).

2.1.2. Hazard Assessment and Characterization. Airborne LiDAR had been used for assessment landslide especially the mass movement for a long time because its good efficiency, high precision and wide scanning range. Terrestrial LiDAR also can be used for characterizing and assessment of landslides and it has higher accuracy and better efficiency than ALS. For example, the International Earth Rotation and Reference Systems Services (IERS) use laser ranging and achieve less than 1 cm accuracy when measuring the distance to geodetic satellites in orbit around the earth over 3500 miles away (Renslow, M.S. ed., 2012). But the accuracy of TLS can easily reach 0.3mm (Maerz, N.H. et al., 2016). The key point of TLS technology can improve the site-specific

modeling. For instance, a detailed slope profile extracted from a TLS-DEM has permitted a researcher to identify the destabilized zone of an earth-flow using a standard Bishop analysis (Jaboyedoff, M. et al., 2012).

A designed experiment helped Travellettia, J. et al. (2008) to conclude the TLS is a powerful tool to assess the movement of slow landslides. The controlled rain experiment was designed in the Super-Sauze mudslide (South French Alps) and the research landslide was 120m². After 5 days monitoring work from 10-July 2007, five scanning point cloud results by LiDAR were gotten. These scanning results were compared with other measurement methods, such as benchmark method and the shaded relief image correlation method. The conclusion of comparison proved the laser scanner can detect average displacement of 3.2 cm/day in the direction 027°/30° of landslide (Travelletti, J. et al., 2008).

Prokop, A. and Panholzer, H. (2009) assessed the capability of LiDAR for monitoring slow moving landslides. They used the TLS technology to monitor the mass movement and estimate the volume change of landslide. Through compared the scanning result with orthophotos, the DEM was provided by TLS can easily assess the displacement of mass by the point cloud. But because of the limitation of precision of laser scanner and monitor method used, the conclusion showed LiDAR scanner used in the research cannot determine the movement rate smaller than 50mm per period. If the quality of scanning point density is described and area has very low point density, the changes smaller 100mm still can be detected (Prokop, A. and Panholzer, H., 2009).

Kasperski, J. et al. (2010) used TLS technology to assess the movement of the Séchilienne landslide (Isère, France) between 2004 to 2007. The time-series of terrestrial

laser scanning results help research team to monitor the three-dimensional displacement of the research area. Even the scanning point cloud had some homogeneous data, but the results were reliable. The sequential monitoring results helped to conclude the volume change of landslide can be deduced by the movement of scanning points and DEM. The efficiency of LiDAR technology to character the landslide had been proved by this research (Kasperski, J. et al., 2010).

Carrea, D. et al. (2015) published an article "Correction of terrestrial LiDAR intensity channel using Oren–Nayar reflectance model: An application to lithological differentiation". The author used black/white matte paper to test the intensity and precision of laser scanner in different scan ranges and incidence laser angles. After the proof test, the author did another test for real rock blocks of different lithologies and surface conditions. The two designed tests showed that the non-perfect diffuse reflectance of rock surfaces can be practically handled by the proposed correction method. The method proposed in this research can improve the LiDAR technology to identify the characteristics of lithological surface for geological mapping purposes (Carrea, D. et al., 2015).

To describe the characteristics of landslide and to define the deformation of underground, Wang, D. et al. (2016) used TLS to use the rotation of the tree stem shapes to indicate the shallow landslide. The author proposed a new monitoring method which uses LiDAR to obtain the point cloud data to calculate the inclination angle of the stem and stem volume. The diameter at breast height (DBH) of tree was 1.6cm and the inclination angle was 8.2° which revealed that characterization of trees and then these data can indicate shallow landslide activities (Wang, D. et al., 2016).

Franz, M. et al. (2016) developed an extension research method with LiDAR technology which is using artificial scanning targets to avoid the influence of vegetation. The research team used LiDAR and 14 polystyrene targets to monitor the displacement of the Peney landslide (Geneva, Switzerland). The laser scanning results was compared with other traditional methods showing reliable results which proved the artificial scanning targets in highly vegetated areas can help LiDAR to obtain efficient scanning result (Franz, M. et al., 2016).

2.1.3. Methods of Forecasting and Monitoring. For forecasting and monitoring landslide purpose, numerous tools are used, such as GIS, mathematic model, computer simulation, borehole observation and so on. LiDAR is one of the most efficient research tools. Combined with several other research tools, the time-of-failure semi-empirical prediction functions have been developed and used for different types of landslide with mixed methods (Jaboyedoff, M. et al., 2012). LiDAR technology has been used for the continuous monitoring several years and it is already a popular research tool to forecasting the landslide even if few published papers exist (Biasion, A. et al., 2005; Prokop, A. and Panholzer, H., 2009; Jaboyedoff, M. et al., 2009).

Oppikofer, T. et al. (2008) concluded a reliable monitoring result through TLS. The author set the research target slope at the eastern flank of the Eiger (Switzerland). The monitor results revealed the movement of slope by more than 70 cm/day during the paroxysmal activity (Oppikofer, T. et al., 2008).

Prokop, A. and Panholzer, H. (2009) used TLS to collect the point cloud data to build a 3D model for a slope. In the case of geohazard management, the 3D model which is built by LiDAR is useful to acquire and monitor the progress activity situations of

landslide (Prokop, A. and Panholzer, H., 2009). The example showed in the research which result of using laser scanner Riegl LMS Z420i to monitor the research area for 1 year.

Abellán, A. et al. (2010) proposed to do detection and spatial prediction of rockfalls by TLS technology. The research area is the main scarp of the 1881 Puigcercós landslide (Pallars Jussà, Catalonia, Spain). The author focused on the past volume change of rockfall first and then used pre-failure deformation as a precursory indicator to do deal with the spatial prediction of rockfalls (Abellán, A. et al., 2010).

Benni Thiebes et al. (2016) wrote an overview to conclude the existing conceptual methods for the Landslide Early Warning Systems (LEWS) and find the TLS technology is an efficient monitoring tool to support the LEWS. The LiDAR applications are not typically published in engineering literature. A few landslide forecasting methods related to TLS had been reported from Austria (Canli, E. et al., 2015). The main reason the TLS is not frequently shown in LEWS is the cost of laser scanner (Thiebes, B. et al., 2016).

Michel Jaboyedoff et al. (2012) concluded the monitor function of TLS is more useful than ALS because of the higher precision and efficiency of TLS, even both of these two technologies use same measurement principles. The precision of ALS was around 15cm but TLS' precision was only 1.5cm. The author also proposed that monitoring the rockfalls is much easier than landslide, because the displacements of rockfall can be considered as rigid body transformations (Jaboyedoff, M. et al., 2012).

To monitor the landslide and rockfall by LiDAR, there are two key precursory indicators: 1) the volume increase reveals the more frequency of rockfall activity before the final collapse (Rosser, N. et al., 2007); 2) the detection of precursory displacements is

investigated for large scale landslides or rockfalls (e.g. 125cm/day displacement was detected before a 170,000m^3 partial collapse of the Eiger rockslide (Oppikofer, T. et al., 2008).

2.1.4. Discussions. Through the research background conclusions above, the TLS technology started to be used in landslide studies from 2000. At beginning the ALS was first used in the geohazard research, and TLS developed later because of the lack of related software for three-dimensional data processing. Previous researchers not only used the TLS for detecting the movement and volume change of slope or monitoring and description the features of landslide, but also developed different extension methods to support the scanning process. But the key problem which has not solved yet is how to use LiDAR to research the subsurface features of landslide. As is known to all, the displacement of landslide always occurs along subsurface failure surfaces or shear planes (Maerz, N.H. et al., 2016). Some scientists tried to develop new methods to extend the scope of LiDAR application. For example, Wang, D. et al. (2016) used the inclination angle of the stem and stem volume of trees to describe the subsurface features of landslide even the results were not precise enough but the measurement method is creative (Wang, D. et al., 2016); Franz, M. et al. (2016) used artificial scanning targets to avoid the influence of the vegetation to improve the precision of scanning results (Franz, M. et al., 2016). Also, there are some researchers that try to extend the LiDAR function to use this technology to study the underground deformation.

2.2. COMBINING LIDAR TECHNOLOGY WITH COMPUTER SIMULATION METHODS TO STUDY LANDSLIDES

Computer simulation is a very important tool to support research for landslide. Previous research developed four kinds of software to study landslide: (1) Mapping software, such as Arc GIS or Global Mapper; (2) Factor of safety calculation software, such as Geo-slope and Slide; (3) Comprehensive analyze and simulation software, such as Praxis and UDEC; (4) Data processing software which support analyze LiDAR scanning result, such as FARO Scene or Leica Cyclone. This section mainly discusses the simulation and data processing software which used in this research to combine the LiDAR technology to study landslide.

2.2.1. Data Processing. Following the development of LiDAR technology, the data processing software become popular in the market and most of them are bundled software with laser scanner. For instance, the FARO Scene and Leica Cyclone are developed for use with the FARO and Leica laser scanners. Another type of data processing software, Lidarsw, which developed by Dr. Norbert H. Maerz and Kenneth J. Boyko at Missouri University of Science and Technology, is stand-alone software which can process the LiDAR scanning results file. Lidarsw will be introduced in Section 3.

The main principle of these two kinds of software is using internal algorithm to process the millions of points reflected from scan target surface. The scanning result from three-dimensional laser scanner is always presents the scanning targets as a three-dimensional set of points which all points have a (x,y,z) position. All scanning results from LiDAR are visualized by point, but details need to extract. Different commercial process software has different extended functions but same core functionality: Visualization, Segmentation, Filtering, Transformation and Gridding.

Visualization means the software creates a visible scanning point cloud and the user can view the related information. Segmentation function means the user can segment single point or points group from the original scan point cloud based on the properties or positions of point. Filtering function means the users can use software to remove data points that are outliers or in error. Transformation means aligning, clipping, stretching or rotating of the point cloud. Gridding is special process of Lidarsw which creates a hypothetical surface from a cloud points, and arrange all scanning points according to certain rules.

2.2.2. Simulation. Previous research used computer simulation models with natural slope and new technologies of LiDAR to study the landslide. For example, some scientists used LiDAR data to combine with hydraulic models to understand the potential risk of a mudslide. Also, LiDAR technology is a significant tool to do scanning work in tunnels, and engineers tried to combine computer software with detection of scanning targets to make an automatic alert system (Conforti, D., 2014).

Agliardi, F. et al. (2001) proposed a new approach to research deep-seated slope deformation kinematics, which combined the geological information and geotechnical parameters to compare with the numerical modeling which used FLAC v 3.40. The results seem to be not suitable to explain the studied phenomenon, but the methods which used comprehensive knowledge is worth emulating (Agliardi, F. et al., 2001).

Chen, C.Y. and Martin, G.R. (2002) proposed using FLAC to simulate the interaction between the stabilizing piles and soil structure. The results reveal that the formation and shape of the arching zone are functions of pile arrangement, relative

pile/soil displacement, pile shape, interface roughness, and soil dilation angle (Chen, C.Y. and Martin, G.R., 2002).

The typical research case of combination of monitoring technology and computer simulation to study landslides is Petley, D.N. et al. proposal in 2005. The research objective is the Tessina landslide located on the southern slopes of Mt. Teverone, in the Alpago valley of NE Italy. To study the landslide movement patterns, the author used an Electronic Distance Measurement (EDM) system to obtain the surface displacement patterns of slope. The FLAC simulation code were used to build a model for the landslide and supported analysis. The conclusion is the movement of slope occurred initially at the toe of the landslide (Petley, D.N. et al., 2005).

Poisel, R. and Preh, A. (2008) modeled a landslide in Aknes (Norway) by PFC3D which simulates the soil flow along the slope as numerous soil particles. In this research, the author introduced the function of PFC which based on the Distinct Element Method to simulate the movement and interaction of 3D particles on the slope by the laws of motion and of force-displacement (Poisel, R. and Preh, A., 2008).

Natural targets also could be a part of simulation model. Conner, J.C. and Olsen, M.J. (2014) proposed a novel algorithm to automatically detect landslide movement by using displacements of tree trunks distributed across the landslide. The author used the relative distance of tree trunks to be optimal parameter to monitor the movement of landslide (Conner, J.C. and Olsen, M.J., 2014).

Dong, M. et al. (2018) proposed a comprehensive methodology for three-dimensional slope stability analysis which combined mathematic three-dimensional modeling for creating the slope 3D simulation models and finite-element method for

stability analyses combined. The research also used an automatic strength reduction method to analyze comprehensive geological hazard (Dong, M. et al., 2018).

2.2.3. Discussions. Computer science is very meaningful to landslide research. Data processing software can help the LiDAR technology to extract the landslide information by visible point cloud. Simulation methods can support scientists to understand the internal transformation of the landslide, especially the mechanism and interaction of mass movement. If the high precision measurement tools like LiDAR can combine the simulation analysis to research the landslide, more regularity would be revealed.

3. EQUIPMENT AND METHODOLOGY

This section describes the equipment and methodology used for the research. This includes the LiDAR scanner, data processing and simulation software used in the research, and experiment design, experiment tools and experiment procedures.

3.1. EQUIPMENT AND SOFTWARE

The research tools used in this research included the following:

1. Measuring apparatus;
2. Software for processing scanning results.

3.1.1. Measuring Apparatus. The measuring apparatus include laser scanner and distance and angle measurement equipment.

3.1.1.1. LiDAR scanner. The laser scanner used in this research is FARO Focus3D X130. This unit consists of a FARO Focus3D X130 laser scanner (Figure 3.1a), scanner tripod stand (Figure 3.1b), and a laptop for data processing. The FARO scanner was used for all scanning work in this research. The main features are:

1. High accuracy;
2. High resolution;
3. High scanning speed;
4. Intuitive control via the built-in touch screen display;
5. High mobility because of small size, light weight, and the integrated quick charge battery;
6. Photorealistic 3D color overlays due to the integrated optical camera;

7. Integrated dual axis compensator to automatically level the captured scan points.These scan points will automatic form three-dimensional scanning result in the scanner.

(a) (b)

Figure 3.1 The FARO Focus3D laser scanner and the scanner tripod; (a) The FARO Focus3D laser scanner which includes the battery, the charger cable, the protective glasses; (b) The tripod for the FARO Focus3D laser scanner.

The principle of FARO Focus3D works by sending an infrared laser beam pulse to the rotational mirror in the scanner. Then the mirror deflects the laser beam using a vertical rotation around the environment being scanned. The scanner itself rotates in a horizontal direction. The scanning result is obtained from the back scattered laser light which is reflected from the surface of scanning target back into the scanner (Figure 3.2a) (FARO® Laser Scanner Focus3D X 130 Manual). The scanner area covers a 360° horizontal x 300° vertical range (Figure 3.2b).

To measure the distance between the scanner and the scan target, the FARO Focus3D uses phase shift technology, which means the scanner projects constant waves

of laser light of varying length outward from the laser sensor. Upon contact with an object, they are reflected back to the scanner. The distance between the laser scanner and the scanning target is accurately measuring by the phase shifts in the waves of the infrared laser light beam.

The scanner actually measures distance (δ), vertical rotational angle (α) and horizontal rotational angle (β) which give each individual measurement a spherical coordinate triplet. The α and β angles are generated using angle encoders to measure the rotational angle of the mirror and scanner at the time of each measurement (Figure 3.3). These two angles are encoded simultaneously with the distance measurement. (Richard G. Brown, 1996). After each scanning, the polar coordinate (δ, α, β), which is then transformed to a Cartesian coordinate (x, y, z). The measurement result is stored in three-dimensional form (x, y, z). Each scanning point has an (x, y, z) coordinate position and all scanning information are saved to the SD-card in the scanner.

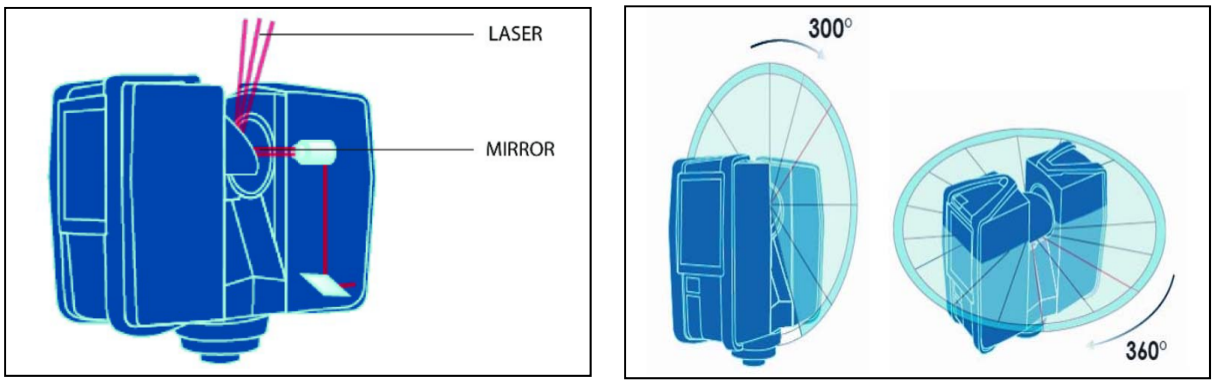

(a) (b)

Figure 3.2 The work principle of FARO Focus3D X130; (a) The position of the laser sensor and the reflection mirror in the scanner; (b) Scanning range of the laser scanner (FARO® Laser Scanner Focus3D X130 Manual, 2014).

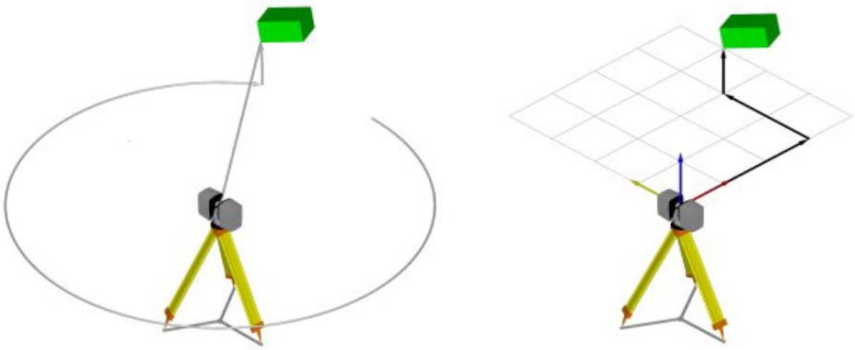

(a) (b)

Figure 3.3 The Polar coordinates transfer to the Cartesian coordinates. (a) The Polar coordinates; (b) The Cartesian coordinates (FARO® SCENE Manual, 2014)

The features and specifications of the FARO Focus3D X130 are as follows (Table 3.1) (FARO® Laser Scanner Focus3D X130 Manual, 2014):

Table 3.1 Features and specifications of FARO Focus3D X130 (modified from FARO® Laser Scanner Focus3D X130 Manual, 2014)

Feature	Specification
General Information	
Power supply voltage	19V (external supply); 14.4V (internal battery)
Power consumption	40W and 80W (while battery charges)
Battery life	4.5 hours
Ambient temperature	5° - 40°C
Humidity	Non-condensing
Cable connector	Located in scanner mount
Weight	5.2kg
Size	240 x 200 x 100mm
Maintenance / calibration	Annual
Ranging Unit	
Unambiguity interval	130m
Range Focus3D X130	0.2m-130m indoor or outdoor with upright incidence to a 90% reflective surface
Measurement speed (pts/sec)	122,000 / 244,000 / 488,000 / 976,000

Table 3.1 Features and specifications of FARO Focus3D X130 (modified from FARO® Laser Scanner Focus3D X130 Manual, 2014)(Cont.)

Feature	Specification
Deflection Unit	
Field of view	Vertical/horizontal: 300° / 360°
Step size	0.009° (40,960 3D-Pixel on 360°) / 0.009° (40,960 3D-Pixel on 360°)
Max. vertical scan speed	5,820 rpm or 97 Hz
Laser parameters	
Laser class	Laser class 1
Wavelength	1550 nm
Beam divergence	Typical 0.19 mrad (0.011°) (1/e, half angle)
Beam diameter at exit	Typical 2.25 mm (1/e)

3.1.1.2. Distance and angle measurement equipment. To verify the LiDAR technology can be used to detect the tiny movement, there are several other pieces of measurement equipment used in this research, such as a Controlled Displacement Device (CDD), dial gauge and Electronic Digital Display Protractor (EDDP).

Controlled Displacement Device: To prove the accuracy and precision of LiDAR technology, a designed controlled displacement device used in this research: Linear Motion Actuator EZC4-05M Mechanism. This mechanism is designed by Kenneth J. Boyko and it is used to simulate the movement of any target. The movement can be controlled by computer (Figure 3.4). The mechanism principle of this device is the screw mechanism which can generate precise motion to simulate the slow movement. Software is designed for this device and the minimum displacement is 1 mil (0.001 inch).

Dial Indicator: In these tests, two dial indicators were used on the CDD which used to verify the CDD displacements (Figure 3.5). In various science and engineering fields, the indicator is an important instrument that can accurately measure small

displacements to 0.0254mm (0.001 inch). The measurement range of the dial indicators which used in this research are 2.54cm (1 inch) and 5.08cm (2 inch).

(a) (b)

Figure 3.4 The controlled displacement device. (a) the linear actuator; (b) the plate which controlled by the linear actuator is used to simulate small displacements and user also can attach other artificial scanning references like spherical target on it.

Electronic Digital Display Protractor (EDDP): In this research the Electronic Digital Display Protractor is used to measure the rotational angle of scanning target rods. The digital protractor is a typical angle measurement tool used for measuring angles with of the target rod with respect to the vertical (gravity) direction (Figure 3.6) (Table 3.2). The rotational angle of the scanning rod which is measured by the protractor is a three-dimensional angle.

3.1.2. Software for Data Processing. The laser scanning result processing software used in this research are “Lidarsw” and “Faro SCENE”. This section will mainly introduce the processing software.

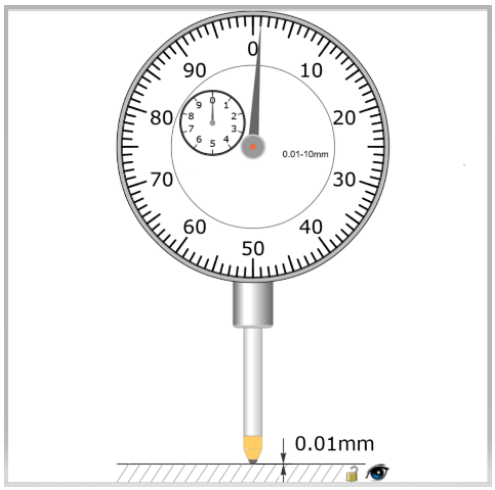

Figure 3.5 The work principle of dial indicator

Figure 3.6 The digital protractor used in the research to monitor the rotational angle of the scanning target rod

Table 3.2 Features and specifications of RISEPRO® Digital Protractor (modify from RISEPRO® Digital Protractor Product description, 2018)

RISEPRO® Digital Protractor	
Outline	Base plate has V-groove with built-in magnets for attaching on curved surfaces or cylinders
Measuring Range	4 x 90˚, 1000mm/m, %: 100%, in/ft: 12in/ft
Accuracy	0˚ and 90˚: +/- 0.05˚
Resolution	0.05˚
Operating Temperature	32 to 122 ˚F (0 to 50 ˚C)
Operating Humidity	0 to 85% R.H.
Dimensions	5.94' x 2.36' x 1.26' inch (151 x 60 x 32 mm)
Weight	10.3 oz (292 g) batteries excluded

3.1.2.1. Faro SCENE. The software "Faro SCENE" is commercial software developed by Faro for their terrestrial and hand-held laser scanners, especially for the Faro laser scanner. The main function of SCENE is for scan data processing and registration. The processing is efficient in real time onsite scan registration. The software can generate full color scanning data by assigning RGB (Red, Green, and Blue) values from the camera to the nearest point. This can help users to visualize better than only seeing a cloud of three-dimensional points.

The features of SCENE are: Impressive Virtual Reality Viewer; Flexible Data Registration; Real Time On-Site Registration; Scanner Control Task; Powerful solid 3D surface rendering; Intuitive user interface; and HDR mapping (Figure 3.7).

In this research the Faro SCENE was mainly used for processing the raw laser scanning data and exporting the special point cloud data in special file form to let the "Lidarsw" do the further processing. SCENE can generate the three-dimensional position (x, y, z) of every scanning point and provide the laser scanning parameters, such as

scanning time, range and resolution (Figure 3.8). SCENE can also automatically detect the natural and artificial references which include: checkerboards patterns and spheres; and natural references: such as corner points, rectangles and planes (Figure 3.9). These references are used to transfer the scanning results of different dates to a single three-dimensional coordinate system, or define the position of the scanning targets and to help the software to find them in different scanning dates.

To recognize the artificial references and natural references, there are some requirements by the software and SCENE can automatic detect the scanning targets only when the scan results satisfy specific requirements (Table 3.3).

Table 3.3 Artificial Reference Requirement of SCENE (modify from FARO® SCENE Manual, 2014)

Artificial Reference Requirement of SCENE	
General Requirement	As artificial targets you should use checkerboard or sphere targets;
	Use artificial targets with a non-reflecting surface;
	Print paper targets with laser printers only;
	The artificial targets should be easily and clearly visible in the scans;
	Artificial targets should not be positioned symmetrically
Checkerboard Requirement	The angle of incidence between the laser beam and the checkerboard target should not be less than 45°;
	Depending on the selected scanning resolution, the automatic detection of checkerboard targets may get unreliable beyond a certain distance to the scanner;
	Have sufficient scan points on the checkerboard targets. They need four or more scan points per quadrant;
	Checkerboard targets should not be attached to a curved surface
Spheres Requirement	Spherical targets should be fully visible in the scan;
	The minimum scan points to recognize a sphere target is 80

Actually, most of the function of SCENE was not used in this research. Two of main functions used in this research are: (1) preprocessing the raw laser scanning result to

a colorful scanning point cloud; and (2) export the data in a file format which can be accepted by “Lidarsw”. SCENE can export several kinds of file format, such as CPE, DXF, XYZ, PTS and so on (the CPE file type is primarily associated with Fax by Microsoft Corporation; The DXF file is a CAD data file format developed by Autodesk for enabling data interoperability between AutoCAD and other programs; the XYZ file contains X, Y, and Z coordinates; the PTS files are often referred to as 3D Points File Graphics). Because the Lidarsw can accept the PTS format, so the final export scan result file from SCENE is PTS file format. The PTS file contains 7 items: x, y, z, intensity, R, G, and B. The x, y, and z are the three-dimensional position and normally in units of decimal mm; the intensity is a signed integer ranging from -2000 to +2000 and represents a relative brightness value; and the R, G, and B numbers are unsigned 8-bit numbers defining the red, green and blue color components.

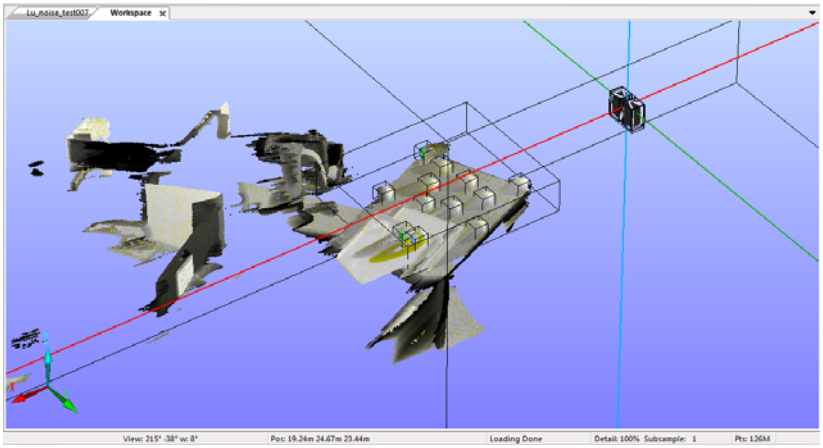

Figure 3.7 The example of Faro SCENE showing the three-dimensional position of artificial targets; Each scan point has a unique three-dimensional position (x, y, z). The position of laser scanner is by default (0, 0, 0).

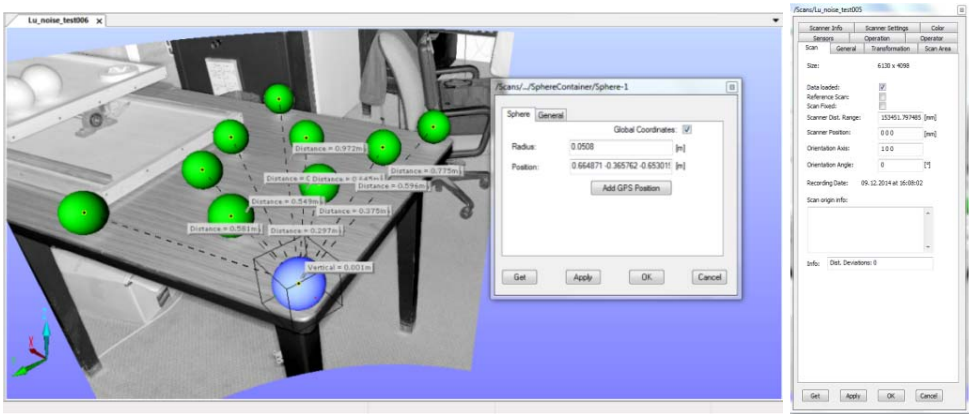

Figure 3.8 SCENE can generate a three-dimensional position (x, y, z) automatically for all scanning targets or point positions identified by mouse click.

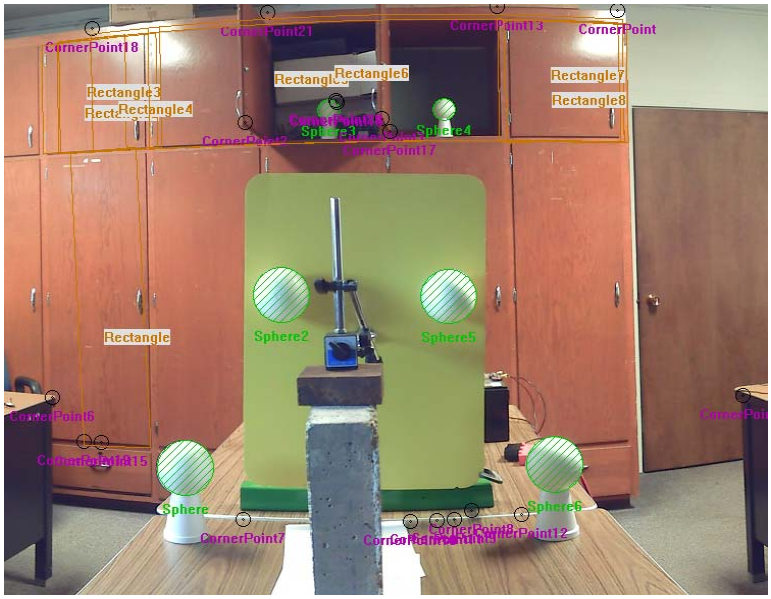

Figure 3.9 The artificial targets and the natural references identified in the SCENE software.

3.1.2.2. Missouri S&T LiDAR Software. The Lidarsw software used in this research has another name: Missouri S&T LiDAR Software which was developed at the Missouri University of Science and Technology. The author of this software is Mr. Kenneth J. Boyko. Lidarsw is written in C++, using the GNU GCC compiler and the main functions of Lidarsw focus on laser scanning data processing and change detection.

The basic concept of using Lidarsw to detect the change of scan area or target is to acquire a high-resolution laser scan at two different dates/times, then register them to a common global coordinate system and analyze the difference of surface position which has occurred over time (Kenneth J. Boyko, 2014).

The whole principle of Lidarsw can be divided to three parts: Structure, Registration and Calculation:

The first part of processing "Structure" means the raw point-cloud data collected from laser scanner (e.g. FARO Focus3D) in PTS file format is unstructured. The raw scanning points file are sorted much like a random bucket of (x, y, z) position information of all scan points in no particular order. If user wants to conduct higher level operations, some degree of structure has to be created. In the software, the command "findminmax" and "load" are responsible to provide the certain degree of structure to point cloud file to support further processing (Kenneth J. Boyko, 2014).

The second part is "Registration". When the researchers want to process the structural scanning to compare the scanning results from different dates or time, they have to make sure these scanning results are comparable. As we known, every scanning point has three-dimensional information (x, y, z) in each scanning result and the scanner position always (0, 0, 0). But the scanner cannot be repositioned in exactly the same position every time, which means every three-dimensional coordinate system at a different date is unique and uncomparable. To calculate the difference of volume change or scanning target movement, the comparability is necessary. "Registration" is software to subtract the two Lidar scanning point cloud acquired at different dates to a common three-dimensional coordinate system to give comparability to the scanning data. In this

process, the scanning data sometimes needs to be. In the software, the command “regpts”, “register”, “view2surf”, “clipspheres” and “findspheres” help to complete this step (Kenneth J. Boyko, 2014).

The final part is “Calculation”. As the development objective of the software, the processing target is to obtain the volume change or displacement. After putting two scanned data sets from different three-dimensional coordinate systems into same coordinate system, the software will use “diff”, “calvol” and “regballs” to finish the calculation process and get the final difference of two or more scan results (Kenneth J. Boyko, 2014). In Lidarsw, there are two individual calculation objectives: the volume change detection and the scan target displacement calculation. Both of them use the same calculation principle which is using the position change of scanning points to obtain the volume change or the displacement. The difference in these two calculation objectives is that volume change needs to consider millions of position change and it is an estimated result because the resolution of laser scanner cannot cover every details of scan area, and to calculate the artificial reference movement it is just needed to find several position changes of reference centers.

To calculate the volume change of rockfall or landslide, the Lidarsw needs nine steps: ckrmse, regpts, findMinMax, load, register, elimVeg, diff, calcvol and view2Surf (Figure 3.10).

To achieve the research objective in this project, the Lidarsw needs seven steps: findminmax, Load, View2surf, Clipspheres, Findspheres, Regballs and Surf2surfer (Figure 3.11).

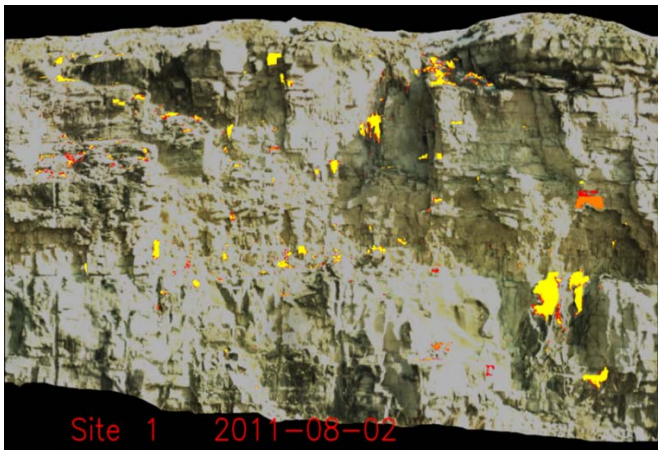

Figure 3.10 Using Lidarsw to calculate the progressive raveling loss (Maerz, N.H. et al., 2015); the yellow parts and the red parts show the date of volume change in a rock fall monitoring application.

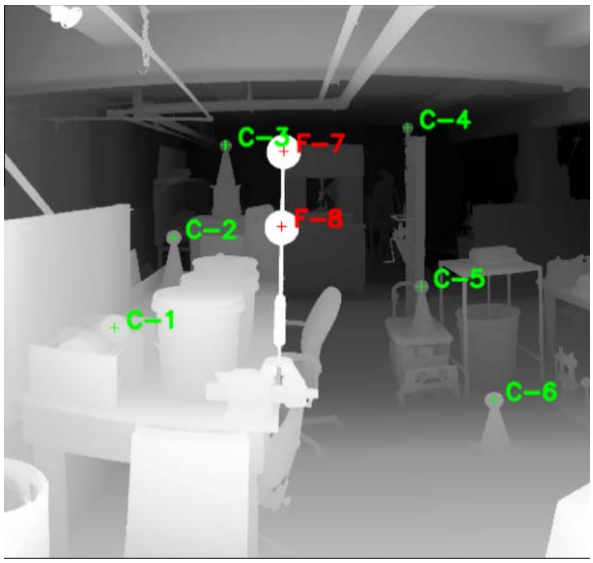

Figure 3.11 Using Lidarsw to obtain the position change of artificial references. The green targets are the control targets which are fixed and used to help registration; the red targets are the floating targets which are used to measuring the displacement.

Using Lidarsw has some processing limitations, and if the user wants to obtain the correct result, he needs to follow some restrictions. The first limitation is file format which needs the user to input the right file format: (xxx.PTS) into the software. The second limitation is all PTS file which needs importing to the software have to be

renamed in such a way to encode the date, time, and site in the following format “yyyy-mm-dd-s.pts” (yyyy is year, mm is month, dd is date and s is site number which is help Lidarsw to recognize the file location). The third limitation is the scanning range. “The internal cell structure used for all the programs utilizes statically allocated fixed-size arrays for the performance advantages they offer. The arrays were sized to handle a wide variety of research requirements, but do have limitations.” (Kenneth J. Boyko, 2014) The maximum internal cell number limitation is: the horizontal extent is limited to 4300 cells and the vertical extent is limited to 3400 cells. The maximum scanning range depends on the mesh resolution used which means the maximum scanning range can be calculated:

4300 cells×Mesh Resolution (mm)/cell=Maximum Horizontal Scanning Range (3.1)

3400 cell×Mesh Resolution (mm)/cell=Maximum Vertical Scanning Range (3.2)

The structural cell number is a certain parameter and the mesh resolution is a variable parameter defined by the software user and the value depends on the laser scanning resolution. Using equation 3.1, 3.2 and the mesh resolution set up in the software and the maximum scan area can be estimated.

The data processing steps of Lidarsw will be introduced in next section.

3.2. METHODOLOGY

Using LiDAR to study landslide movement has two key problems which need to be solved: (1) The accuracy of the measurement methods; (2) The methodology to extend

the function of LiDAR technology to obtain both surface and subsurface motion of landslide.

To improve the measurement accuracy of LiDAR technology, there are numerous examples of research about laser scanner using different types of laser scanners and different methods with different measurement accuracy to study the landslides. For instance, Franz, M. et al. (2016) found the artificial targets can improve the scanning accuracy when he monitored the landslide in the Peney landslide (Geneva, Switzerland). In this research, the author used the polyfoam cube to be the scanning references. Another research conclusion from Maerz, N.H. et al. (2016) used the spherical targets to improve the accuracy level of the laser scanning result to 0.3 mm. Depending on the data processing software, different shapes or sizes of scanning references are used under difference research conditions.

In this research, all scanning reference artificial targets used are spheres. There are two reasons to use the sphere shape targets in the scanning processes. The first reason has been discussed above which is an artificial reference can help to improve the precision of LiDAR scanning result as described in Section 2 and Section 3.2, and also can avoid the noise in the scanning process, such as vegetation on the slope or cars on the road between the scanner and scan area. The second reason for using spherical targets is the target which has a spherical shape can significantly enhance the accuracy of the scanning result because of the algorithm of data processing software. In both the Faro SCENE and Lidarsw, several types of targets and natural references can be automatic detected, such as planes, sharp rock corners, or checkerboard centers, but the spherical target is the best choice because spherical targets have the unique property of omni-

directional stability - no matter what angle the sphere is scanned at, the computed position of the sphere center will always be the same. This property is critical for applications where multiple scans separated over long periods of time are required. The FARO SCENE and Lidarsw use a recursive algorithm to find the (x, y, z) position which results in the smallest standard deviation of distances to each of the surface observations (Figure 3.12).

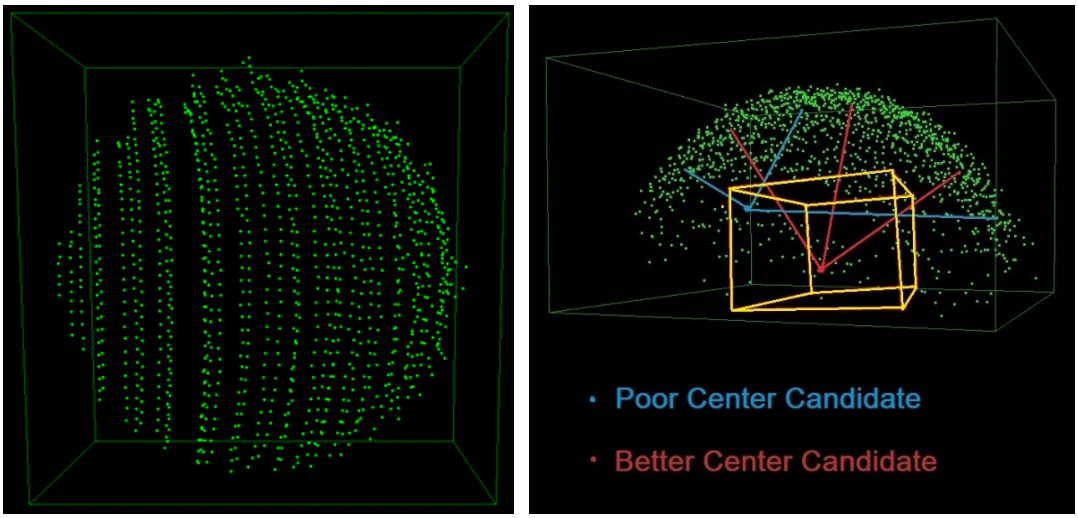

(a) (b)

Figure 3.12 The Lidarsw uses are cursive algorithm to find the three-dimensional center position of spherical scanning reference. (a) The omni-directional stability of sphere (Maerz, N.H. et al. 2016); (b) The recursive algorithm method to calculate the center of the sphere target in Lidarsw (Kenneth J. Boyko, 2014). The calculation process "findspheres" can recognize the point which is the closest one to the real center of the spherical target. For example, the red point has better standard deviation value than blue point which means the red point is closer to the actual center of the sphere than the blue point. Using the scanning points on the scanning target, "findspheres" can calculate thousand times to find the best result of the center of the scanning target in the scanning result.

The conclusion is that the spherical shaped target is better than other kinds of references, such as planes, cubes or chessboard targets is because: (1) The omni-

directional stability of sphere which means no matter the scanning direction, the scanning result of sphere target will be same; (2) The recursive algorithm method can be used to calculate the center of sphere instead of plane, cube or chessboard, which means the position of sphere center in the scanning result has better precision than other kinds of artificial and natural reference.

To extend the function of LiDAR technology to obtain the subsurface motion of landslide, a new methodology is developed to extend the function of LiDAR technology in landslide research (Maerz, N.H. et al. 2016). To present the subsurface motion, rigid aluminum rods and Styrofoam ball targets mounted on the rod are designed for this research (Figure 3.13).

As shown in Figure 3.13, these artificial references which include the rod and sphere targets make it possible to get sub-mm measurements by LiDAR scanning. When the aluminum rod is installed into the slope, both inside and outside the slide area, the motion of the spherical targets inside the slide area relative to the targets outside the slide area can be measured. Meanwhile, because there are two spherical targets on the same rigid rod, the rotation angle of the rod which is generated by the motion of subsurface soil can be detected by LiDAR scanning technology when the two spherical targets on the rod can be used to measure the rotation and displacement. Also, no matter which kind of relationship between the rod and shear surface (Figure 3.13-1, 2, 3 and 4), both the surface or subsurface movement of soil can be shown by the scanning sphere references on the aluminum rod. Thus, depending on whether the base of the rod is above or below the slip/failure surface, different displacement/rotation of soil body will be obtained by LiDAR.

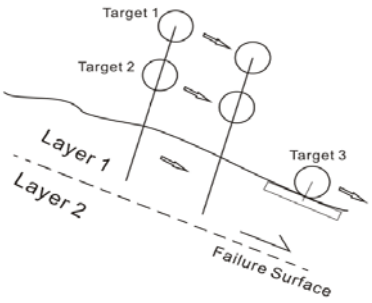

Figure 3.13-1: Movement of Styrofoam target spheres above a planar shear surface, when the base of the rod is above the shear surface.

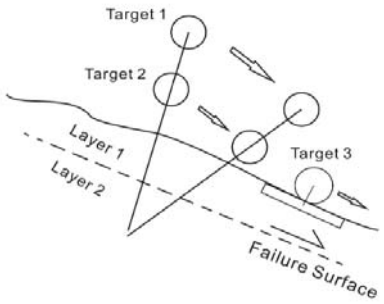

Figure 3.13-2: Movement of Styrofoam target spheres above a planar shear surface, when the base of the rod is below the shear surface.

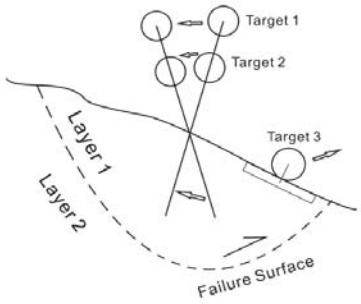

Figure 3.13-3: Movement of Styrofoam target spheres above a circular shear surface, when the base of the rod is above the shear surface.

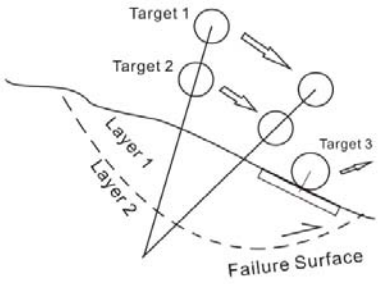

Figure 3.13-4: Movement of Styrofoam target spheres above a circular shear surface, when the base of the rod is below the shear surface.

Figure 3.13 The four types of relationship between the scanning targets and type of soil slide/shear surface: the two kinds of scanning targets are designed for the scan by LiDAR; These two kinds of targets will be used in the further experiments.

To prove this methodology, the analysis of the rod and soil interaction as a result of movement is necessary. The computer simulation method will combine the LiDAR scanning result to explain this new methodology.

According discussed above, the methodology for this research involved the following three steps:

1. Scanning and data processing;

2. Experimental design;

3. Test result analysis.

3.2.1. Scanning Prepare and Data Processing. According the background, the research objective and the developed methodology, a series of experiments to prove the developed method were designed. But before the experiment design is explained it is necessary to understand the scanning procedure and data processing is necessary.

The entire scanning process of the Faro Focus3D terrestrial laser scanner includes five steps:

1. Set up the scanner tripod and estimate the scan distance to make sure the scanning range is not above the limitation of the scanner;

2. Mount the Faro Focus3D on the tripod and set up the scanning parameters; The scanning resolution is the most important parameter which needs to be recorded to fit the mesh resolution to be used in Lidarsw;

3. Set up the scanning direction and fix the position of the control targets and float targets the location of which depends on the research objectives;

4. Do a fast scan to make sure the scanning targets are covered and then conduct the detailed scan;

5. Import the raw scanning data to the Faro SCENE program;

The data processing of the FARO SCENE includes four steps:

1. Transfer the raw scanning data to the Faro SCENE by SD card used in the FARO Focus3D;

2. Find the data file folder (the data base name is same as the user defined in the laser scanner) in the software and preprocess each scanning file;

3. Decide if automatic detection of the artificial and natural references in the Faro SCENE is satisfactory and process the scan data to points cloud;

4. Choose the xxx.pts file format for the export scan file.

The third step of scan data processing is using Lidarsw to do the final process and the detail of each command will be described as follow (Kenneth J. Boyko, 2014):

"findminmax": After the xxx.pts file is imported to Lidarsw, the first command is "findminmax" which can examine the file and determine the maximum and minimum extent of the three-dimensional position information (x, y, z). This program also can find if the scan area is beyond the limit of the software (Equation 3.1 and Equation 3.2).

"load": This program is used to load the xxx.pts file into the internal binary data structure and use the metadata file which contained the set-up information produced by "findminmax". The set-up information includes all information require by Lidarsw, such as the mesh resolution. This program is used to sort space of scanning point and bin each scanning points to the appropriate cell to load that point in, and loads in the information about that point.

"view2surf": This program is used to examine the image of scanning result which is composed of scanned points. In this step, there are two kinds of scanned targets: control target and floating target. The control targets (Figure 3.14) is used to help the Lidarsw to register different scan results to a single three-dimensional coordinate system. The floating target (Figure 3.14) is the monitor target which allows LiDAR to obtain the displacement of soil body. In this step, all control spherical targets and floating targets are

labeled and wait for further processing (Figure 3.14). In this step, the approximated center of the sphere is picked by the user and named. It is better to pick close to the center of the sphere as this will let the next program calculation the center of the spherical target more quickly.

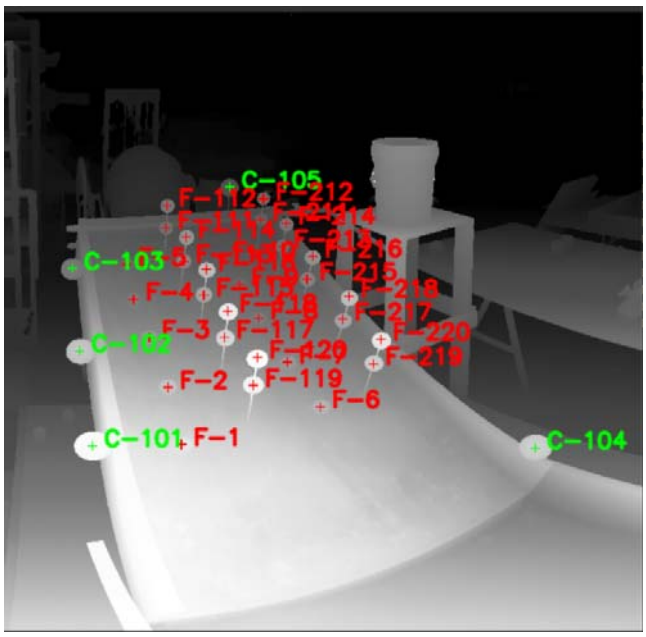

Figure 3.14 The program "view2surf" which help the Lidarsw to locate the control sphere targets and float sphere targets. The green marks show the position of control targets and the red marks show the position of floating targets.

"clipspheres": This program helps the Lidarsw to prepare to calculate the three-dimensional position of the center of the sphere target. The "view2surf" has let the software know the estimate center of sphere, and this program will clip a square space around the estimate center. The side length of the square is set to twice of the diameter of sphere. The benefit of using the side length twice of the diameter of sphere is wherever the mark in "view2surf" located in the scan points on the sphere target, the next program "findspheres" always can calculate the center (x, y, z) position of the sphere.

“findspheres”: After the software uses “clipspheres” to zone the sphere target, “findspheres” calculates the center of each of the spherical targets. This program uses two steps to calculate the center position by recursive algorithm (Figure 3.12). The first step is using the marked center, which is labeled by the user in the “view2surf” program, to calculate the center (x, y, z). The second step is using the center which was calculated in the first step and the diameter which user defined to delete the abnormal scanning points around the sphere targets. If the distance between any scanned point and the calculation center is 10% larger or smaller than the set-up diameter, then the Lidarsw will judge this scanning point is an outlier and delete it in the second calculation step. The calculation result of the second step will be the final three-dimensional calculation center of the sphere target.

“regballs”: The function of the final step is that uses the calculated center of spheres to find the difference of each sphere center position between two different scan dates and obtain the displacement of scanning targets.

The final result of data processing by the Lidarsw is a three-dimensional position report which include all scan targets position (x, y, z), the position change of scanning references and some scanning information such as the root-mean-square error which generated in the registration processing. The further analysis in build on the scanning procedure and the scanning data processing.

3.2.2. Experimental Design. To develop the method of using LiDAR technology and the designed artificial references to study the landslide, three steps are required: (1) Analysis of the principle of the method; (2) Laboratory verification tests; (3) Practical

application. This research will focus on (1) and (2), but also provide analysis and suggestions for the further practical tests.

After understanding the scanning procedure and the data processing and according the research objective and methodology, the experiment of this research would focus on three parts: (1) Error tests to prove the precision level of LiDAR scanner; (2) Sandbox tests to prove the feasibility of LiDAR technology and the new research methodology; and (3) Bench model tests to prove the practicability of LiDAR technology and the new methodology.

The error generated in scanning process can be divided into three types: (1) The error of three-dimensional position of scanning targets; (2) The displacement error of scanning targets; (3) The error of rotational angle of the scanning target rod. To understand these three types of error can help to measure the accuracy and precision of the new research method. Furthermore, the error tests will support all further research which use the LiDAR technology or other similar research methods.

To analyze the feasibility of LiDAR technology and the new research methodology, the laboratory is necessary. The sandbox test is designed and there are two objectives of this test: (1) To prove the combination of the Aluminum rod and the spherical scanning targets can represent the movement of internal of sand or soil masses; (2) Using computer simulation method to analyze the interaction between the rod and the soil.

To prove the research method can be used in real environment, a bench model test is designed. The test objective is to test if this method can find the movement of surface and subsurface of large-scale slope.

4. THE ERROR TESTS

This section elaborates on the process of the error test and relevant results.

4.1. THE THREE-DIMENSIONAL POSITION ERROR (PRECISION) TEST

The definition of three-dimensional position error is the difference between the true position of the scanning targets and the LiDAR scanning result. To know the error range of the three-dimensional position is one of the most important elements of this research project, because all further tests and analysis, such as displacement or rotational angle of scan target, uses the three-dimensional position of the scanning target. But the true position of the targets is hard to accurate measure. Therefore, this research uses the precision test method to calculate the three-dimensional position error.

The three-dimensional position error test has two purposes: (1) Obtain the inherent three-dimensional position error of the FARO Focus3D LiDAR scanner; (2) Prepare for the displacement error test.

4.1.1. Experimental Process. To obtain the three-dimensional position error, there are three basic experimental conditions that need to be met during multiple scans of the same target: (1) Set the laser scanner in a fixed position to scan the targets; (2) Set consistent scan parameters in each scanning to let the scan results to be comparable; (3) Fix the scanning targets in same position to let the position of scan targets to be comparable.

The scanning targets used in this experiment are 10.16 cm (4 inch) diameter Styrofoam spheres. The spherical target is a good artificial scanning reference because of

the omni-directional stability of sphere and the ease of identification in the recursive algorithm method of Lidarsw. Both SCENE and Lidarsw use (x, y, z) position of scanning points on the surface of the spherical scanning target to calculate the center point position of the sphere which is used to represent the position of the scanning target.

All scanning targets are fixed in a stable position (Figure 4.1a). The entire test process is as follows:

1. Fix 10 scanning spherical target on table;

2. Use FARO Focus3D to scan all targets 11 times (replicates). All targets are in the same scanner position; the scanner uses the same scanning direction and range and using the same scanning parameters in entire experiment process;

3. Obtain the three-dimensional location (x, y, z) of each scanning target in scanning results;

4. Set the 1st scanning result to be the base scanning result;

5. Compare the 2nd to 11th scanning results with the 1st scanning result;

6. Calculate the three-dimensional position error of FARO Focus3D in three directions (X, Y, Z) by the Lidarsw program (Figure 4.1 b, c, d).

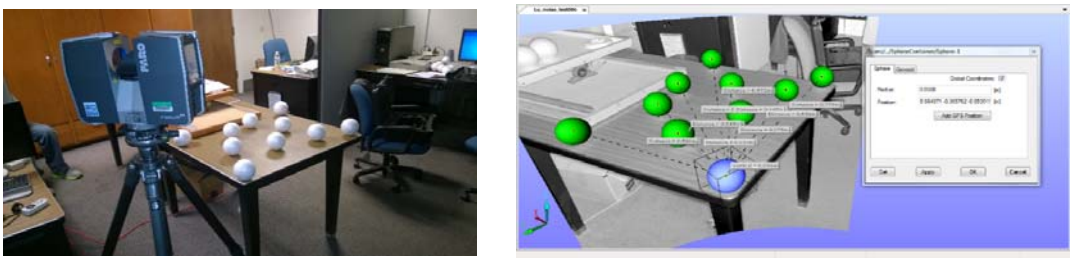

(a) (b)

Figure 4.1 The three-dimensional position error test. (a) Scanning targets on table; (b) Scanning results in SCENE; (c) Three-dimensional coordinate system of scanning result in SCENE; (d) The scanning result shown in Lidarsw. Red “F” is used to identify floating targets in Lidarsw, and the number is the ID of the scanning targets.

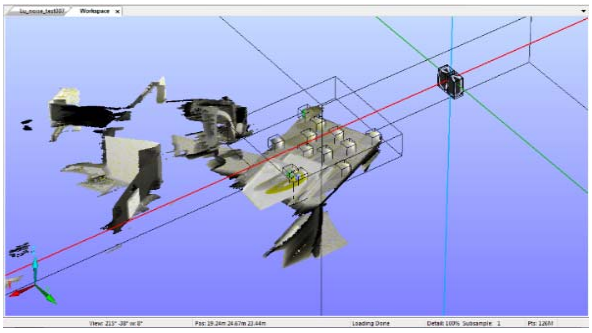

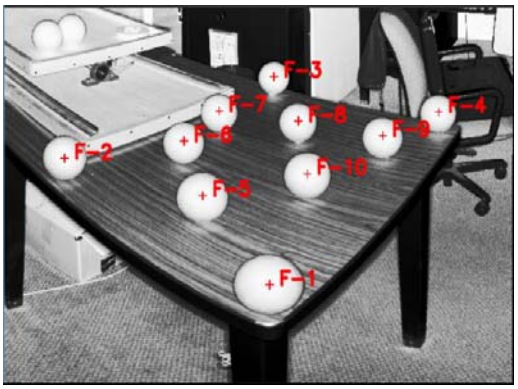

(c) (d)

Figure 4.1 The three-dimensional position error test. (a) Scanning targets on table; (b) Scanning results in SCENE; (c) Three-dimensional coordinate system of scanning result in SCENE; (d) The scanning result shown in Lidarsw. Red "F" is used to identify floating targets in Lidarsw, and the number is the ID of the scanning targets. (Cont)

4.1.2. Test Results and Conclusion. The scanning results of three-dimensional error test are shown below:

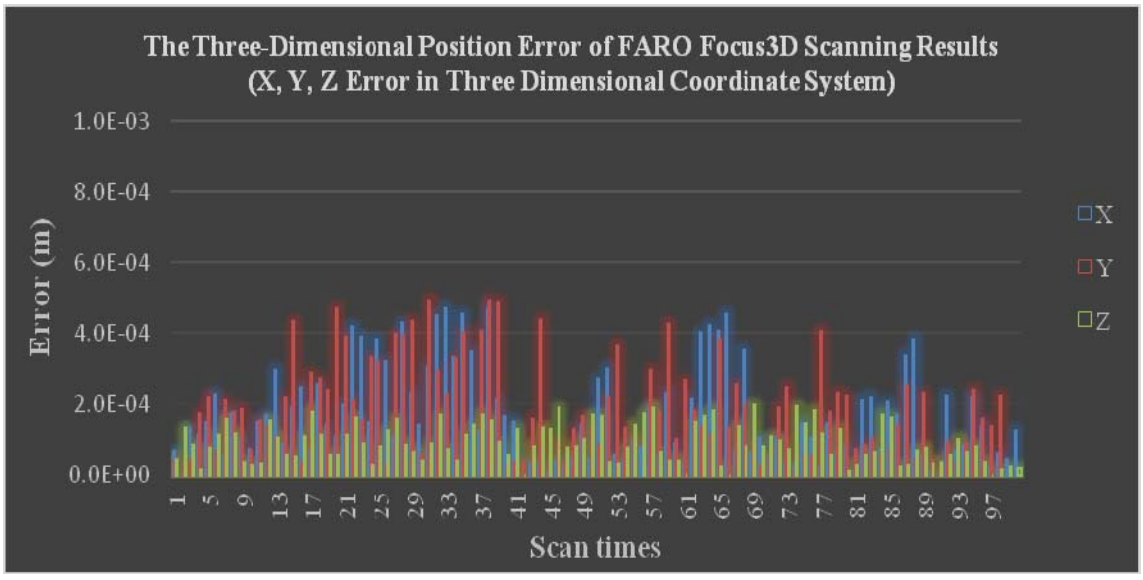

Figure 4.2 The three-dimensional positional error of FARO Focus3D in three-dimensional Cartesian coordinate system. There are 10 matched group (the 2nd to 11th scanning results), and each group has 10 scanning targets need to compare with the control group (the 1st scanning result). Therefore, there are 100 results of comparison.

Table 4.1 The average three-dimensional position error

	X (mm)	Y (mm)	Z (mm)	Average three-dimensional position error (mm)
Average error	0.168	0.185	0.090	0.265

Table 4.2 The maximum three-dimensional position error

	X (mm)	Y (mm)	Z (mm)	Maximum three-dimensional position error (mm)
Maximum error	0.471	0.492	0.191	0.707

The Lidarsw uses the same three-dimensional coordinate system with FARO Focus3D, which means the same scanning point has the same (x, y, z) position in the LiDAR scanner, the software “SCENE” and “Lidarsw”.

After repeated error tests, each direction of the three-dimensional coordinate system has different error range. The average and maximum three-dimensional position errors are shown in Tables 4.1 and 4.2. The average three-dimensional error is 0.265 mm and the maximum three-dimensional error is 0.707 mm.

The precision of the three-dimensional position obviously is influenced by the number of the scanning points of the sphere target. More scanning point means the software calculation result has better precision level because more scan points on the spherical target surface means the calculation result of the center of sphere by the recursive algorithm is closer to the real sphere target center (Kenneth J. Boyko, 2014). Previous research (Maerz, N.H. et al., 2016) shows the scan precision of the sphere artificial reference is increased as the number of the scan points of the reference increases, but little improvement in precision is achieved beyond 1000 scanning points. In this research, the spherical target which has the minimum number of the scanning points is

the target F3 (Figure 4.1d) which has the longest distance with the laser scanner. The spherical target F3 has 8458 scanning points on its surface and it has 10777 scan points before the second calculation step of "findspheres" to wipe off the abnormity scan points. When the scanner uses same scanning resolution and all targets are one size but distances from the scanner are different, the farthest targets have less scan points than the closer targets, because of the divergence of the laser beam paths.

4.2. THE DISPLACEMENT ERROR (ACCURACY) TEST

To obtain the displacement of surface and subsurface movement of a slope, the scanning target can help LiDAR technology to detect the minute displacement. Using a known displacement of a scanning target allows the determination of measurement accuracy.

Using the displacement of scanning targets to reveal the landslide movement will generate errors because of the three-dimensional position error and the registration process. Therefore, to test the displacement error range of the scanning target is necessary.

A controlled displacement device was designed for this test (introduced in Section 3) (Figure 3.4). The device has three components (Figure 4.3): (1) the linear actuator controlled by computer (the minimum displacement of the linear actuator is 0.0254 mm (1 mil)); (2) the simulation circuit board controlled by the linear actuator; (3) a dial indicator fixed in the device which can verify the intended displacement.

The displacement error test has three main goals: (1) to find the minimum displacement which can be detected by the LiDAR technology; (2) to find the minimum displacement which can be detected by the LiDAR scanner and the error which is

generated in the scanning target displacement processing; (3) to test if the size of scanning target has an influence on the scanning error. All of these three research goals will verify the former research result which suggests that more than 1000 points on the spherical will not significantly improve accuracy. (Maerz, N.H. et al., 2016).

4.2.1. Experimental Process. To identify the minimum displacement which can be detected by the LiDAR technology, the displacement error test needs: (1) to use one scanner for all scans; (2) to do all scans with same scanning parameters; (3) and to use the floating target to measure the precision of scanning result. To point out if the size of scanning target has influence about the scanning result, this research using different sizes of the floating targets.

All control targets (used for registration) in this experiment are 10.16 cm (4 inch) diameter Styrofoam spheres, and the floating targets used in this research are 10.16 cm (4 inch) and 6.35 cm (2.5 inch) diameter Styrofoam spheres. All control targets are fixed on a stable position and the floating targets are fixed to the displacement simulator. The entire test process is as follows (Figure 4.3):

1. Set the controlled displacement device to its initial position (Figure 4.3) and prepare the computer program for controlling the movement of the simulator;
2. Fix the control sphere targets around the displacement simulator;
3. Fix the floating sphere targets onto the surface of the moving metal plate of the controlled displacement device (Figure 4.3);
4. Scan all targets in the starting position to be the baseline scanning result;
5. Use the computer to move the floating targets 0.0254 mm (1 mil) and repeat the scan;

6. Set the displacement simulator back to the original position and redo the baseline scan;

7. Use the computer to move the floating targets 0.0508 mm (2 mil) and repeat the scanning;

8. Set the metal board back to original position and redo the Baseline Scanning;

9. Repeat the step 7 and 8, and double the displacement of the simulation metal board until the displacement to 26.01 mm (1024 mil) and the maximum displacement in this test is 43.18 mm (1700 mil);

10. Register each scanning result to the corresponding baseline scanning result to compare the true displacement of the floating targets and the LiDAR scanning results and to calculate the error in each step;

11. Change the size of the floating targets and repeat the scanning process;

12. Compare the scanning results in the step 10 and 11 to find if the scanning target size could significantly affect the scanning error.

Figure 4.3 The controlled displacement device and the scanning targets. The spherical targets on the metal plate are the floating targets and the spherical targets on the table are the control targets. (a) The diameter of the floating target is 10.16 cm (4 inch); (b) The diameter of the floating target is 6.35 cm (2.5 inch).

4.2.2. Test Result. The displacement error test results are shown in Table 4.3 and 4.4 and Figure 4.4 and 4.5:

Table 4.3 The displacement error test result for 10.16 cm (4 inch) spherical target

Scan ID	Controlled Distance (mil)	Measured Displacement (mm)	LiDAR Scanning Result (mm)	Absolute Error (mm)
1	0	0.0000	0.0000	0.0000
2	1	0.0254	0.1843	0.1589
3	2	0.0508	0.6528	0.6020
4	4	0.1016	0.3406	0.2390
5	8	0.2032	0.3967	0.1935
6	12	0.3048	0.8930	0.5882
7	16	0.4064	1.0272	0.6208
8	20	0.5080	0.4965	0.0115
9	24	0.6096	0.6126	0.0030
10	28	0.7112	0.7428	0.0316
11	32	0.8128	0.8445	0.0317
12	64	1.6256	1.6547	0.0291
13	128	3.2512	3.6602	0.4090
14	256	6.5024	6.4387	0.0637
15	512	13.0048	12.9141	0.0907
16	1024	26.0096	26.4688	0.4592
17	1700	43.1800	43.3490	0.1690

The result of the displacement error test which used the 10.16 cm (4 inch) scanning target is shown in Figure 4.4 and Table 4.3 (Table 4.3). The result shows the LiDAR technology can obtain the displacement of the scanning targets and the minimum displacement that can be identified by the scanner is 0.508 mm (20 mil), which means if the displacement of the scanning targets is smaller than 0.508 mm (20 mil), the absolute error may be larger than or close to the actual displacement of the targets (Figure 4.4) and this phenomenon can make it difficult to recognize the displacement and the error. The mean value of absolute error is 0.2313 mm.

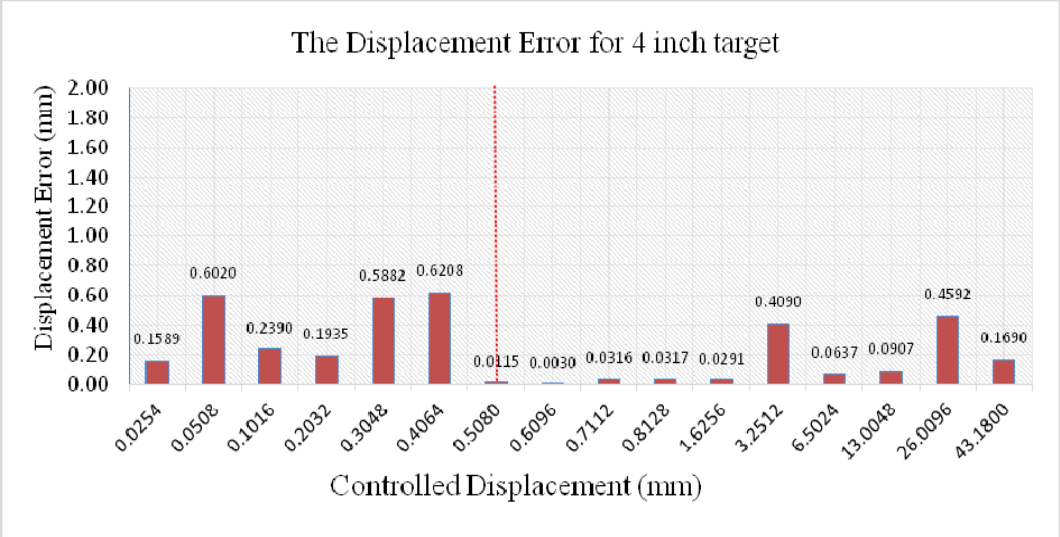

Figure 4.4 The displacement error of the 10.16 cm (4 inch) sphere target. The red line is the value boundary for the FARO Focus3D scanner to differ the displacement of scanning target with the displacement error. If the displacement smaller than 0.508mm (in the left side of the red line), the scanner can not differ the displacement with error.

Table 4.4 The displacement error test result for 6.35 cm (2.5 inches) sphere target

Scan ID	Controlled Distance (mil)	Measured Displacement (mm)	LiDAR scanning result (mm)	Absolute Error (mm)
1	0	0.0000	0.0000	0.0000
2	1	0.0254	0.1114	0.0860
3	2	0.0508	0.0949	0.0441
4	4	0.1016	0.1206	0.0190
5	8	0.2032	0.5313	0.3281
6	12	0.3048	0.4253	0.1205
7	16	0.4064	0.9564	0.5500
8	20	0.5080	0.5220	0.0140
9	24	0.6096	0.6150	0.0054
10	28	0.7112	0.7309	0.0197
11	32	0.8128	0.7939	0.0189
12	64	1.6256	1.7578	0.1322
13	128	3.2512	3.1935	0.0577
14	256	6.5024	6.4962	0.0062
15	512	13.0048	13.0446	0.0398
16	1024	26.0096	26.3901	0.3805
17	1700	43.1800	43.4172	0.2372

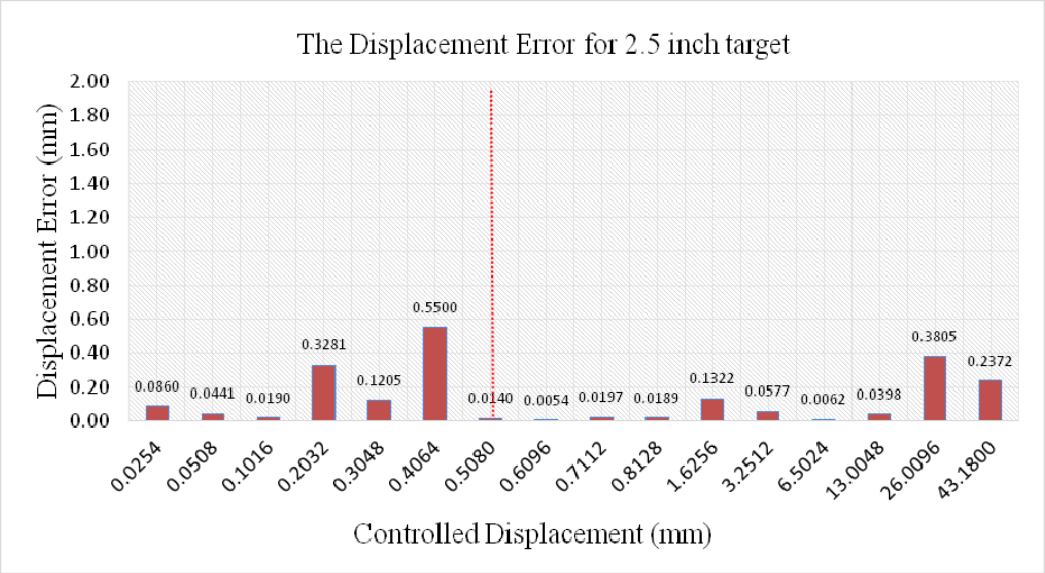

Figure 4.5 The displacement error of the 6.35 cm (2.5 inch) sphere target. The red line is the value boundary for the FARO Focus3D scanner to differ the displacement of scanning target with the displacement error. If the displacement smaller than 0.508mm (in the left side of the red line), the scanner can not differ the displacement with error.

The displacement error test result which used the 6.35 cm (2.5 inch) scanning target shows in Table 4.4. The result shows the LiDAR technology can obtain the displacement of the scanning targets and the minimum displacement that can be identified by the scanner is 0.508 mm (20 mil) which is similar with the minimum displacement of the 10.16 cm (4 inches) scanning target. This means if the displacement of the scanning target is smaller than 0.508 mm (20 mil), the absolute error may be larger than or close to the actual displacement of the target (Table 4.4). The mean value of absolute error is 0.1287 mm.

4.2.3. Conclusion. The test results show the FARO Focus3D can recognize the scanning target displacement greater than or equal to 0.5080 mm (20 mil) no matter the scanning target is 10.16 cm (4 inches) or 6.35 cm (2.5 inches). When the displacement of target less than 0.4064 mm (16 mil), the software can not differ the actual displacement

from error because the error is larger than or close to the displacement (Table 4.3 and 4.4). When the displacement of scanning target reaches 0.5080 mm, the absolute error of LiDAR scanner is always smaller than 0.46 mm.

In this test, there two sizes of the scanning target were used and the number of scanning points on all the control targets and the floating targets are well over 1000, which means the scanning point number should have no influence on the accuracy of the scanning result. Under the known conditions above, the mean value of absolute error of the 10.16 cm (4 inches) target is 0.2313 mm and the mean value of absolute error of 6.35 cm (2.5 inches) target is 0.1287 mm (Table 4.5). The conclusion is if the scanning point number of scanning sphere target is larger than 1000, the size of sphere appears not to have a significant impact to the displacement error.

Table 4.5 The mean of the displacement error for different size of the scanning targets

Diameter of the Scanning Target	Mean of the Displacement Error
10.16 cm (4 inch)	0.2313 mm
6.35 cm (2.5 inch)	0.1287 mm

The displacement error test proves that the artificial spherical target not only can improve the scanning precision (Franz, M. et al., 2016), but also can be used to help LiDAR technology to measure the displacement of the displacement simulator used in this research. Also, this test result indicates that the LiDAR technology can keep the scanning error smaller 0.46 mm when the scan parameters and targets can follow specific requirements: (1) The number of scan points on the scanning target is larger than 1000 which require the scan distance, the scan resolution and the scan target size; (2) The

scanning artificial spherical targets are used in the research to be the control targets and the floating targets to help the software registration and improve the scan precision; (3) The displacement of scan target need to meet the certain value which is 0.508 mm.

4.3. THE ROTATIONAL ANGLE ERROR TEST

To reveal the subsurface displacement of soil, the design philosophy is shown in Section 3.2 and Figure 3.13 which uses the rigid aluminum rod and the spherical targets on the rod to measure the movement both of surface and subsurface of soil. The LiDAR technology has been proven that it can detect the sphere target displacement in Section 4.2 and in this section the rotational angle error test is designed to test if this method can accurately measure the rotational angle. Furthermore, this test is also designed to test the rotational angle error range.

The reason that LiDAR can detect the rotational angle can be shown in Figure 4.6 as follow:

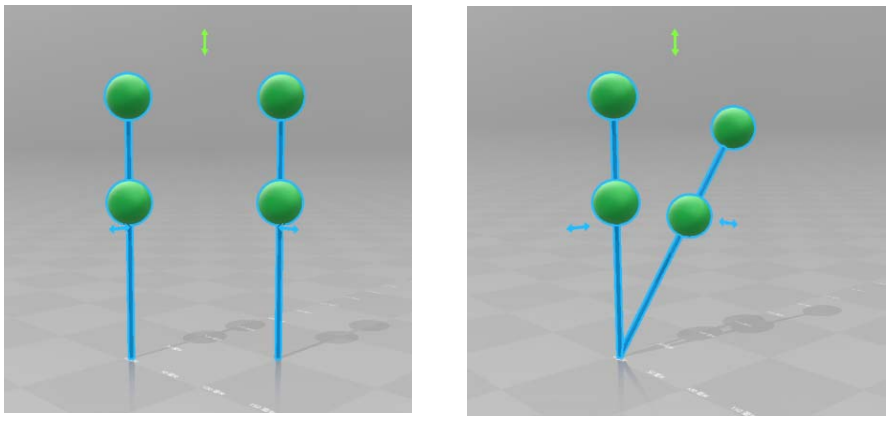

(a) (b)

Figure 4.6 The principle of using twin target rods to measure rotation. (a) Target rod moves such that the targets move in parallel; (b) Target rod shows rotation only. (c) Target rods move in parallel and in rotation; (d) Target rods move in parallel and in rotation but move laterally as well.

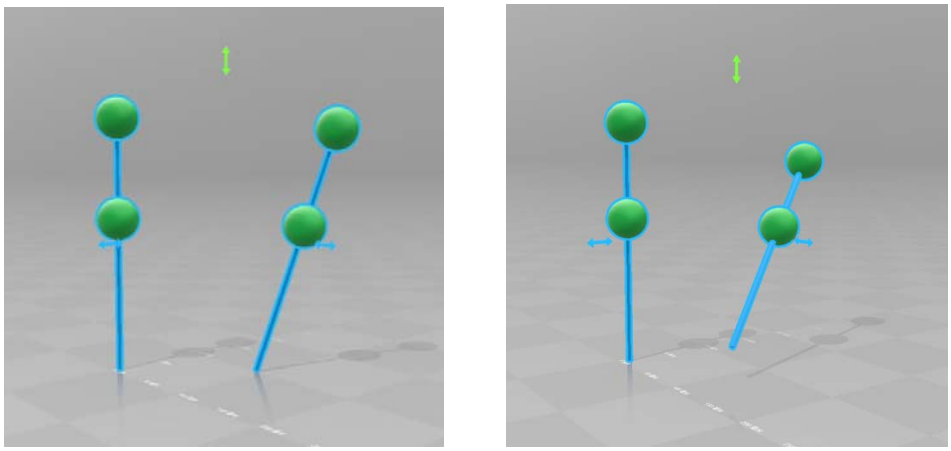

(c) (d)

Figure 4.6 The principle of using twin target rods to measure rotation. (a) Target rod moves such that the targets move in parallel; (b) Target rod shows rotation only. (c) Target rods move in parallel and in rotation; (d) Target rods move in parallel and in rotation but move laterally as well. (Cont)

The three-dimensional position of the two spherical scanning targets on the rigid aluminum rod can be detected by the LiDAR scanner. Given two three-dimensional positions of the scanning targets the angle of the target rod can be calculated. The definition of the rotational angle is that the inclined angle generated between the original attitude of the rod and the attitude after rotation. The rotational angle between these two spatial vectors can indicate the displacement and motion tendency of the subsurface of the landslide.

The rotational angle test will focus on the first type of target and test: error in measuring the rotational angle.

For this experiment, the targets used in this research which need to fixed on a rod is built as shown in Figure 4.7. To minimize displacement measurement errors, the target needs to be precisely centered on the rods.

Figure 4.7 To fixed the sphere scanning target to the metal rod and keep the three-dimensional error of scanning results to minimum, all spherical targets used in this research are drilled precisely through their centers to let the rod can pass precisely through the center of the sphere target.

4.3.1. Experimental Process. In the rotational angle error test, the main research objective is to test the ability of the LiDAR technology to obtain the inclined angle of the target rods which are composed of two spherical targets set on a single rigid metal rod. The three-dimensional error test and the displacement error test results have shown the LiDAR technology can be used to detect the three-dimensional position and the displacement of the artificial scanning targets. Therefore, the rotational angle error test just needs to focus on: 1) measuring the rotational angle error range; (2) determining if the size of the scanning sphere target will influence the test results.

To achieve the research objectives, this test uses six control targets to improve the scanning precision and reduce the error in the registration processing, and two floating targets impaled on a metal rod which is fixed on a stable table to be rotated at determined angles. The metal rod used in this research is rigid and can only be rotated (Figure 4.8).

To monitor the rotational angle and use the true value to compare with the LiDAR measurement value, a digital protractor is attached to the metal rod (Figure 3.6 and Figure 4.8). The details of the digital protractor were introduced in the Section 3.1.1.2.

Figure 4.8 The designed scanning target which include two floating target spheres on a metal rod that can be rotated in one direction. A digital protractor is attached to the target rod to verify the angle changes.

The floating targets used in this experiment were of three sizes of diameter: 6.35 cm (2.5 inch), 10.16 cm (4 inch) and 15.24 cm (6 inch). All control targets used in this experiment were 10.16 cm (4 inch). The length of the metal rod is 70.48 cm (27.75 inch). The experiment processes are described as follow:

1. Design and build the scanning target by impaling the target balls on the target rods. The designed target includes two sphere targets (15.24 cm (6 inch)) impaled on to a steel rod space and their center position is apart from each other in certain distance (Figure 4.9);

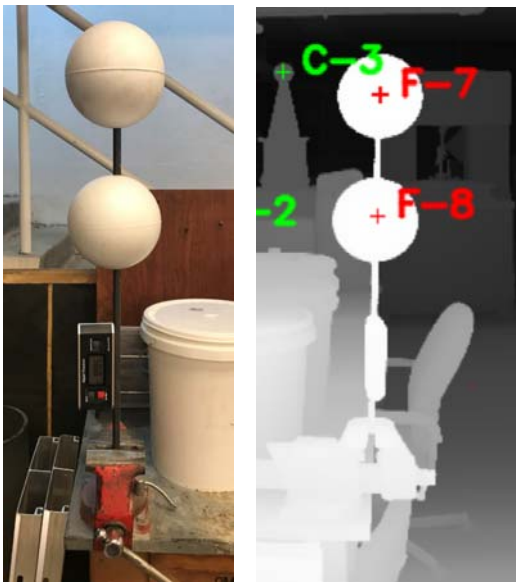

Figure 4.9 The principle of using the scanning targets to measure the rotational angle in scans. The left figure is the original target and the right figure is the scanning point result showed in Lidarsw. The red mark indicates the three-dimensional center of each target. Green "C" is used to identify the control target; red "F" is used to identify floating targets in Lidarsw; and the number is the ID of the scanning targets.

2. Fix the iron rod in a vice so the rod can only rotate around a fixed point in a single direction.

3. An electronic digital display protractor is attached to the rod (Figure 4.9), the resolution value of the protractor used in the experiment is 0.05°;

4. Fix the control targets (all control targets are 10.16 cm (4 inch) plastic sphere) around the floating targets (the control targets are fixed and used to register successive LiDAR scans so they are in a common coordinate system) (Figure 4.10);

5. Erect the rod vertically and set the initialize the protractor measurement to 90.00°, then use the LiDAR to do the baseline scanning three times;

6. Rotate the rod and set up the rotational angle to 0.50°, then redo the scanning three times;

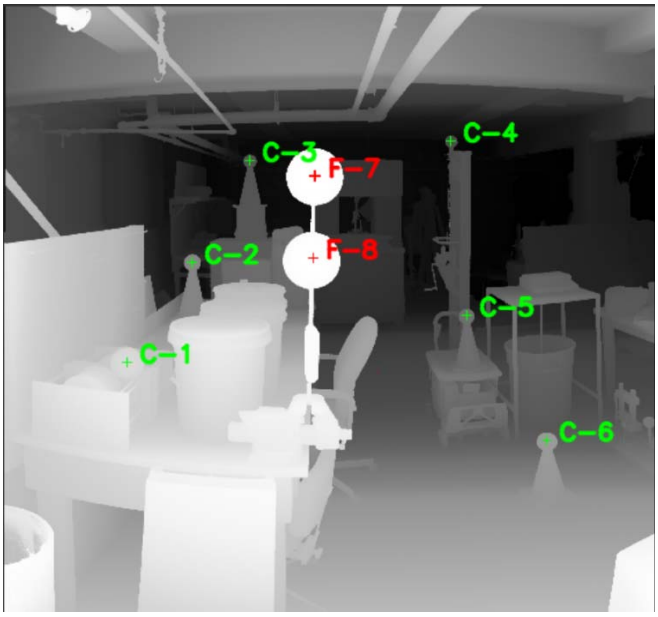

Figure 4.10 The scan points cloud figure shows the position of the control targets and floating targets. The green targets are the control sphere references and the red targets are the floating sphere targets. Green “C” is used to identify the control target; red “F” is used to identify floating targets in Lidarsw; and the number is the ID of the scanning targets.

7. Set the rod back to 90.00°, redo the baseline scanning three times;

8. Rotate the rod and set up the rotational angle to 1.00°, then do the measurement scanning three times;

9. Respectively rotate the rod and set up the rotational angle to 2.00°, 5.00°, 10.00°, 20.00° and 30.00°, then repeat the steps 7 and 8;

10. Register the baseline scanning results and each subsequent scanning results by Lidarsw to a common coordinate system.

11. Calculate the rotational angle for each step above, using the LiDAR derived midpoint coordinates of the upper and lower target balls;

12. Compare the measurement rotational angle by LiDAR with the true rotational angle obtain by electronic digital display protractor to get the error of rotational angle;

13. Change the size of the floating target to 10.16 cm (4 inch) and 6.35 cm (2.5 inch), and repeat each scanning step above;

14. Compare the rotational angle error in different size of floating target to find if the size of scanning target could significantly affect the value of error.

4.3.2. Test Result and Conclusion. All floating and control targets in this experiment have met the minimum scanning point number requirement of 1000 based on previous research results (Maerz, N.H. et al., 2016). For this experiment, the minimum number of scanning points was 6102 which is greater than 1000, so the size of scanning target should have no bias for the three-dimensional error and the displacement error. The different target size experiments results are shown in Table 4.6, Table 4.7 and Table 4.8.

Table 4.6 The rotational angle error for the 6.35 cm (2.5 inch) floating target

Scan ID	True Rotational Angle	LiDAR Scanning Result (°)	Avg Scanning Result (°)	Abs Error (°)	Avg Error (°)
2	0.5°	0.578	0.568	0.078	0.068
3		0.587		0.087	
4		0.538		0.038	
5	1°	0.938	0.979	0.062	0.043
6		0.966		0.034	
7		1.032		0.032	
8	2°	1.872	1.865	0.128	0.135

Table 4.6 The rotational angle error for the 6.35 cm (2.5 inch) floating target (Cont.)

Scan ID	True Rotational Angle	LiDAR Scanning Result (°)	Avg Scanning Result (°)	Abs Error (°)	Avg Error (°)
9		1.854		0.146	
10		1.870		0.130	
11		5.153		0.153	
12	5°	5.140	5.141	0.140	0.141
13		5.131		0.131	
14		9.854		0.146	
15	10°	9.828	9.835	0.172	0.165
16		9.824		0.176	
17		20.278		0.278	
18	20°	20.255	20.270	0.255	0.270
19		20.276		0.276	
20		29.778		0.222	
21	30°	29.782	29.775	0.218	0.225
22		29.766		0.234	

Table 4.7 The rotational angle error for the 10.16 cm (4 inch) floating target

Scan ID	True Rotational Angle (°)	LiDAR Scanning Result (°)	Avg Scanning Result (°)	Abs Error (°)	Avg Error (°)
2		0.672		0.172	
3	0.5	0.592	0.635	0.092	0.135
4		0.640		0.140	
5		1.134		0.134	
6	1	1.116	1.142	0.116	0.142
7		1.175		0.175	
8		2.110		0.110	
9	2	2.109	2.111	0.109	0.111
10		2.115		0.115	
11		5.026		0.026	
12	5	4.999	5.004	0.001	0.013
13		4.987		0.013	
14	10	10.246	10.249	0.246	0.249
15		10.256		0.256	

Table 4.7 The rotational angle error for the 10.16 cm (4 inch) floating target (Cont.)

Scan ID	True Rotational Angle (°)	LiDAR Scanning Result (°)	Avg Scanning Result (°)	Abs Error (°)	Avg Error (°)
16		10.246		0.246	
17		19.926		0.074	
18	20	19.887	19.915	0.113	0.085
19		19.931		0.069	
20		30.046		0.046	
21	30	30.049	30.037	0.049	0.037
22		30.017		0.017	

Table 4.8 The rotational angle error for the 15.24 cm (6 inch) floating target

Scan ID	True Rotational Angle (°)	LiDAR Scanning Result (°)	Avg Scanning Result (°)	Abs Error (°)	Avg Error (°)
2		0.552		0.052	
3	0.5	0.530	0.544	0.030	0.044
4		0.550		0.050	
5		0.958		0.042	
6	1	0.970	0.978	0.030	0.027
7		1.008		0.008	
8		1.706		0.294	
9	2	1.702	1.702	0.298	0.298
10		1.696		0.304	
11		4.876		0.124	
12	5	4.874	4.870	0.126	0.130
13		4.860		0.140	
14		9.996		0.004	
15	10	10.021	10.010	0.021	0.013
16		10.014		0.014	
17		20.115		0.115	
18	20	20.169	20.144	0.169	0.144
19		20.150		0.150	
20		29.802		0.198	
21	30	29.802	29.800	0.198	0.200
22		29.797		0.203	

The experiment results show the LiDAR can recognize the rotational angle of the designed scanning target. Because of the resolution of the digital protractor is 0.05°, the test results the maximum absolute error is 0.304°, the minimum absolute error is 0.001°, the maximum average error is 0.298°, and the minimum average error is 0.013°. The average error of all data of different sizes of targets are (Table 4.9):

Table 4.9 The average error for the different size of scanning target

Target Size	Avg Error (°)
6.35 cm (2.5 inch)	0.149
10.16 cm (4 inch)	0.110
15.24 cm (6 inch)	0.122

Figure 4.11 The average rotational angle error for the different sizes of the scanning target

The average error results of three sizes of scanning target have no obvious difference (Figure 4.11) and it indicates the size of the scanning target has no obvious impact on the rotational angle scanning result if the scanning point number meet the software requirement. Furthermore, the curves in Figure 4.11 show the average error of

the scanning targets do not have obvious increase with the rotational angle increase. The rotational angle error of FARO Focus3D scanning result keeps small and prove the LiDAR technology which has enough accuracy to detect the tiny movement and rotation of the designed artificial scanning targets.

5. THE SANDBOX TESTS AND COMPUTER SIMULATION RESULTS

In accordance with the research principles in Section 3 and the error test results in Section 4, a series of experiments have been designed in Section 5 to determine the interaction between the target rod and the soil so as to prove if the target rods can accurately reflect the subsurface movement of the soil. As the designed scanning target shown in Figure 3-13, there are four modes of target motion which are caused by the displacement difference of soil layers and the position of the failure surface. Therefore, Section 5 focuses on both physical tests and computer simulation to verify that the rod movement accurately reflect the subsurface soil movement.

The main differences between the categories of Figure 3-13 are the position of the failure surface and the resulting motion of the target rod. The LiDAR technology detects the displacement of the scanning targets and uses the rotational angle of the rod to determine the location of the displacement surface and relative subsurface movement of soil layers above and below the displacement surface. In Section 4, it has been shown that LiDAR technology can be used to obtain the displacement of the spherical scanning target and the rotational angle of the rod. In Section 5, the sandbox test is used to prove that the LiDAR technology can be used to obtain the accurate movement of real soil materials. Furthermore, computer simulation methods are used to analyze the target rod/soil interaction.

Shear box test used in this section to determine if the target rods can be used in conjunction with the LiDAR technology to monitor the movement of surface and subsurface of soil. FLAC3D and PFC3D have also been adopted in this section so as to

simulate the shear box test procedure and analyze the interaction between the soil and the rod in entire experiment process.

5.1. SANDBOX TEST 1

The sandbox model is design for the sandbox test which simulated the shear plane between different soil layers, and test the scanning target rod reaction by the movement of soil.

5.1.1. Model Design. The sandbox model has four component parts: sandbox frame, displacement control leadscrew, dial gauge, and scanning targets. There are two boxes in the sandbox frame (Figure 5.1), the bottom box is fixed onto a testbed and unmovable, and the top box can slide over the bottom box and the displacement is controlled by the displacement control leadscrew. Two metal plates are fixed onto the sandbox frame and are used to ensure that the top box can slide only in a parallel direction with the bottom sandbox (Figure 5.2). A threaded rod (leadscrew) is linked to the testbed and the top sandbox, whose function is to pull the top box across the lower one to simulate the movement of the soil, slow and precise. It is driven by the manual tightening of a nut on the end of the threaded rod. A dial type displacement gauge is used to set the desired displacement. There are two types of scanning targets: the control targets and the floating targets. The control targets are used to register different scans to a single three-dimensional coordinate system. These are mounted independently of the moving box. There are two types of floating targets (Figure 5.2): The floating type 1 consists of two target balls impaled on an aluminum rod, being used to monitor the subsurface soil movement. The floating type 2 is a target ball fixed onto a wood board

which is buried in very top layer of soil, which can accurately measure the movement of the surface soil (Figure 5.2). In Figure 5.2, the aluminum target rod and the target balls F6 and F7 are the floating type 1 targets and the target ball F8 remains the floating type 2 target.

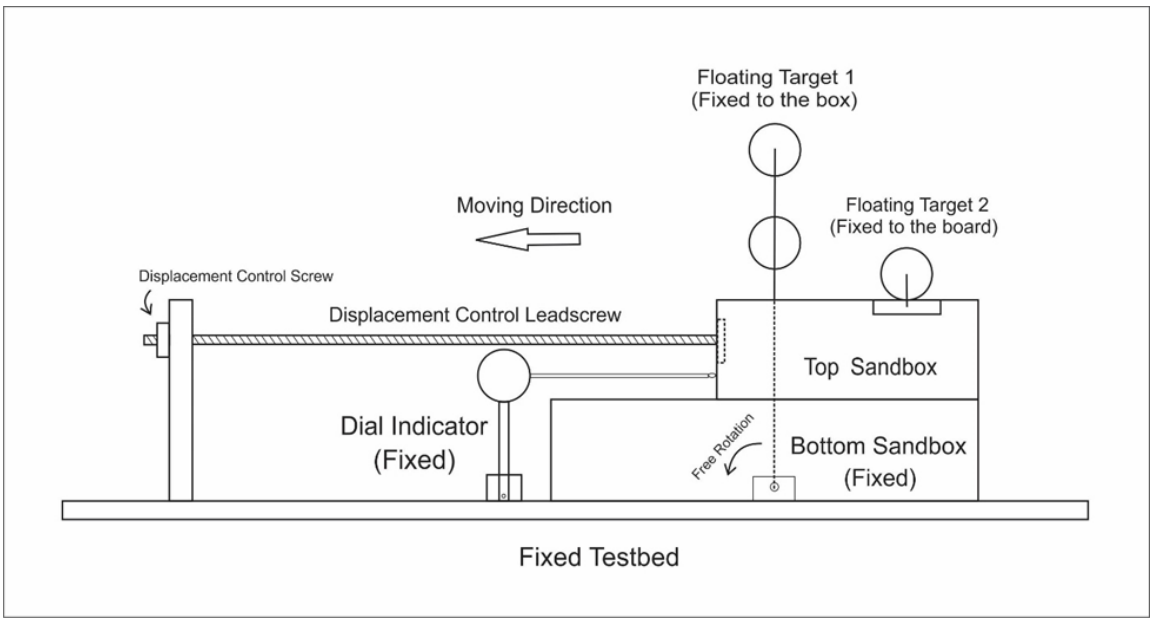

Figure 5.1 The Sandbox Model Design

The sandbox test 1 is used to find out if the LiDAR scanning method and the two spherical scanning targets fixed onto the target rod can measure the motion of soil body or the displacement difference between soil layers. In the sandbox test 1, the shear plane is between the top and bottom sandbox. The key intent of the sandbox test 1 is the bottom layer of soil that is motionless when the top soil moves to simulate the landslide.

To simulate the failure surface and soil layers, the special sandbox is built as Figure 5.2.

To complete the research objective, the sandbox was set up as is shown in Figure 5.1, which consists of two boxes with the bottom one fixed onto the testbed and the top one staying movable by means of the displacement control leadscrew. The specification of the sandbox test is described as below:

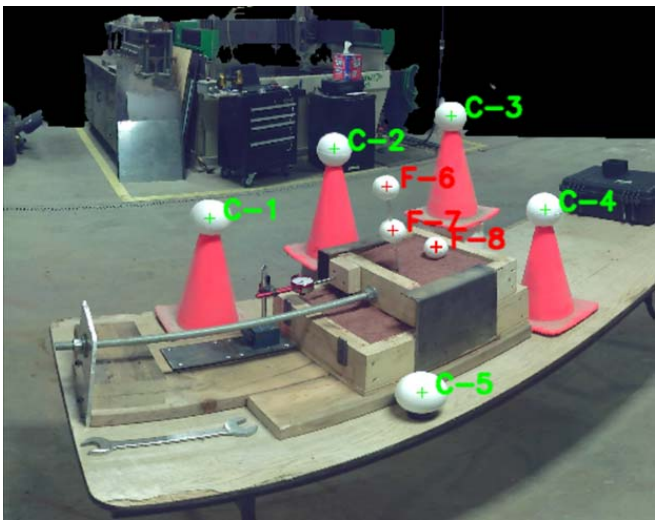

Figure 5.2 The scanning result of the sandbox model in Lidarsw. The scanning targets with green marks are the control targets, and the scanning targets with red mark are the floating targets. The target F6 and F7 are fixed onto the scanning target rod.

1. Specification of the Scanning Targets:

(1) Size of Scanning Target Spheres: The diameter is 6.35cm (2.5 inch) and 10.16cm (4 inch);

(2) Material of Target Spheres: Styrofoam;

(3) Types of Scanning Target used in the test: The control spherical 10.16cm (4 inch) targets are fixed (stationary) around the sandbox; the floating 6.35cm (2.5 inch) spherical targets are fixed onto an aluminum rod which is hinges to the bottom of sandbox and the diameter is 6.35cm (2.5 inch).

(4) Size of Target Rod: The length of rod is 45.72cm; the diameter of the target rod is 0.635cm.

2. Specification of the Sandbox:

(1) Materials of Sandbox: Sandbox frame is made of wooden boards that are 3.8cm thick; a steel plate acts as a track used to constrain the movement direction of top sandbox along the bottom sandbox.

(2) Size of Sandbox: The width of both top and bottom sandboxes is 37.6cm; the length of top sandbox is 30cm; the length of bottom sandbox is 50cm; the height of both top and bottom sandbox is 10cm without the plank thickness;

(3) Structure of Sandbox: The bottom box is fixed onto the table and unmovable; the top box is set up above the bottom box and can only move only in parallel with the long side of bottom box. The displacement of the top box is controlled by the leadscrew.

3. Materials of Target Rod and Soil:

(1) The metal rod is made of aluminum.

(2) The soil materials used for this test are: garnet sand and topsoil. The garnet sand and the topsoil are supplied by the Rock Mechanics and Explosives Research Center of Missouri University of Science and Technology.

4. Research Method:

(1) To test the ability of the LiDAR to measure the movement of the scanning targets, the test displaces of the top sandbox a distance of 5.08cm (2inch) in 10 equal increments, which means the displacement of each step is 0.508cm (0.2inch). A LiDAR scan is conducted between each step.

5.1.2. Test Procedure and Scan Result of Sandbox Test 1. The entire scan process of the sandbox test 1 is as follows:

(1) Fix the target rod onto the sandbox;

(2) Fill the garnet sand into the sandbox;

(3) Set up the control targets around the scanning area, and fix the floating targets F6 and F7 onto the aluminum rod and F8 on the surface of soil in the sandbox (Figure 5.2);

(4) Conduct a baseline LiDAR scan when the sandbox is in the original position;

(5) Pull the top sandbox 0.58cm (0.2 inch), and re-scan the sandbox model;

(6) Repeat process (5) 10 times until the displacement of the top box reaches 5.08cm (2 inch);

(7) Remove the garnet sand to the topsoil to fill in the sandbox and repeat process (3) to (6);

(8) Process the scanning data to obtain the displacement of the floating targets 1 and 2 and the rotation angle of target rod (Figure 5.1);

(9) Compare the results to find out if the LiDAR measured displacement match with the actual ones.

The scanning result of the sandbox test 1 are shown in Figure 5.3 to Figure 5.8:

The scanning target rod which is fixed to the bottom sandbox is rotated by the movement of the top sandbox when the bottom sandbox is motionless. The rotation of the rod and two spherical scanning targets on the rod extend the function of the LiDAR scanner to allow the measurement of the rotational angle (Figure 4.6, 5.1, 5.7 and 5.8).

5.1.3. Conclusion of the Sandbox Test 1. Uniting the scanning result of the sandbox test 1, some conclusions can be drawn via the figures as shown:

(1) The displacement of the scanning target F8 have similar displacement values in both of soil types with respect to the movement of the top sandbox. It means the target F8 can help the LiDAR scanner to extend its function to obtain the surface displacement of landslide no matter which kinds of soil it is (Figure 5.3-5.6).

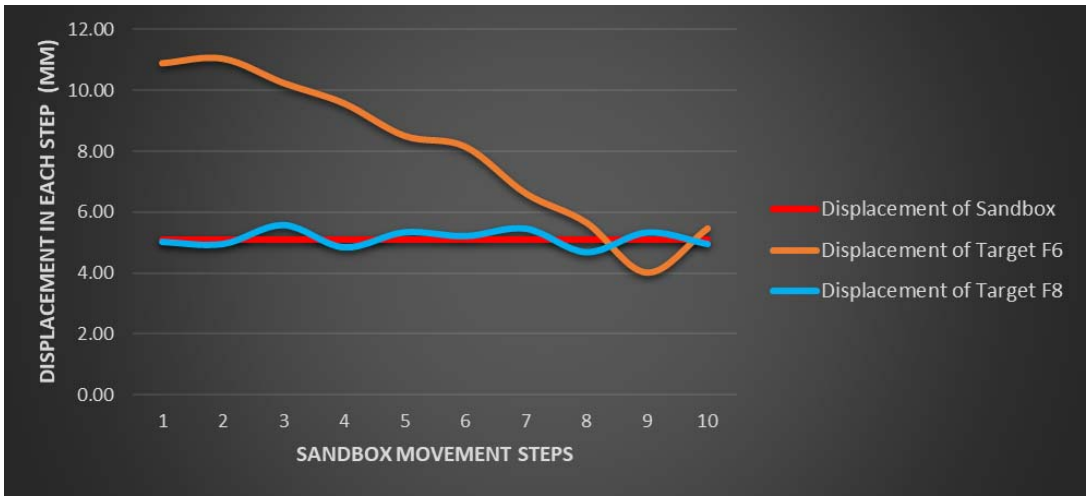

Figure 5.3 The true displacement of the floating target and the top sandbox (filled with garnet sand). The curves show the true displacement of the target F6 (the floating target 1 as shown in Figure 5.1) and F8 (the floating target 2 as shown in Figure 5.1) as well as the top sandbox. The true displacement includes the displacement in x, y and z direction (In Lidarsw, the x and y direction are the horizontal movement directions, and the z direction is the vertical movement direction). The horizontal displacement directions of the target F6, F8 and the top sandbox are similar while the vertical displacement directions of the target F6, F8 and the top sandbox are different. The change tendency of the true displacement of the target F8 and the top sandbox are close. The true displacement of the target F6 is larger than the target F8 and the top sandbox from step 1 to 7, and it is similar to the target F8 and the top sandbox from step 8 to 10. The difference of the scanning result of the displacement of the scanning target F6 and F8 is because of the scanning target position and the geometric characteristics of the target rod.

(2) The curves in Figure 5.3 and 5.5 show the LiDAR scanning results use the displacement of the scanning targets to reveal the surface and subsurface of soil movement tendency in different types of soil. The displacement of the target F6 has same decreasing tendency in both the garnet sand and the topsoil. This phenomenon reveals the fact that the displacement difference between soil layers can push the target rod to rotated in the same direction in both cases.

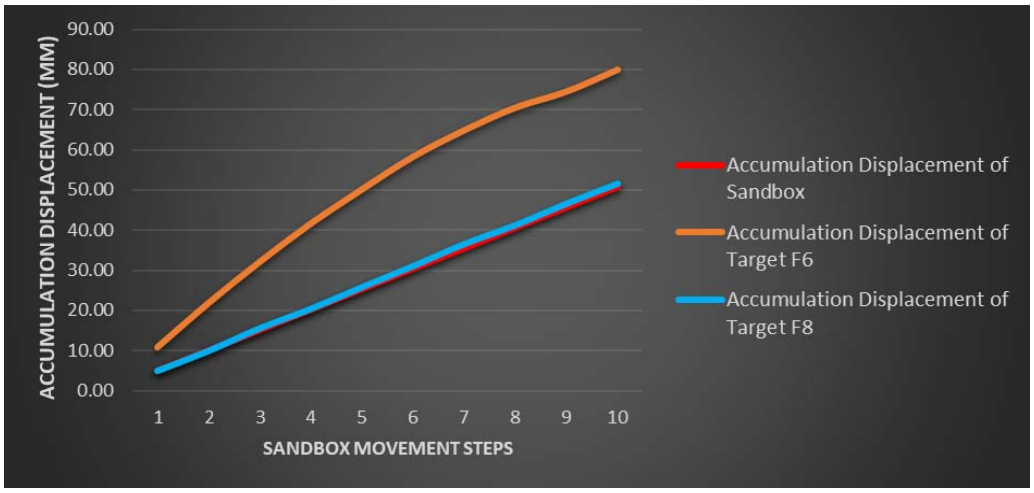

Figure 5.4 The accumulation displacement of the floating targets and the top sandbox (filled with garnet sand). The curves show the accumulation displacement of the target F6 and F8 and the top sandbox. The accumulation displacement of the target F8 have similar variation tendency with the top sandbox. The accumulation displacement of the target F6 is larger than the target F8 and the top sandbox in entire experiment procedure. The reason is that the angle of inclination and the rotational speed of the target rod keep increase in entire experiment procedure. The influences of the accumulation displacement of the target F6 may include but are not limited to the geometrical change of the target rod and the soil layers and the soil properties (e.g. particle size, bulk density, cohesion and water content).

(3) Miscellaneous displacement values of the same scanning target (F6) in different soil types reveal the fact that the rotation of the target rod by soil movement is different owing to the properties of soil (Figure 5.3-5.6). The properties of soil, such as

particle size, bulk density, water content, and cohesion, can change the mechanical behaviors of the soil that will leave the interaction between soil and the scanning target rod become different and eventually change the rotational process of the scanning target rod. Therefore, when researchers use this scanning method to monitor the subsurface movement of soil slope, the impact on the rotational process of the scanning target rod by the soil properties needs to be considered or measured;

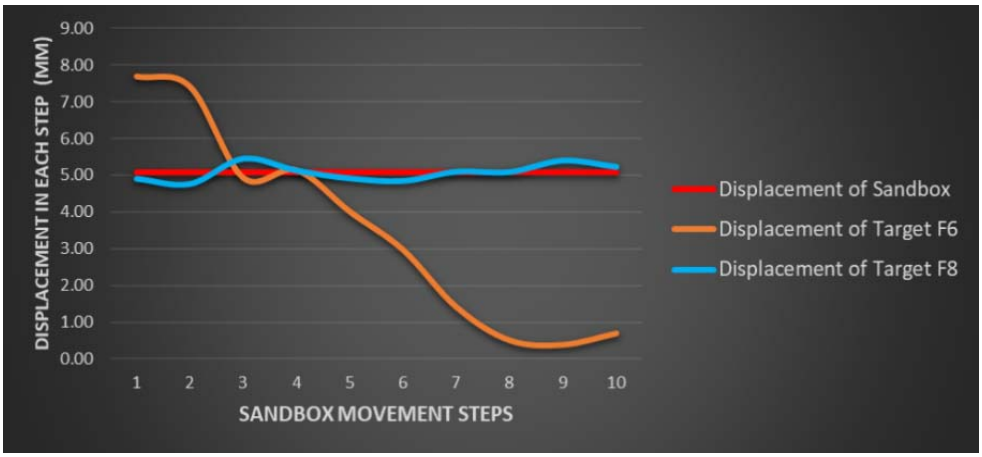

Figure 5.5 The displacement of the floating target and the top sandbox (filled with topsoil).The curves show the true displacement of the target F6 and F8 and the top sandbox. The true displacement includes the displacement in x, y and z direction (In Lidarsw, the x and y direction are the horizontal movement directions, and the z direction is the vertical movement direction). The horizontal displacement directions of the target F6, F8 and the top sandbox are similar, meanwhile, the vertical displacement directions of the target F6, F8 and the top sandbox are different. The change tendency of the true displacement of the target F8 and the top sandbox are close. The true displacement of the target F6 is larger than the target F8 and the top sandbox from step 1 to 2, and it is smaller than the target F8 and the top sandbox from step 3 to 10. The difference of the displacement of the scanning target F6 and F8 is because of the scanning target position and the geometric characteristics of the target rod.

(4) In the garnet sand (Figure 5.3), the true displacement of the target F6 is larger than that in the target F8 and the top sandbox from step 1 to 7 in that the position of the target F6 is on the top of the target rod. When the top sandbox movement makes the

target rod begin to tilt, the displacement of the target F6 is larger than that in the target F8 which is on the soil surface. The true displacement value of the target F6 is similar to the target F8 from step 8 to 10 because when the inclination angle of the target rod is large enough, and the bottom of the target rod is fixed, the rod cannot keep free rotation tendency and soil may move around or slide with the target rod instead push it rotation or movement. The influences of the displacement of the target F6 and the rotation of the target rod may include but are not limited to the geometrical change of the scanning target rod and the soil properties (e.g. particle size, bulk density, cohesion or water content).

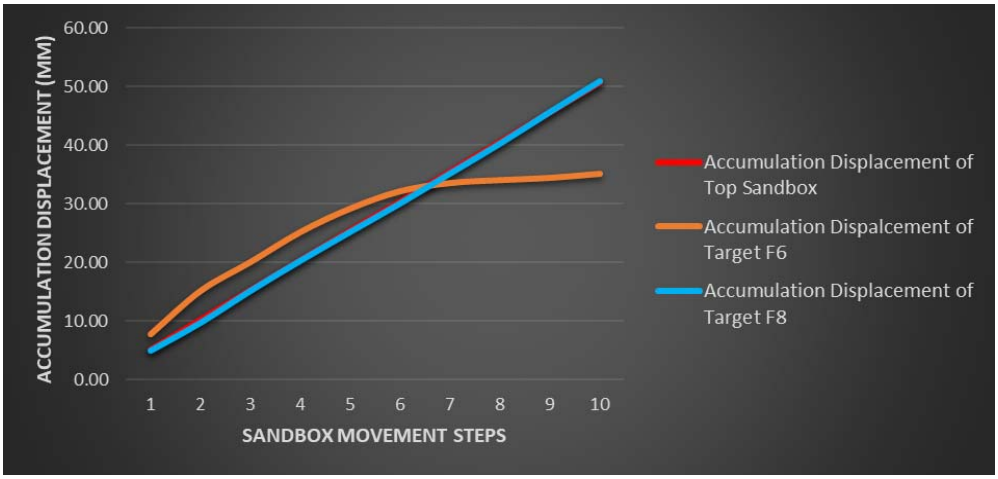

Figure 5.6 The accumulation displacement of the floating target and the top sandbox (filled with topsoil).The curves show the accumulation displacement of the target F6 and F8 and the top sandbox. The accumulation displacement of the target F8 have similar variation tendency with the top sandbox. The accumulation displacement of the target F6 is larger than the target F8 and the top sandbox from step 1 to 6, but smaller than the target F8 and the top sandbox from step 7 to 10. The reason of the accumulation displacement of the floating target F6 decreases from the step 6 is the increase rate of the inclination angle and the rotational speed of the target rod decrease. The reason for this phenomenon may include but is not limited to the geometrical change of the target rod and the soil layers and the soil properties (e.g. particle size, bulk density, cohesion and water content).

(5) The true displacement of the target F6 is larger than that in the target F8 and the top sandbox from step 1 to 2 (Figure 5.5), because the position of the target F6 is on the top of the target rod. When the top sandbox movement causes the target rod start to tilt, the displacement of the top position of the target rod is larger than that in the target F8 displacement. The true displacement of the target F6 is smaller than that of the target F8 and the top sandbox from step 3 to 10 which means the rotation speed of the target rod in the topsoil is smaller than that in the rod in the garnet sand (Figure 5.3) (the top sandbox has same displacement in both cases of the sandbox test 1). The reason for the difference includes but is not limited to the geometrical change of the scanning target rod and the soil properties (e.g. particle size, bulk density, cohesion or water content).

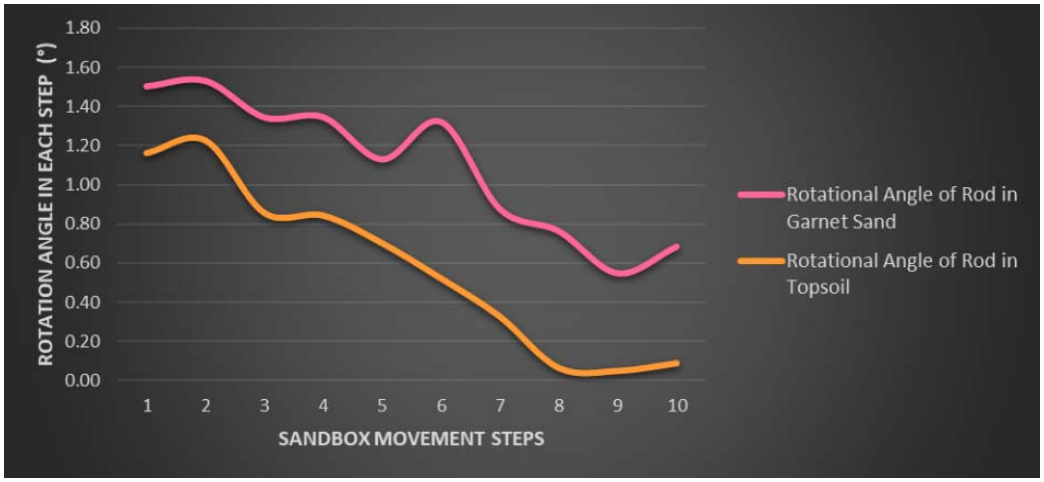

Figure 5.7 The rotational angle of the target rod in different types of soil. The rotational direction of the target rod in the garnet sand is same as in the topsoil. The rotational angle change of the target rod has similar increasing tendency in both garnet sand and topsoil. The rotational angle of the target rod in the garnet sand is larger than that in topsoil.

(6) The accumulation displacement of the scanning target F6 is larger than that in the displacement of the top sandbox and the target F8 in the garnet sand (Figures 5.4) and

remains on an upward trend during the entire displacement process. In the topsoil, the accumulated displacement of the target F6 is larger than that in the top sandbox at the beginning stage, but the growth rate has a sharp decrease after the displacement exceeds 3.56cm (1.4 inch) and then the accumulated displacement of the target F6 becomes smaller than that of the sandbox (Figures 5.6). The reason for this difference in the two case of the sandbox test 1 is the same as the conclusion (5): the only difference of two experiments of the sandbox test 1 is the soil type, and the fact that the test results of the displacement of the same scanning target are different reveals that the properties of soil can change the mechanical behaviors of soil and have some impacts on the gradient change of the scanning target rod.

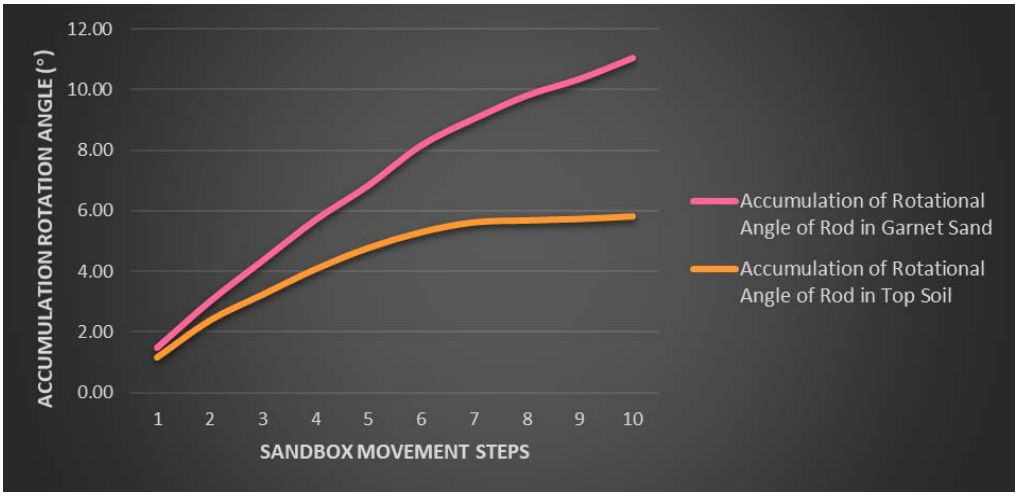

Figure 5.8 The accumulation rotational angle of the target rod in different types of soil. The accumulation rotational angle of the target rod in the garnet sand is larger than that in the topsoil.

(7) As the curves shown in Figure 5.7, the rotational angle has increasing tendency in both garnet sand and topsoil. The rates of rotational angle increase in both

garnet sand and topsoil have a decreasing trend. Geometric reasons result in this phenomenon. On the threshold of the experiment, the target rod is rotated with the soil movement. When the inclination angle of the target rod increases with the top sandbox movement, some soil particles will slide around or along the target rod instead of perpendicular with the target rod. Therefore, the rotational speed of the target rod is decreasing with the angle of inclination increasing.

(8) The rotational angle and the accumulation rotational angle of the target rod in the garnet sand are larger than in the topsoil (Figure 5.7 and 5.8). The reason is same as the displacement value of the target F6 is because different types of soil has different mechanical behavior. As a result, the interaction between soil and the target rod is different.

The results of the sandbox test 1 demonstrates that the type 1 targets (the scanning target F8) can be used for the surface of soil down-slope movement measurements, and the scanning target rod and twin spherical targets (the scanning target F6 and F7 and the aluminum rod used in the sandbox test 1) can be used for the soil downhill movement measurements. Both of two scanning targets can extend the function of the LiDAR scanning technology. The surface target (F8) can extend the function of LiDAR scanning technology to measure the surface soil movement. The target rod and the two spherical scanning targets on the rod can be used to measure the displacement differences of different soil layers.

This new measurement method is influenced by two factors: the underground geometric characteristics, such as the position of the target rod and the shear surface between soil layers; the properties of soil, such as the water content, the soil particles size,

the bulk density and the soil type. The underground geometric characteristics have impacts on the displacement and rotation of the target rod. Different properties of soil are of different mechanical behaviors which can influence the LiDAR scanning measurement result by the change of interaction between the soil and the target rod.

5.2. COMPUTER SIMULATION FOR THE SANDBOX TEST 1

From the standpoint of engineering, the interaction between the metal rod of the floating target 1 and soil is necessary to understand for practical application, especially if the shear stress or normal stress produced with soil movement can make the rod of the floating target 1 bend or slip to affect the LiDAR scanning results. However, there are several factors (e.g. the soil particle size, the water content, the bulk density and cohesion) affecting the accuracy of the artificial calculation result of the interaction between the soil and the scanning target rod. Therefore, the author of the research attempts to use computer simulation methods as an analysis tool to explain the interaction between the soil and the target rod in the sandbox test 1.

To study the interaction between the soil and the aluminum rod, two computer simulation software, FLAC3D and PFC3D are used in this research to simulate the sandbox test 1. The main reason to choose these two software was that FLAC3D and PFC3D use different simulation methods: FLAC3D uses Finite Difference Method (FDM) to simulate the model, and PFC3D uses the Discrete Element Method (DEM). FDM is mostly used to simulate the large scale and uniform materials model from macro-perspective, but DEM is mostly used to simulate the model by material particles from micro-perspective. Therefore, simulation results from these two different simulation

methods in this research will be compared so as to analyze the interaction between soil and rod.

FDM is a method for solving partial differential (or ordinary differential) equations and systems of equations to determine the numerical solution of the problem, referred to as the difference method. Its basic idea is to firstly divide the problem's definition domain into grids, and then change the derivative in the definite solution problem into difference quotient according to the appropriate numerical differential formula on the grid points. Therefore, the original problem is changed into a difference scheme and then the numerical solution will be put forward.

DEM was first proposed in 1971. When Cundall proposed this method (Cundall, P.A., 1971), it adopted the distinct element method to distinguish it from the finite element method in continuous media mechanics. Discrete element method was later used to replace distinct element method to reflect the fact that the system was discrete. Each element in the discrete element method set is independent, and each element has corresponding properties such as size, mass, moment of inertia and contact parameters. It is also in conformity with Newton's Second Law, forcing a displacement theorem on the basis of each unit firstly determining the contact unit in accordance with the amount of overlap among units calculated by using a force displacement theorem, and the contact force between the unit of force and torque is obtained after unit were determined by Newton's Second Law of Motion and the Cycle Calculation until all the particles in the system is evaluated.

Both FDM and DEM need define the properties of the materials in simulation model. The main differences between these two methods are: FDM delimits the boundary

conditions of the model frame first and then defines the properties of the materials inside the certain boundaries; DEM needs to define the properties of each single material particle subsequent to delimiting the boundary conditions of the model.

In this research, the parameters of soil coming from previous research results (American Society for Testing and Materials, 1985; Naval Facilities Engineering Command, 1986; Prat, M. et al., 1995; Swiss Standard, S.N., 1999; Minnesota Department of Transportation, 2007; Das, B.M., 2008; Obrzud, R. and Truty, A., 2012; Yu Lipeng, 2014;) (Table 5.1):

Table 5.1 The Soil Properties for FDM and DEM Simulation

	Young's Modulus	Poisson's Ratio	Cohesion	Friction Angle	Density	Soil Porosity
Garnet Sand (SP)	20 MPa	0.25	0 Kpa	36°	4.1 g/cm^3	0.3
Topsoil (ML-CL)	4.58 MPa	0.33	4 Kpa	32°	1.8 g/cm^3	0.35

To simulate the sandbox model to study the interaction between soil and rod, the properties of aluminum rod is also needed. (Handbook, ASM Metals, 1985; Handbook, Metals, 1990; Structural Alloys Handbook, 1996; Aluminum Association, Inc, 2001) (Table 5.2):

Table 5.2 The Aluminum Rod Properties for FEM and DEM Simulation

Mechanical and Physical Properties of Aluminum 6061-T6			
Property	Metric	English	Comments
Density	2.7 g/cm^3	0.097 lb/in	AA; Typical
Hardness, Brinell	95	95	AA; Typical; 500 g load; 10 mm ball

Table 5.2 The Aluminum Rod Properties for FEM and DEM Simulation (Cont.)

Mechanical and Physical Properties of Aluminum 6061-T6			
Property	Metric	English	Comments
Hardness, Knoop	120	120	Converted from Brinell Hardness Value
Hardness, Rockwell A	40	40	Converted from Brinell Hardness Value
Hardness, Rockwell B	60	60	Converted from Brinell Hardness Value
Hardness, Vickers	107	107	Converted from Brinell Hardness Value
Ultimate Tensile Strength	310 MPa	45000 psi	AA; Typical
Tensile Yield Strength	276 MPa	40000 psi	AA; Typical
Elongation at Break	12 %	12 %	AA; Typical; 1/16 in. (1.6 mm) Thickness
Elongation at Break	17 %	17 %	AA; Typical; 1/2 in. (12.7 mm) Diameter
Modulus of Elasticity	68.9 GPa	10000 ksi	AA; Typical; Average of tension and compression.
Notched Tensile Strength	324 MPa	47000 psi	2.5 cm width x 0.16 cm thick side-notched specimen, Kt = 17
Ultimate Bearing Strength	607 MPa	88000 psi	Edge distance/pin diameter = 2.0
Bearing Yield Strength	386 MPa	56000 psi	Edge distance/pin diameter = 2.0
Poisson's Ratio	0.33	0.33	Estimated from trends in similar Al alloys
Fatigue Strength	96.5 MPa	14000 psi	AA; 500,000,000 cycles completely reversed stress
Fracture Toughness	29 MPa-m	26.4 ksi-in	KIC; TL orientation.
Machinability	50 %	50 %	0-100 Scale of Aluminum Alloys
Shear Modulus	26 GPa	3770 ksi	Estimated from similar Al alloys
Shear Strength	207 MPa	30000 psi	AA; Typical

5.2.1. FLAC3D Simulation. There are three main steps in the simulation process of FLAC3D: (1) Finite difference grid; (2) Constitutive and material properties, which include define constitutive model, boundary of model, cell type, cell property, cell

geometric attribute, cell connectivity, primary function, boundary conditions and loading; (3) Set up the boundary and initial conditions.

The parameters of the sandbox test 1 have been introduced the section 5.1.1, and the computer simulation follows all details of the test to simulate and analyze the interaction between soil and rod. The simulation model assumes the soil used in the test is uniform one, and uses the Mohr-Coulomb model to be the material constitutive model, and the pile unit to simulate the aluminum rod which is fixed to bottom of the simulation sandbox, too. The contact model of soil and aluminum rod uses the elastic model. The coding program follows sandbox test 1 which sets the displacement of the top sandbox to be 5.08cm (2 inch) and divides the displacement into 10 intervals, which means the displacement of each interval is 0.508cm (0.2 inch) (Figure 5.9).

The FLAC3D simulation uses 100,000 steps to meet the 5.08cm (2 inch) displacement and the final simulation results show (1) the pile displacement, (2) the shear stress on the pile; (3) the normal stress on the pile, and (4) the pile yield state. The FLAC3D simulation consists of two parts: one uses the properties of the garnet sand to define the material in the sandbox, and the other uses the properties of the topsoil.

5.2.1.1. FLAC3D simulation result for the sandbox test 1 with garnet sand. The simulation results of the sandbox test 1 with garnet sand by the FDM are shown in this section. There have three kinds of simulation results: (1) the displacement simulation result; (2) the normal and shear stress of the scanning target rod. (3) the shear stress distribution on the slip surface between the top and bottom sandbox. These simulation result use different color scales.

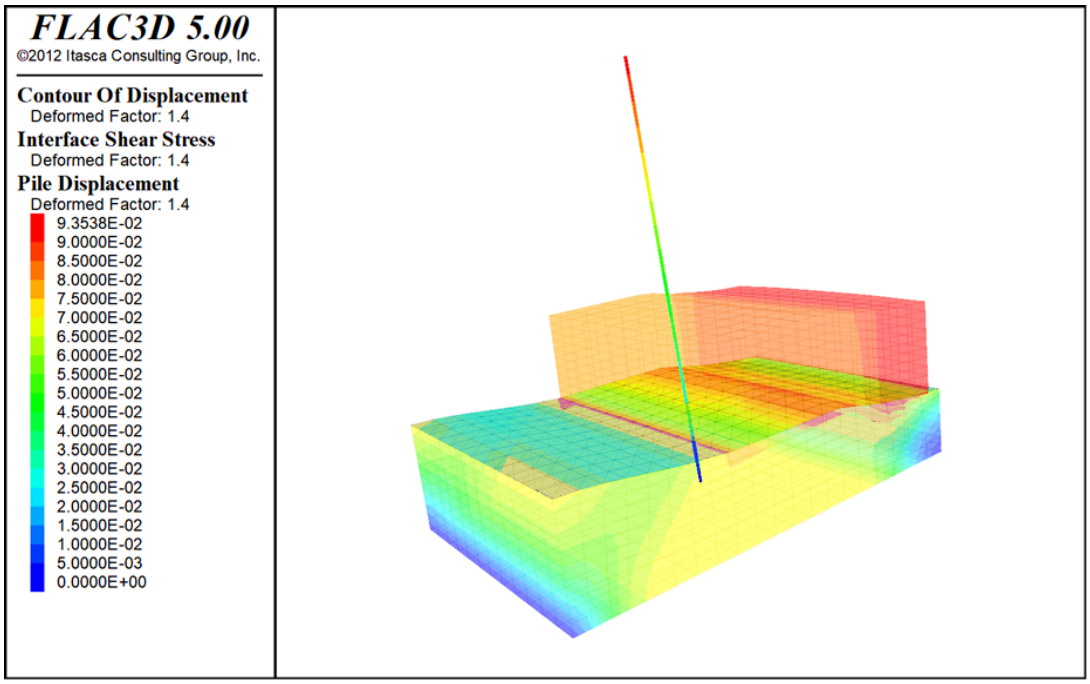

Figure 5.9 The FLAC3D simulation result of the sandbox test 1 (filled with garnet sand).The top sandbox (the top colorful grid) is of 50.8 mm (2 inch) displacement; the bottom sandbox (the bottom colorful grid) is unmovable. This simulation result has three color scales: (1) the color scale used to describe the pile (the target rod) displacement is shown in the left side of the figure. The maximum displacement value is 93.54 mm at the top cell of the pile and the minimum value is 0 mm at the bottom cell; (2) the color scale used to describe the soil displacement is hidden in the left of the figure. The maximum displacement value is 80.06 mm and the minimum value is 0 mm; (3) the color scale used to describe the distribution of the shear stress on the shear surface between the top and bottom soil layer is hidden in the left of the figure. The maximum shear stress on the shear surface is 2995.3N, and the minimum value is 0. All color scales are in red to show the maximum value and are in blue for the minimum value.

As Figure 5.9 shows, the bottom of the rod is fixed to the bottom of the sandbox and displacement at that point is 0 mm. The maximum displacement of the pile is in the top of the rod, and the displacement is 9.3538e-02m (93.54mm). The back part of the top sandbox has larger displacement than that in the front part. The maximum shear stress on slip surface is in the middle part of the shear surface between the top and bottom sandbox. The maximum shear stress value is 2995.3N.

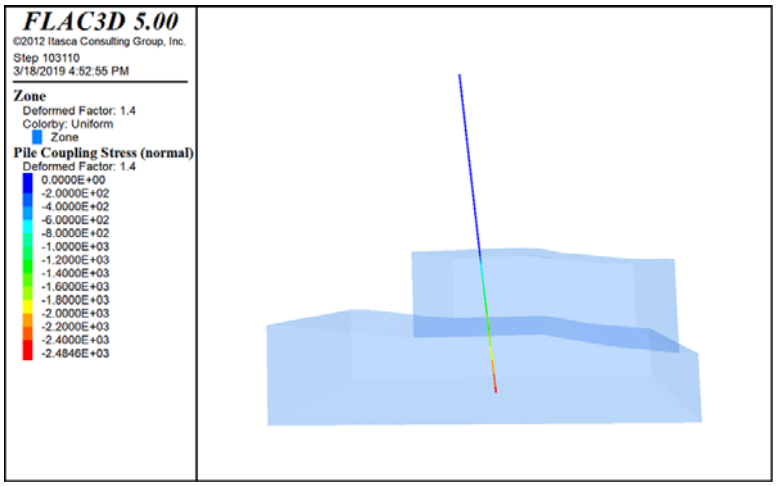

Figure 5.10 The normal stress simulation results by FLAC3D for the sandbox test 1 (filled with garnet sand).The simulation objective is the distribution of the normal stress on the aluminum rod in the garnet sand. The "Zone" presents the sandbox filled with the garnet sand and is shown as blue grid in the figure; the "Pile" is the target rod in the sandbox test 1. The color scale in the left side of the figure is used to describe the normal stress, and the unit is Newton. The maximum value of the normal stress is 2484.6N, and the minimum one is 0N.

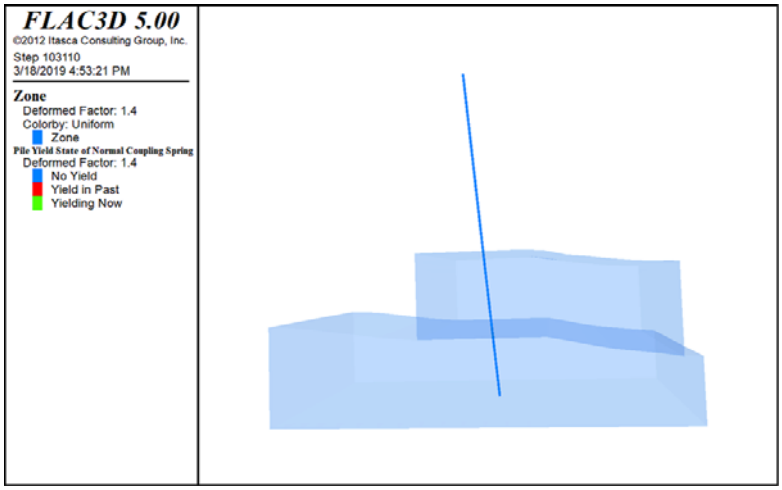

Figure 5.11 The yield state by normal stress simulation result by FLAC3D for the sandbox test 1 (filled with garnet sand).The simulation objective is to simulate if the normal stress can make the target rod yield. The "Zone" presents the sandbox filled with the garnet sand and is shown as blue grid in the figure; the "Pile" is the target rod in the sandbox test 1. The color scale in the left side of the figure is used to describe the yield state of the target rod. The red means the rod was in yield state by the normal stress at some time in the past; the green means the rod is in yield state at present; the blue means the rod is in no yield state in entire simulation process. The simulation result shows the pile has not been in yield state by the normal stress in the entire simulation process.

The normal stress and the shear stress simulation results are shown in Figure 5.10 and Figure 5.12, and the stress distribution on the aluminum rod is described by the color scale. The normal stress distribution indicates when the top sandbox moves, the maximum normal stress generated in the bottom position of the target rod which is fixed on the bottom sandbox. The maximum value of the normal stress is 2484.6N. The shear stress distribution indicates the maximum shear stress is generated in the middle position of the target rod which is in the top sandbox. The maximum value of the shear is 3.42N (Figure 5.14).

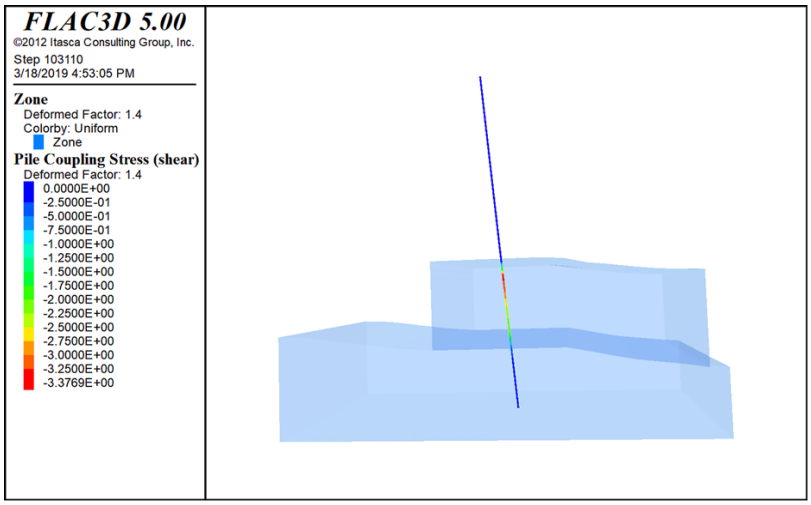

Figure 5.12 The shear stress simulation results by FLAC3D for the sandbox test 1 (filled with garnet sand).The simulation objective is the distribution of the shear stress on the aluminum rod in the garnet sand. The “Zone” is the sandbox filled with the garnet sand and is shown as blue grid in the figure; the “Pile” is the target rod in the sandbox test 1. The color scale in the left side of the figure is used to describe the shear stress, and the unit is Newton. The maximum value of the shear stress on the target rod is 3.38N and the minimum one is 0N.

Through the simulation for the normal stress distribution on the rod, Figure 5.11 demonstrates that the rod has not reached the yield state of normal coupling stress in the

entire simulation process and the maximum stress value is 2484.6N (Figure 5.14). Through the simulation for the shear stress distribution on the rod, Figure 5.13 demonstrates that the rod has not reached yield state of shear coupling stress in the entire simulation process and the maximum shear stress absolute value is 3.42N (Figure 5.14).

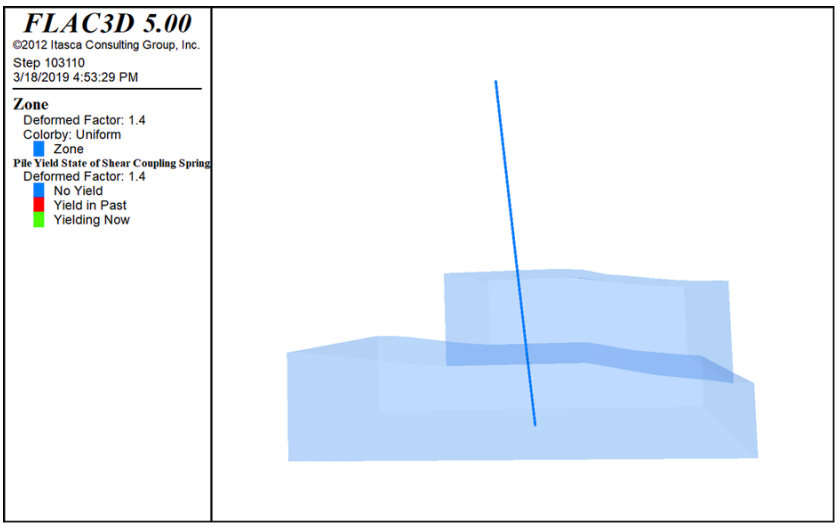

Figure 5.13 The yield state by shear stress simulation result by FLAC3D for the sandbox test 1 (fill with garnet sand).The simulation objective is to simulate if the shear stress could let the target rod yield. The "Zone" is the sandbox filled with the garnet sand and are shown as blue grid in the figure; the "Pile" is the target rod in the sandbox test 1. The color scale in the left side of the figure is used to describe the yield state of the target rod. The red means the rod was in yield state by the shear stress at some time in the past; the green means the rod is in yield state currently; the blue means the rod is in no yield in entire simulation process. The simulation result shows the pile has not been in yield state by shear stress in the entire simulation process.

5.2.1.2. FLAC3D simulation result for the sandbox test 1 with topsoil. As Figure 5.15 shows, the bottom of the rod is fixed to the bottom of the sandbox and displacement at that point is 0 mm. The maximum displacement of the pile is in the top of the rod, and the displacement is 5.8798e-02m (58.80 mm). The back part of the top sandbox has larger displacement than that in the front part.

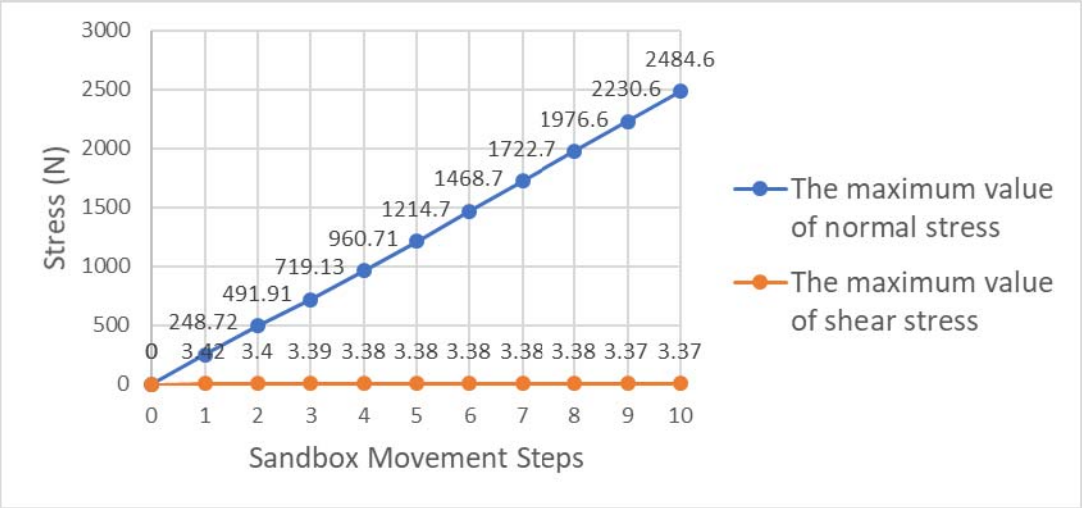

Figure 5.14 The absolute value of the maximum normal and shear stress on the pile in FLAC3D simulation result and the material is the garnet sand.

The normal stress and the shear stress simulation results are shown in Figure 5.16 and Figure 5.18, and the stress distribution on the aluminum rod is described by the color scale. The normal stress distribution indicates when the top sandbox moves, the maximum normal stress generated in the bottom position of the target rod which is fixed on the bottom sandbox. The maximum value of the normal stress is 2260.2N. The shear stress distribution indicates the maximum shear stress is generated in the middle position of the target rod which is in the top sandbox. The maximum value of the shear is 2.61N (Figure 5.20).

Through the simulation results for the normal stress distribution on the rod Figure 5.16 and 5.17 demonstrate that the rod has not reached the yield state of normal coupling stress in the entire simulation process (Figure 5.20). The simulation results for the shear stress distribution on the rod Figure 5.18 and 5.19 demonstrate that the rod has not reached yield state of shear coupling stress in the entire simulation process (Figure 5.20).

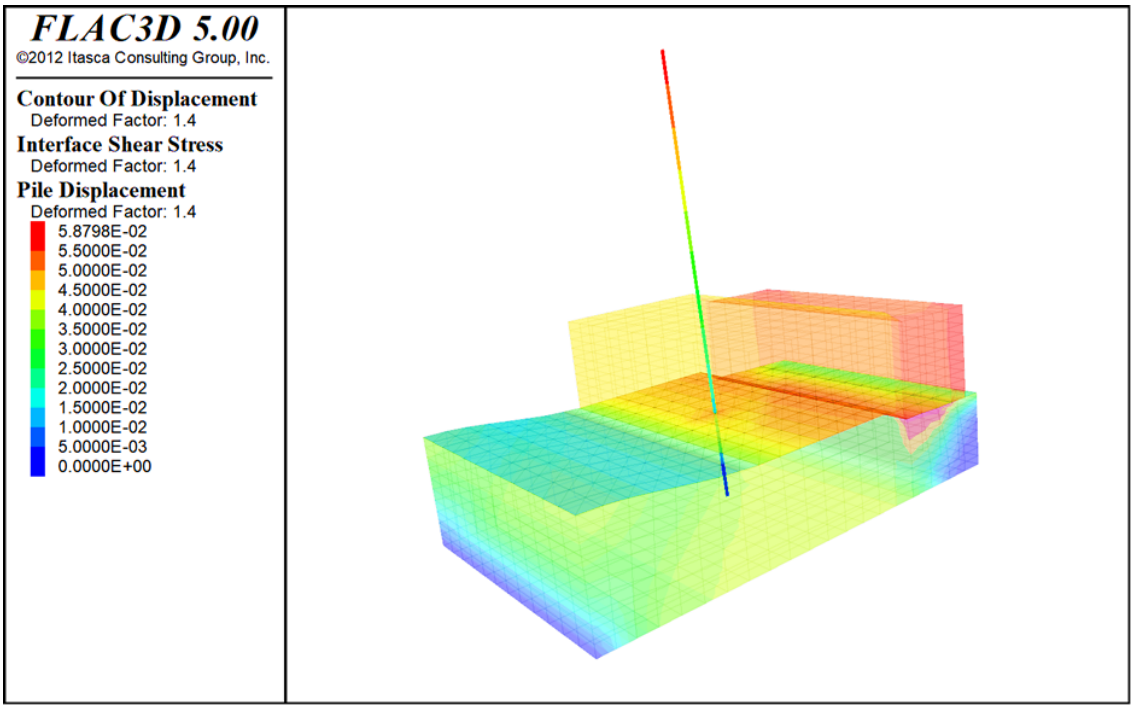

Figure 5.15 The FLAC3D simulation result of the sandbox test 1 (filled with topsoil).The top sandbox (the top colorful grid) has 50.8 mm (2 inch) displacement; the bottom sandbox (the bottom colorful grid) is unmovable. This simulation result has three color scales: (1) the color scale used to describe the pile (the target rod) displacement is shown in the left side of the figure, and the maximum displacement value is 58.80 mm and the minimum one is 0 mm; (2) the color scale used to describe the soil displacement is hidden in the left of the figure. The maximum displacement value is 66.89 mm and the minimum one is 0 mm; (3) the color scale used to describe the distribution of the shear stress on the shear surface between the top and bottom soil layer which is hidden in the left of the figure. The maximum shear stress on the shear surface is 1888.3N, and the minimum one is 0N. All color scales use red to show the maximum value and blue for the minimum value.

5.2.1.3. Discussion for FLAC3D simulation results for the sandbox test 1. The FLAC3D simulation for the sandbox test 1 can help the new LiDAR measurement method to illustrate the relative displacement of the sandbox and the aluminum rod, the maximum value of the normal and shear stress, the variation tendency of the stress value and the stress distribution on the pile, proving there is no yield state in entire experiment process to influence the LiDAR scanning results in the sandbox test 1.

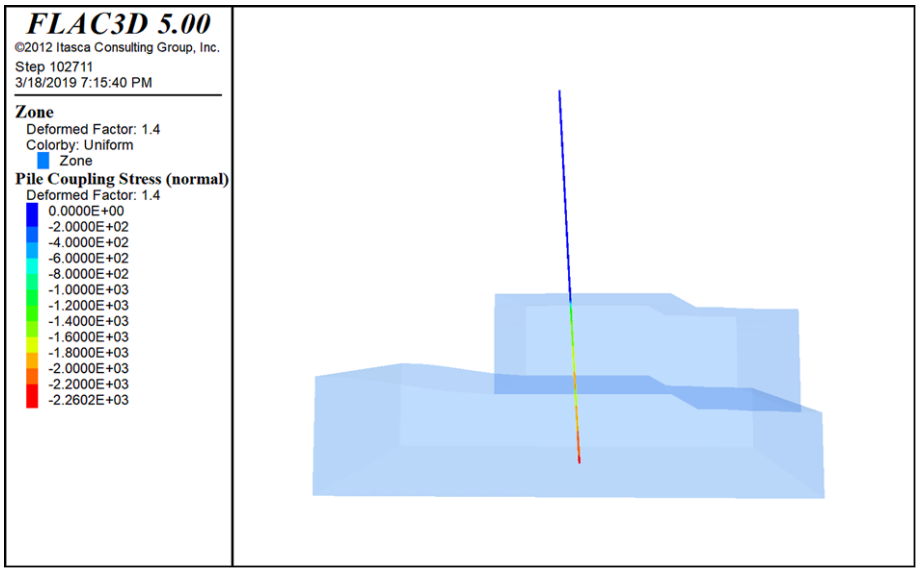

Figure 5.16 The normal stress simulation results by FLAC3D for the sandbox test 1 (filled with topsoil).The simulation objective is the distribution of the normal stress on the aluminum rod in the topsoil. The "Zone" is the sandbox filled with the topsoil and are shown as blue grid in the figure; the "Pile" is the target rod in the sandbox test 1. The color scale in the left side of the figure is used to describe the normal stress, and the unit is Newton. The maximum value of the normal stress is 2260.2 N, and the minimum one is 0 N.

5.2.2. PFC3D Simulation. PFC3D simulation is different from FLAC3D owing to different simulation principles. There are five main steps in the simulation process of DEM: (1) build the model structures and frames in software; (2) generate the simulation particles and then define the properties for each particle; (3) determine contact model, which means definition contact relationship for the different particles or structures; (4) contact detection, which means calculate the distance between each particle and if there has any contact relationship existence, then calculate the interaction force before the simulation process start; (5) set up the simulation process and run the program code.

To compare with the simulation result from FDM and DEM, the simulation models used in two software have same size and experiment processes.

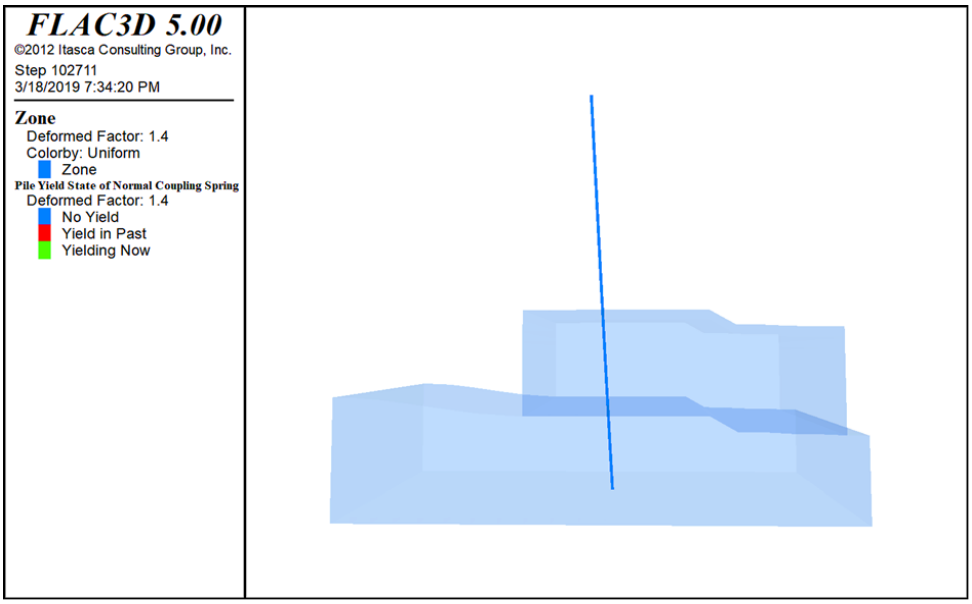

Figure 5.17 The yield state by normal stress simulation result by FLAC3D for the sandbox test 1 (filled with topsoil).The simulation objective is to simulate if the normal stress could let the target rod yield. The "Zone" presents the sandbox filled with the topsoil and is shown as blue grid in the figure; the "Pile" is the target rod in the sandbox test 1. The color scale in the left side of the figure is used to describe the yield state of the target rod. The red means the rod was in yield state by the normal stress at some time in the past; the green means the rod is in yield state at present; the blue means the rod has no yield in entire simulation process. The simulation result shows the pile has not been in yield state by the normal stress in the entire simulation process.

To simulate the sandbox test 1, the DEM model follows all structural details of the sandbox test 1 in Section 5.1.1. In the PFC3D program, the soil and the aluminum rod both need to use particles to simulate, but they are two kinds of particle groups in the simulation program; a soil group and a pile one. The soil group is used to simulate the soil in the sandbox, and the other is used to simulate the aluminum rod in the soil. The aluminum rod is simulated to be a single row of equal sized particles. The simulation program defines the properties of soil particles and pile particles using the parameters from Table 5.1 and Table 5.2. The contact model of the soil group is a liner contact constitutive model and the contact model of the pile group is the parallel binding

constitutive model. Some special properties need describing in the code previous to the start of simulation program:

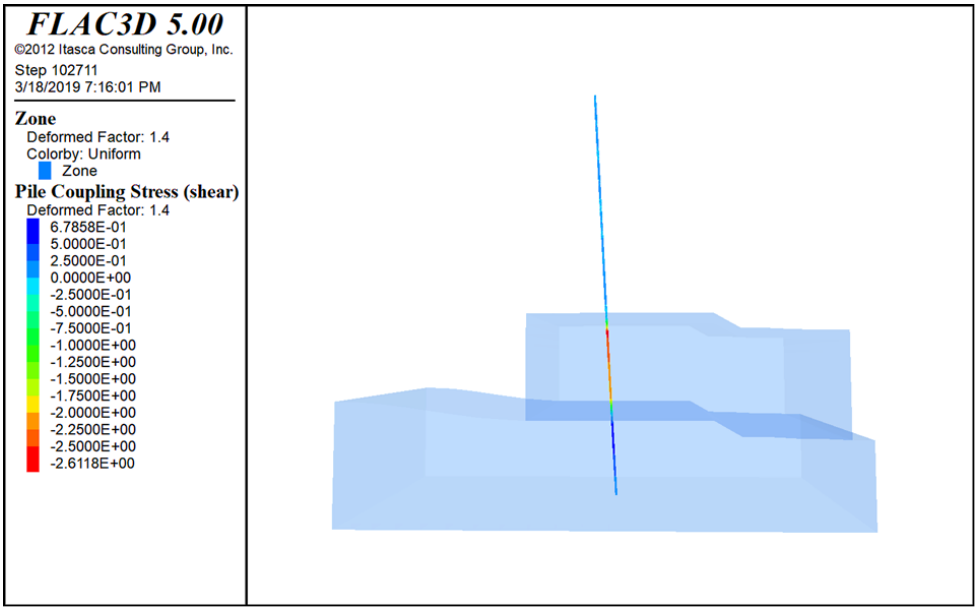

Figure 5.18 The shear stress simulation results by FLAC3D for the sandbox test 1 (filled with topsoil).The simulation objective is the distribution of the shear stress on the aluminum rod in the topsoil. The "Zone" presents the sandbox filled with the topsoil and is shown as blue grid in the figure; the "Pile" is the target rod in the sandbox test 1. The color scale in the left side of the figure is used to describe the shear stress, and the unit is Newton. The maximum value of the shear stress on the target rod is 2.61N and the minimum one is 0N.

(1) Set up the radius of the particle size of the garnet sand (3.5e-03m to 5.0e-03m) and the topsoil (2.0e-03m to 4.5e-03m).

(2) Fix the bottom particle of the aluminum rod to the bottom of the sandbox, but allow this particle freedom to rotate.

(3) Delete the top boundary of the sandbox to allow the top particles to move freely.

(4) Set up the displacement of the top sandbox to 5.08mm (2 inch) and the loading speed of the top sandbox is 0.1m/s.

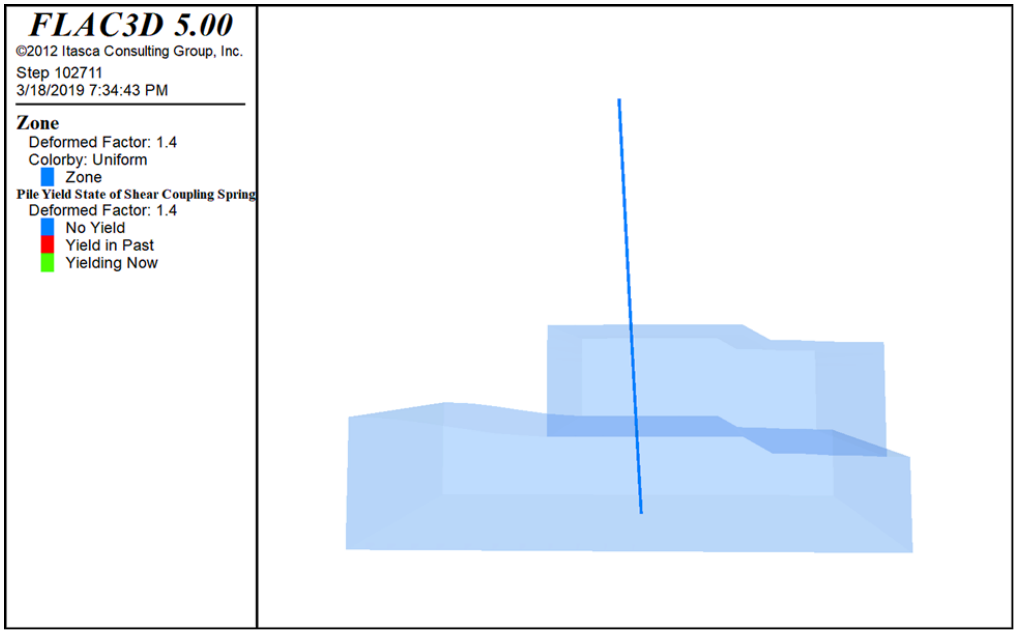

Figure 5.19 The yield state by shear stress simulation result by FLAC3D for the sandbox test 1 (filled with topsoil).The simulation objective is to simulate if the shear stress can make the target rod yield. The "Zone" presents the sandbox filled with the topsoil and is shown as blue grid in the figure; the "Pile" is the target rod in the sandbox test 1. The color scale in the left side of the figure is used to describe the yield state of the target rod. The red means the rod was in yield state by the shear stress at some time in the past; the green means the rod has yield state currently; the blue means the rod is in no yield state in entire simulation process. The simulation result shows the pile has not been in yield state by shear stress in the entire simulation process.

In this research, the simulation process of PFC3D takes over fifty hours to obtain the simulation results. The duration time of simulation depends on several factors that are of impacts: the number of particles, the loading stress or speed, the parameters of particles.

For the sandbox test 1 simulation, the number of particles is determined by the porosity of soil and the radius of particles. In practice, the computing power limits the

number of soil particles, and if the number is too large for the computer calculation ability, for example 500,000 particles, the software crashes. If the simulation uses the real particle size of clay (0.002mm), silt (0.002-0.05mm), or sand (0.05-2.00mm), the number of particles will be 500,000 to 1500,000 and the computer used for this research can not bear such a large computational load. Therefore, the radius of particles in the simulation program needed to consider both the real material size and the computer calculation ability. This is the one important reason why PFC3D sometimes can often not obtain sufficiently accurate simulation results. If the computing power of the computer used in further research can be enhanced, the simulation result will be more realistic.

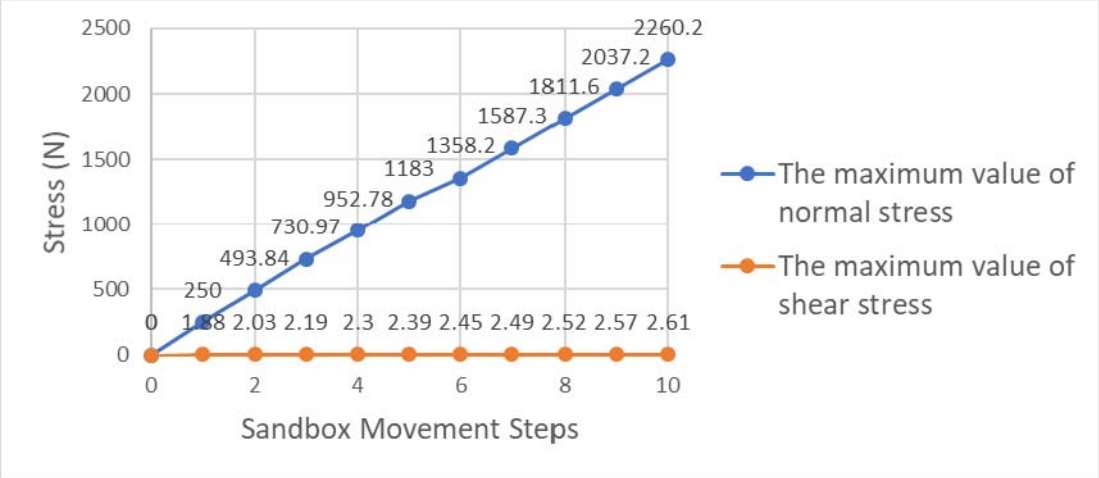

Figure 5.20 The absolute value of the maximum normal and shear stress on the pile in FLAC3D simulation result and the material is the topsoil.

As the number of particles, the loading stress or speed on the sandbox will influence the duration time of simulation. If the loading stress or speed is small enough, the simulation result will be more realistic but the simulation process will use twice as many days.

5.2.2.1. PFC3D simulation result for the sandbox test 1 with garnet sand. The PFC3D simulation results are shown in section 5.2.2.1 and 5.2.2.2.

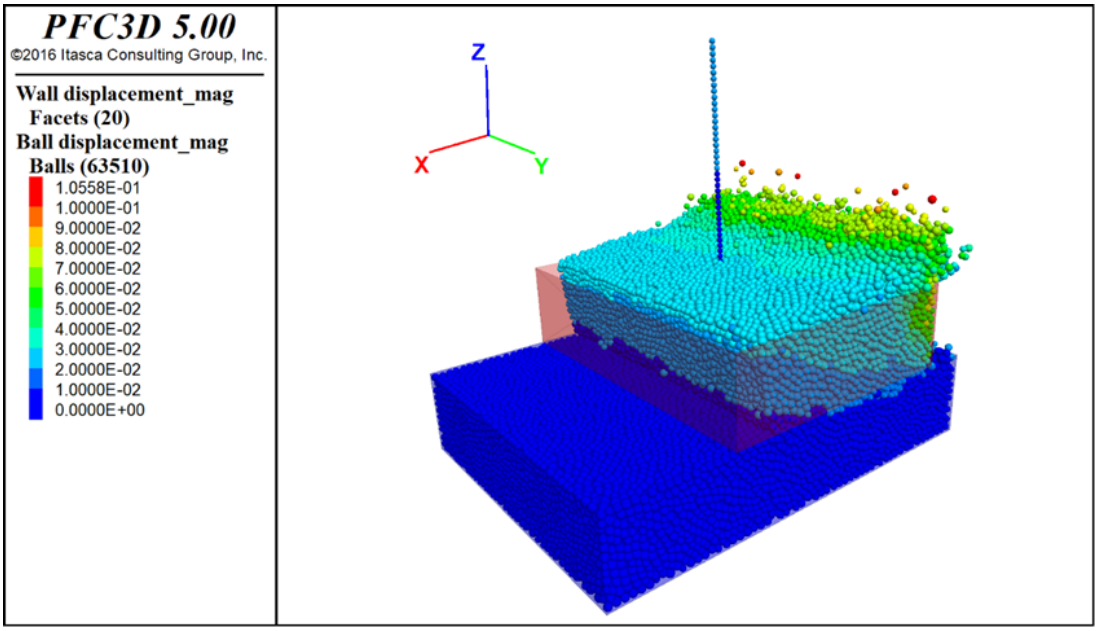

Figure 5.21 The PFC3D simulation result of the sandbox test 1 (soil material is the garnet sand).The simulation objective is the displacement of the garnet sand particles and the scanning target rod. The total displacement of the wall frame is 5.08cm (2 inch). The color scale in the left side is used to display the displacement of all particle groups, and the unit is meter.

The Figure 5.21 shows the displacement of the garnet sand particles and the target rod particles. The maximum displacement of the soil particles is in the back of the top sandbox and the displacement is 105.58mm. The particles of soil in the back of the top sandbox have been pushed up with movement of the wall structure because of the loading speed of the sandbox in the simulation program. If the program decreases the loading speed of the top box, the particles will stay in the box, but the simulation duration time would be too long. The Figure 5.22 shows the displacement of the pile particle

group and the pile is in no obvious yield or bending deformation. The maximum displacement of the pile particle group (rod) at the top particle and the displacement is 13.81mm.

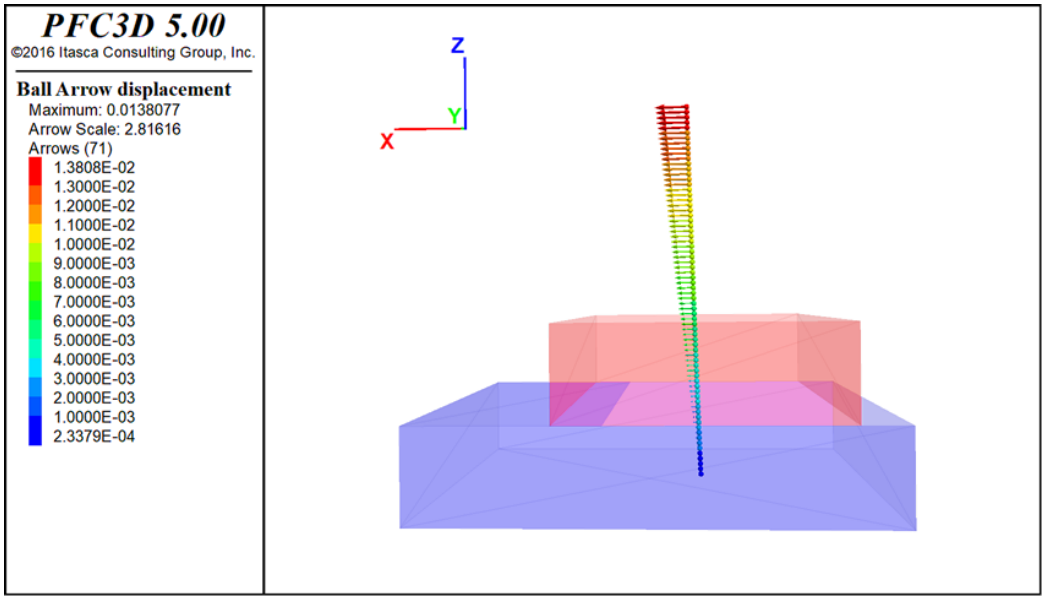

Figure 5.22 The PFC3D simulation result for the particle displacement of the pile group in the garnet sand. The red gird is the top sandbox and its displacement is 5.08cm (2 inch), and the blue gird is the bottom sandbox without any displacement. The color scale in the left side is used to display the displacement of each pile (rod) particle, and the unit is meter.

The DEM simulation result for the force analysis can only analyze the contact force for each pile particle (Figure 5.23). The contact force comes from the impact between the soil particles and the pile particles. The maximum contact force for the pile is at the bottom particle which is fixed onto the sandbox and the contact force of the particle is 15.539N. The contact force direction of most of pile particles is same as the rotational direction, which reveals the particles interaction between the soil and the target rod is the reason for the rod rotation.

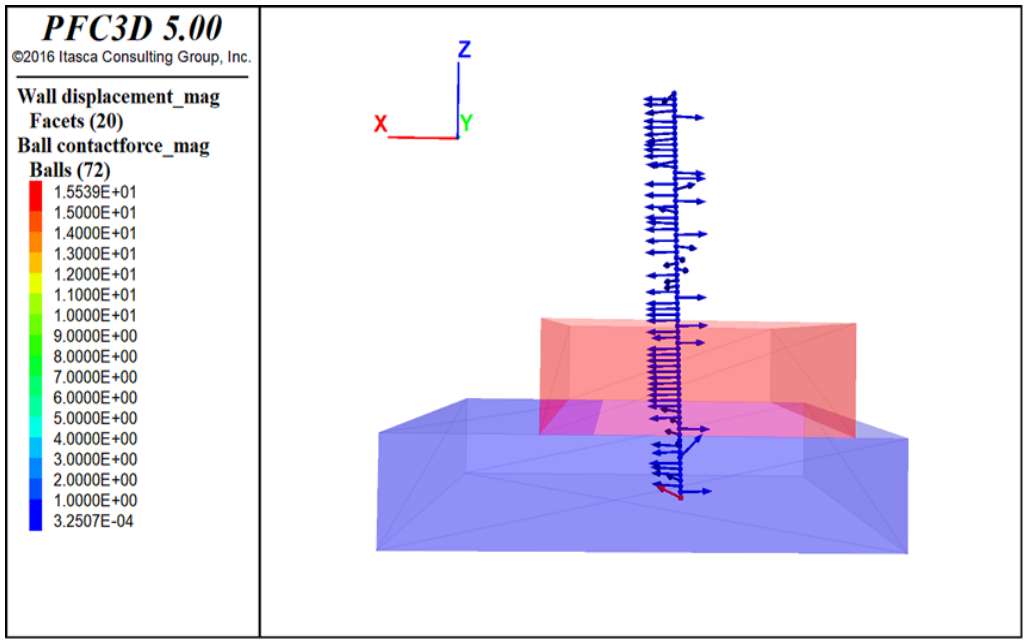

Figure 5.23 The PFC3D simulation result for the contact forces of the pile group with the garnet sand. The red cuboid is the top sandbox in the experiment and its displacement is 5.08cm (2 inch), and the blue cuboid is the bottom sandbox without any displacement. The color scale in the left side is used to display the contact force of each pile particle, and the unit is Newton.

5.2.2.2. PFC3D simulation result for the sandbox test 1 with topsoil. As the simulation result for the sandbox test 1 with the garnet sand, the particles displacement of the topsoil and the target rod are shown in the Figure 5.24. The maximum displacement of particles is the topsoil particle which is in the back of sandbox. The maximum displacement of the topsoil particles is 143.32mm which is larger than the displacement of the garnet sand because the density of the garnet sand particle is larger than the topsoil particle. The maximum displacement of the pile particle is the top one of the pile particle group and the displacement value is 16.53mm. The maximum displacement of the pile in the topsoil is larger than that in the garnet sand.

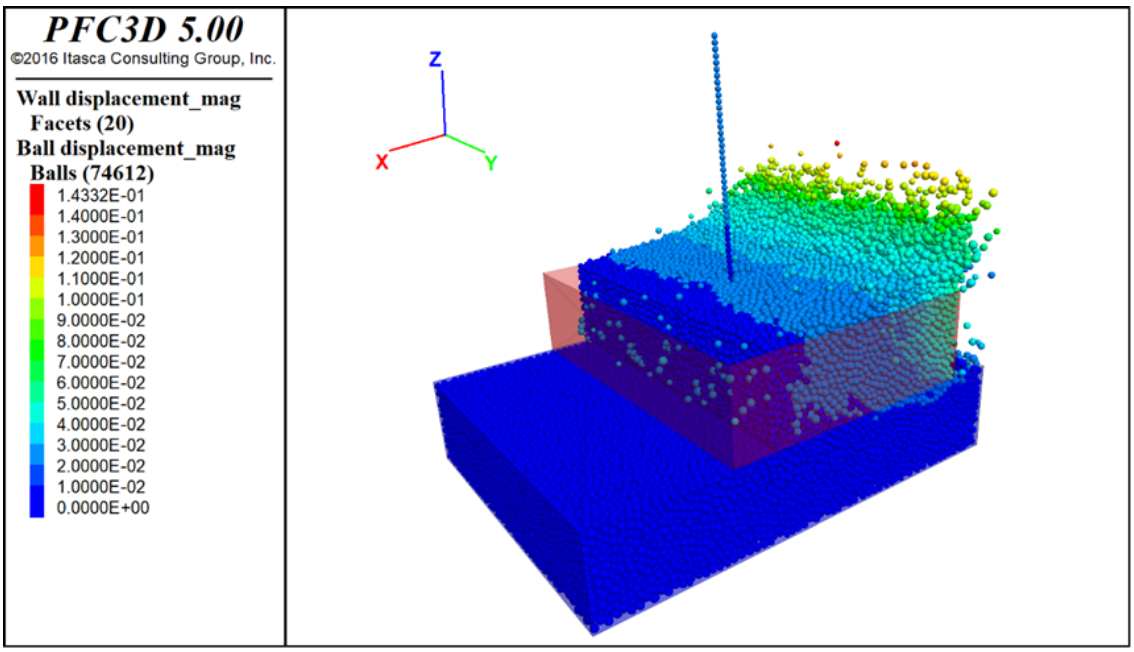

Figure 5.24 The PFC3D simulation result of the sandbox test 1 (soil material is the topsoil).The simulation objective is displacement of the topsoil particles and the aluminum rod. The displacement of the wall structure is 5.08cm (2 inch). The color scale in the left side is used to display the displacement of all particle groups.

The maximum contact force for the pile is the bottom particle which is fixed onto the sandbox and the value is 9.6138N. The contact force direction of most pile particle is same as the rotational direction, which proves the particles interaction force between the soil and the rod is the reason for the rod rotation.There are many factors that are of impacts on the final simulation results, such as cohesion, density and elasticity modulus of soil and loading stress and speed.

5.2.2.3. Discussion for PFC3D simulation results for the sandbox test 1. The PFC3D simulation for the sandbox test 1 can help the new LiDAR measurement method to illustrate the movement tendency of the soil particles and the target rod. Even the simulation result value has a degree distortion because of the limitation of the computer

power, but the PFC3D still can calculate the displacement of all particles and the contact force between particles.

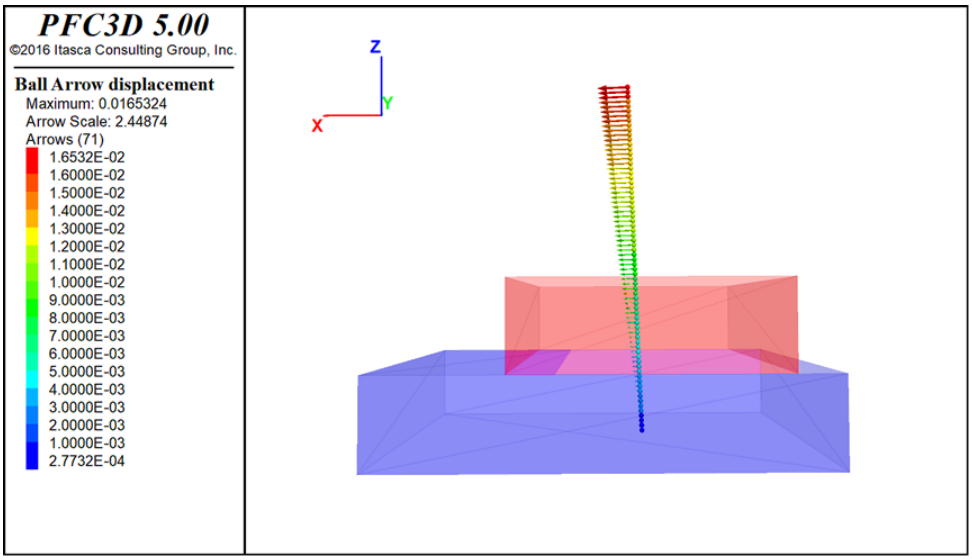

Figure 5.25 The PFC3D simulation result for the particle displacement of the pile group in the topsoil. The red grid is the top sandbox and its displacement is 5.08cm (2 inch), and the blue gird is the bottom sandbox without any displacement. The color scale in the left side is used to display the displacement of pile particle group.

5.2.3. Conclusion for the Computer Simulation Methods. The computer simulation is mainly used to study the interaction between soil and rod, and support the LiDAR technology to develop the new function to monitor slow landslides. Results from both the FLAC3D and the PFC3D simulations can help to understand the rod rotation process (Table 5.3), the soil movement and the interaction of the soil and the target rod in the sandbox test 1.

Table 5.3 The Displacement of Target F6 in Sandbox test 1

Soil type	LiDAR Scanning Results (mm)	FLAC3D (mm)	PFC3D (mm)
Garnet Sand	80.02	93.54	13.81
Topsoil	35.06	58.80	16.53

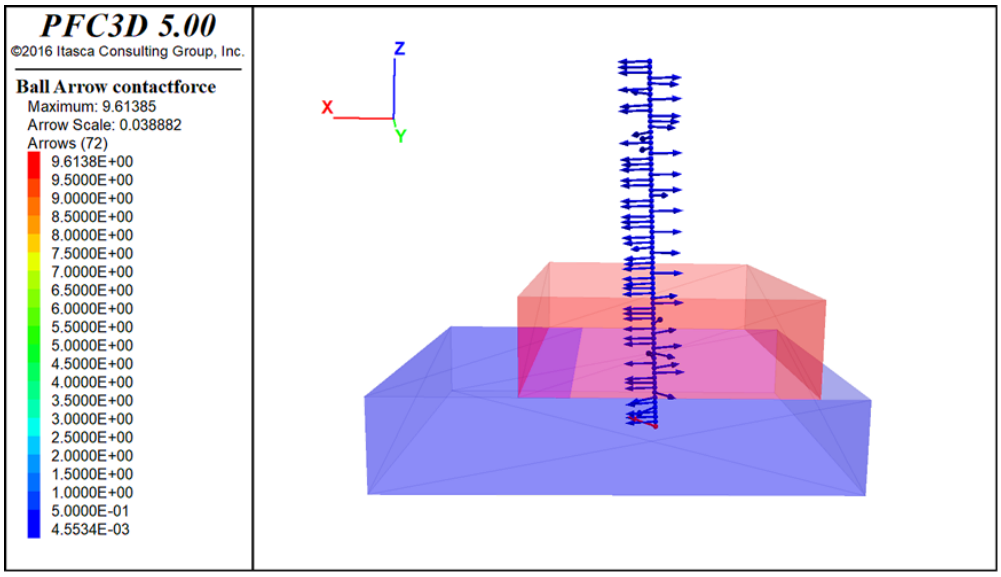

Figure 5.26 The PFC3D simulation result for the contact force of the pile group in the topsoil. The red cuboid is the top sandbox in the experiment and its displacement is 5.08cm (2 inch), and the blue cuboid is the bottom sandbox without any displacement. The color scale in the left side is for the contact force of the pile particle group.

The displacement simulation results from FLAC3D are closer to the LiDAR scanning results, and the data from the PFC3D simulation is distortion because of the compromised parameters used in the simulation program. In the meantime, the stress analysis indicates FLAC3D is more suitable to analyze the interaction stress than PFC3D in the sandbox test 1 and the reason is same as the displacement simulation result.

The PFC3D has the advantage to study the movement tendency of the soil particles, and it can help FLAC3D to explain the stress distribution on the rod (Figure 5.27 and 5.28). The arrow direction of each soil particles in Figure 5.27 and 5.28 is the displacement direction of the soil particles and color scale shows displacement distance. The normal stress on the target rod in the FLAC3D simulation result gradually increases from its middle position and eventually reaches the maximum normal stress value at the bottom of the target rod which is fixed onto the sandbox (Figure 5.10 and 5.16).

Explanation to this phenomenon is that when the top sandbox starts displacement and the bottom sandbox is motionless, the soil in the box would start to move. The difference of the velocity of soil particles between different soil layers is generated by the sandbox movement. Being relative to the particles which are moving faster push the target rod to rotate, the soil particles which are of lower moving speed will impede the rotation of the target rod. Therefore, the normal stress is generated from the boundary of the different velocity of the soil layers and gradually increases until the bottom of the rod. The normal stress direction is opposite to the rotational direction of the target rod.

The comparison between the LiDAR scanning results and computer simulation results of the sandbox test 1 indicates that the displacement of the sandbox and the surface soil (the scanning target F8) are similar and larger than the target rod in same height. The computer simulation models reveal the phenomenon by the three-dimensional models (Figure 5.9, 5.15, 5.21 and 5.24) and the PFC3D simulation results display the reason in Figure 5.29 and 5.30. When the soil particles start to move, some soil particles move around the target rod instead of putting the target rod to rotate. Therefore, the displacement of the surface soil would move further than the target rod in same height.

According the LiDAR scanning result, the FLAC3D and the PFC3D simulation result, the differences of the displacement of the surface soil and the target rod in same height can be calculated (Table 5.4).

As the Table 5.4 shown, the LiDAR scanning result is much closer to the real experiment than computer simulation results. The FLAC3D simulation result is closer to the LiDAR scanning result than that of PFC3D.

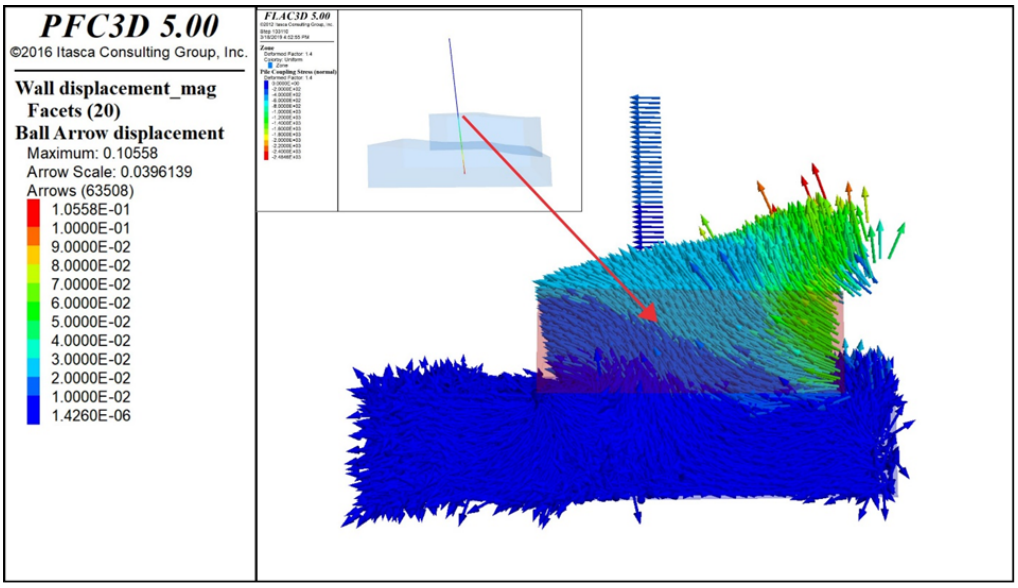

Figure 5.27 The PFC3D simulation result helps to explain the normal stress simulation result by FLAC3D (soil material is the garnet sand). The normal stress is generated in the differentiation boundary of the soil particle displacement. The soil material is the garnet sand.

In most results in Table 5.4, the soil has larger displacement than the target rod in same height. The reason is shown in Figure 5.29 and 5.30, when the soil body start to move, some soil particles would move around the target rod instead of pushing the rod to rotate. The displacement difference between the surface soil and the target rod in same height is an important parameter which need to be considered when using the LiDAR technology to measure the landslide movement. This difference can influence the final measurement results. Meanwhile, the different types of the soil will have difference value of the displacement difference. The computer simulation methods can help to calculate the displacement difference between the surface soil and the target rod in same height before using the LiDAR scanning method to measure the natural landslide. The calculation results need to be taken into the final LiDAR measurement result.

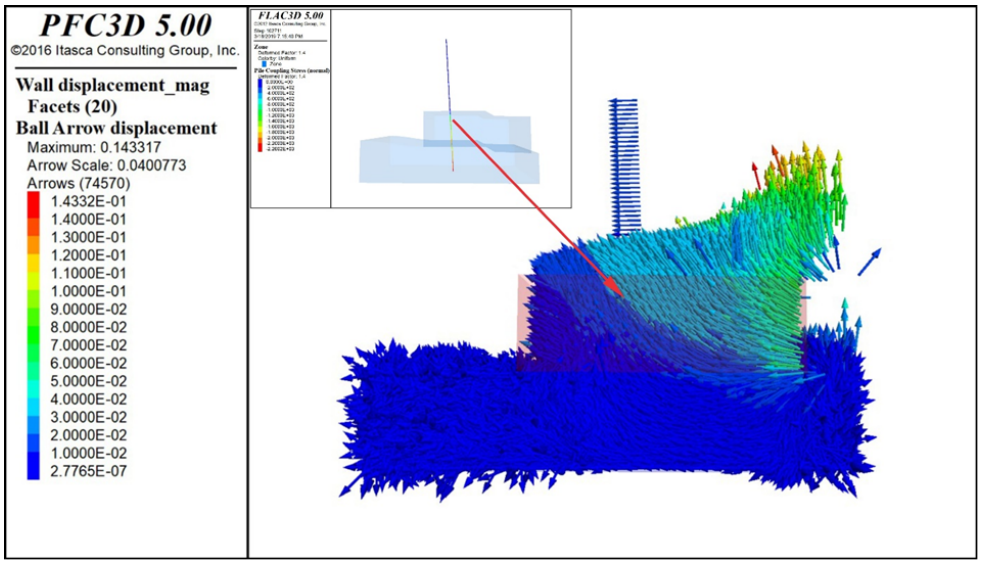

Figure 5.28 The PFC3D simulation result helps to explain the normal stress simulation result by FLAC3D (soil material is the topsoil). The normal stress is generated in the differentiation boundary of the soil particle displacement. The soil material is the topsoil.

The FDM and the DEM can be used to: (1) simulate the sandbox experiments and use three-dimensional figures to display the test model; (2) calculate the displacement for all parts of the model; (3) analyze the interaction between the soil and the target rod; (4) prove if the target rod enters yield state in entire experiment procedure.

In this research project, the displacement simulation results of the FDM is closer to the LiDAR scanning results which can prove that it is better to use at simulating the displacement of the rod and analyzing the stress distribution on the rod. The DEM has distorted results in that some parameters used for the coding were compromised because of computational limits, but it is still useful to simulate the movement of the soil and the target rod. The DEM also can help to explain the mechanism of movement between the soil layers and the target rod in this experiment. As a result, the combination of FDM and DEM can not be an accurate forecasting tool in landslide research, but it is a highly effective tool to help LiDAR measurement method to study the interaction and the

behavior of the soil layers and the scanning target rods in monitoring and analyzing slow moving landslides.

5.3. SANDBOX TEST 2

The experiment model used in the sandbox test 2 is same as the sandbox test 1, because the test results of the sandbox test 2 need to compare with the results in the sandbox test 1.

5.3.1. Model Design. In the sandbox test 1, the target rod is fixed onto the bottom of the box to create more controlled conditions. In a real natural environment, the scanning target rod usually cannot be fixed onto a completely stationary rock or soil layer that can hold its bottom in exactly unmovable position. Therefore, sandbox test 2 is designed to test the movement situation of the target rods with different bottom conditions.

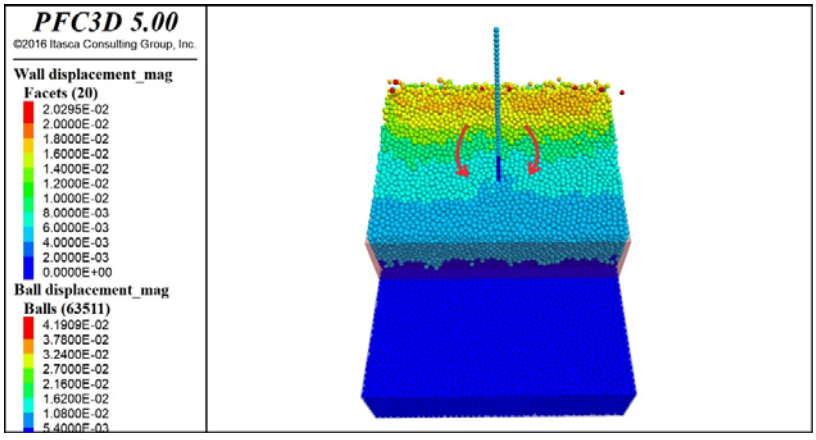

Figure 5.29 The simulation result of PFC3D shows the garnet sand particles move around the scanning target rod. The red arrows display the displacement direction of the soil particles. The color scales in the left side of the figure show: (1) the color scale for the wall displacement indicate the progress of the simulation procedure; (2) the color scale for the balls' displacement indicate the displacement of the soil and pile particles.

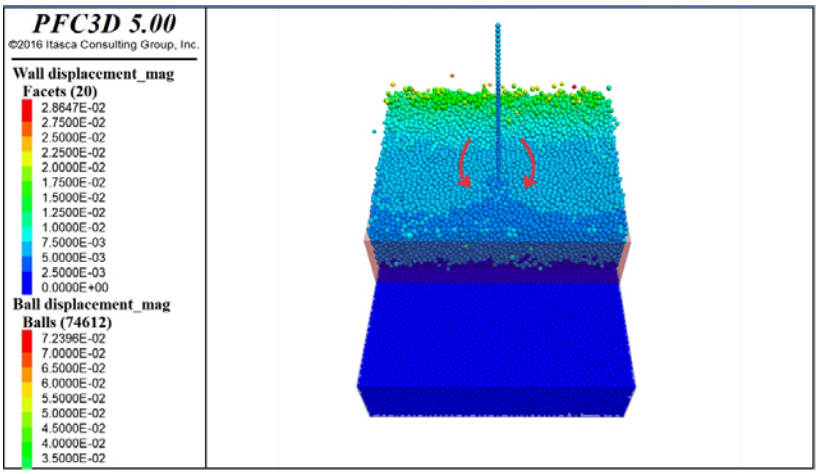

Figure 5.30 The simulation result of PFC3D shows the topsoil particles move around the scanning target rod. The red arrows display the displacement direction of the soil particles. The color scales in the left side of the figure show: (1) the color scale for the wall displacement indicate the progress of the simulation procedure; (2) the color scale for the balls' displacement indicate the displacement of the soil and pile particles.

Table 5.4 The Displacement Difference between the Surface Soil and the Target Rod in Same Height

Soil type	Data type	LiDAR Scanning (mm)	FLAC3D (mm)	PFC3D (mm)
Garnet Sand	Surface Soil Displacement	51.46	50.80	18.12
	The Target Rod	62.22	37.22	6.90
	Difference	-10.76	13.58	11.22
Topsoil	Surface Soil Displacement	50.85	50.80	14.23
	The Target Rod	27.26	24.40	8.04
	Difference	23.59	26.40	6.19

The model design of the sandbox test 2 is same as the sandbox test 1 (Figure 5.1) and the only difference is more scanning targets were used in addition to not being fixed onto the bottom of the target rod (Figure 5.31). In the sandbox test 2, there are three types of the target rods (Figure 5.32): the #1 rod is unfixed and the bottom position is above the

boundary between the top and bottom sandbox; the #2 rod is fixed onto the bottom sandbox which is same as the rod in sandbox test 1; the #3 rod is in the same depth as the #2 rod however t the bottom of the #3 rod is not fixed to the bottom of the box. The design of the different insertion modes of rod is used to simulate the possible different rods inserted in natural landslides.

The specification of the scanning targets in sandbox test 2:

1. Specification of the Scanning Targets:

(1) Size of Scanning Target Spheres: The diameter is 6.35cm (2.5 inch) and 10.16cm (4 inch);

(2) Material of Target Spheres: Styrofoam;

(3) Types of Scanning Target used in the test: The control spherical 10.16cm (4 inch) targets are fixed (stationary) around the sandbox; the floating 6.35cm (2.5 inch) spherical targets are fixed onto an aluminum rod which is hinges to the bottom of sandbox and the diameter is 6.35cm (2.5 inch).

(4) Size of Target Rods: The length of rods is 45.72cm; the diameter of rods is 0.635cm.

2. Specifications of the Sandbox:

(1) Materials of Sandbox: Sandbox frame is made of wooden boards 3.8cm thick; a steel plate acts as a track used to constrain the movement direction of top sandbox along the bottom sandbox.

(2) Size of Sandbox: The width of both top and bottom sandbox is 37.6cm; the length of top sandbox is 30cm; the length of bottom sandbox is 50cm; the height of both top and bottom sandbox is 10cm without the plank thickness;

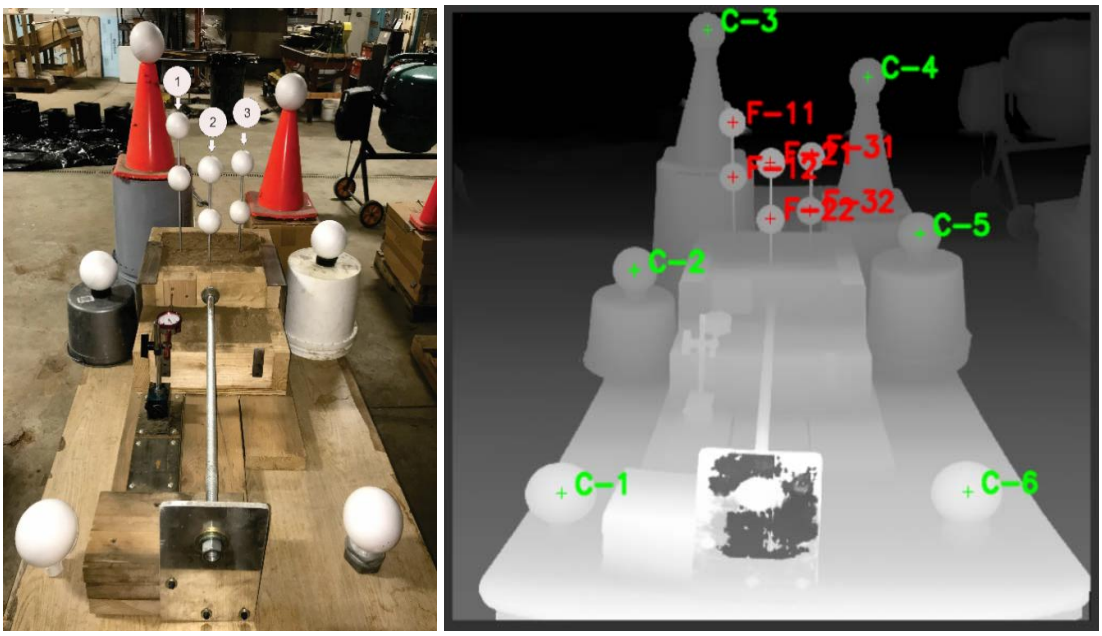

(a) (b)

Figure 5.31 The design of sandbox test 2 and the scanning result of the sandbox model in Lidarsw. (a) The model of sandbox test and the ID of the aluminum rods; (b) The scanning targets in Lidarsw with green marks denoting the control targets, and the floating targets are denoted with red marks.

(3) Structure of Sandbox: The bottom box is fixed to the table and unmovable; the top box is set up above the bottom box and can only move only in parallel with the long side of bottom box. The displacement of the top box is controlled by the leadscrew.

3. Materials of Target Rod and Soil:

(1) The metal rod is made of aluminum.

(2) The soil materials used for this test are: garnet sand and topsoil. The garnet sand and the topsoil are supplied by the Rock Mechanics and Explosives Research Center of Missouri University of Science and Technology.

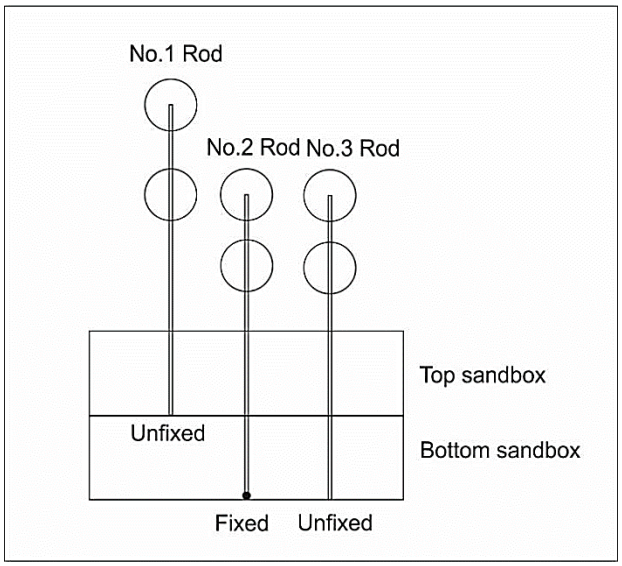

Figure 5.32 The illustration of the three targets rods in sandbox test 2

4. Research Method:

To test the ability of the LiDAR to measure the movement of the scanning targets, the test displaces of the top sandbox a distance of 5.08cm (2inch) in 10 equal increments, which means the displacement of each step is 0.508cm (0.2inch). A LiDAR scan is conducted between each step. Three scanning target rods which have same size but are in different bottom conditions and the spherical scanning targets on the rods are the measurement targets. This test will test if the target rods without fixed bottom can still help the LiDAR scanner to obtain the movement of subsurface soil or displacement difference of soil layers.

5.3.2. The Process and Scanning Results of the Sandbox Test 2. The entire scanning process of the sandbox test 2:

(1) Fix the #2 target rod in the sandbox;

(2) Fill the garnet sand into the sandbox;

(3) Insert the #1 and #3 target rod in the soil;

(4) Set up the control targets around the scanning area, and fix the floating targets 11, 12, 21, 22, 31 and 32 onto the three target rods (Figure 5.31);

(5) Conduct a baseline LiDAR scan when the sandbox is in the original position;

(6) Pull the top sandbox 0.58cm (0.2 inch), and re-scan the sandbox model;

(7) Repeat process (5) 10 times until the displacement of the top box reaches 5.08cm (2 inch);

(8) Remove the garnet sand to the topsoil to fill in the sandbox and repeat process (3) to (6);

(9) Process the scanning data to obtain the displacement of the floating targets and the rotation angle of the three target rods (Figure 5.31);

(10) Compare the results to find if the LiDAR measured displacement match the actual ones.

The scan results of the sandbox test 2 are shown in Figure 5.33 and Figure 5.34.

5.3.3. Conclusion for the Sandbox Test 2. In accordance with the curves in Figure 5.33 and 5.34, the scan results of three target rods have clear variation trends with the top sandbox movement. The comparison of the Figure 5.33 and 5.34 demonstrates that the #2 rod which is fixed onto the bottom sandbox has the same rotational angle change tendency as that in the sandbox test 1 (Figure 5.7), no matter in which kind of soil material. The rotational angle of the #2 rod in both garnet sand and topsoil show expected rotation at the beginning stage of the top sandbox movement and then rapidly decreases, as the movement is restrained by the fixed attachment.

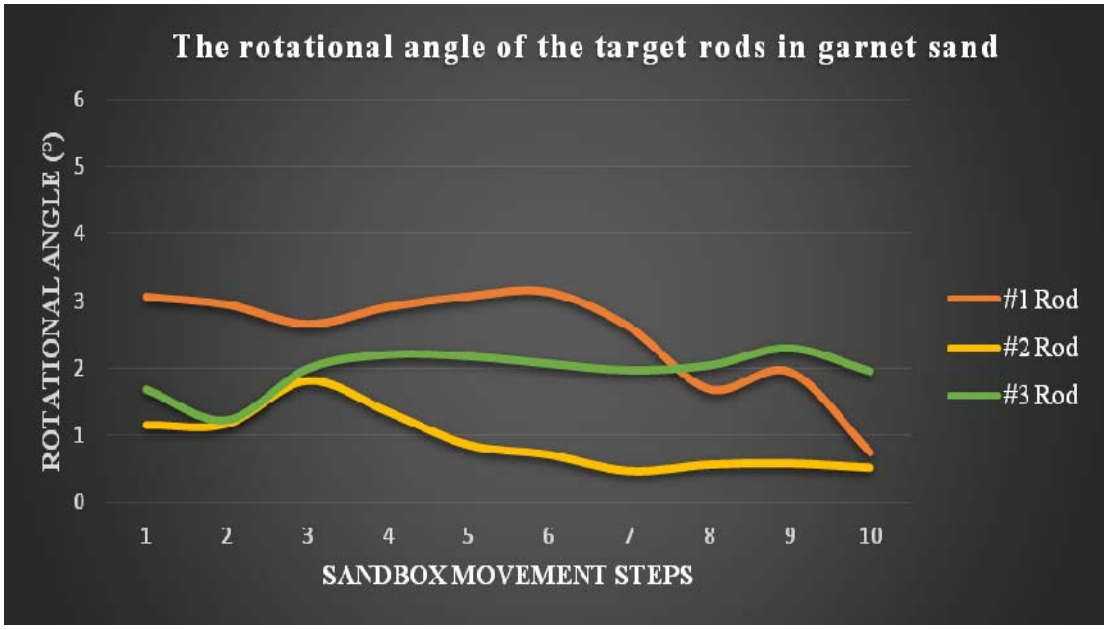

Figure 5.33 The change tendency of the rotational angle of three scanning target rods in the garnet sand. Each sandbox movement step is 5.08mm (0.2 inch).

The #3 rod which is not fixed onto the bottom sandbox has the same rotational angle change as the #2 rod early in the test in both garnet sand and topsoil. As the curves shown in Figure 5.33 and 5.34, later in the test, unlike the #2 rod, the rotation continues at approximately the same rate. As a result, the fixed bottom of the rod will lead to a smaller rotational angle. Therefore, the conclusion can be drawn that if the rod is not fixed onto the bottom, it would be more obvious that the rotational phenomenon would be detected by LiDAR scanner.

The biggest difference of rotational angle change of three target rods is the #1 rod and it has bigger rotational angle in topsoil. In the curves of all three rods, the rotational angle of the #1 rod is the one that has the maximum change, no matter in which soil material. The reason is the position of the #1 rod is different with other two rods because it does not penetrate through the shear plane which means the #1 rod can move in parallel

and in rotation but also laterally as well (Figure 5.35). The rotational angle of the #3 rod is smaller than that of the #1 rod because of the bottom soil layer is unmovable which holds the #3 rod to prevent it from free rotation (Figure 5.36). Notwithstanding, the rotational angle of the #3 rod is larger than that of the #2 rod because its bottom is not fixed onto the bottom sandbox and can move freely(Figure 5.37).

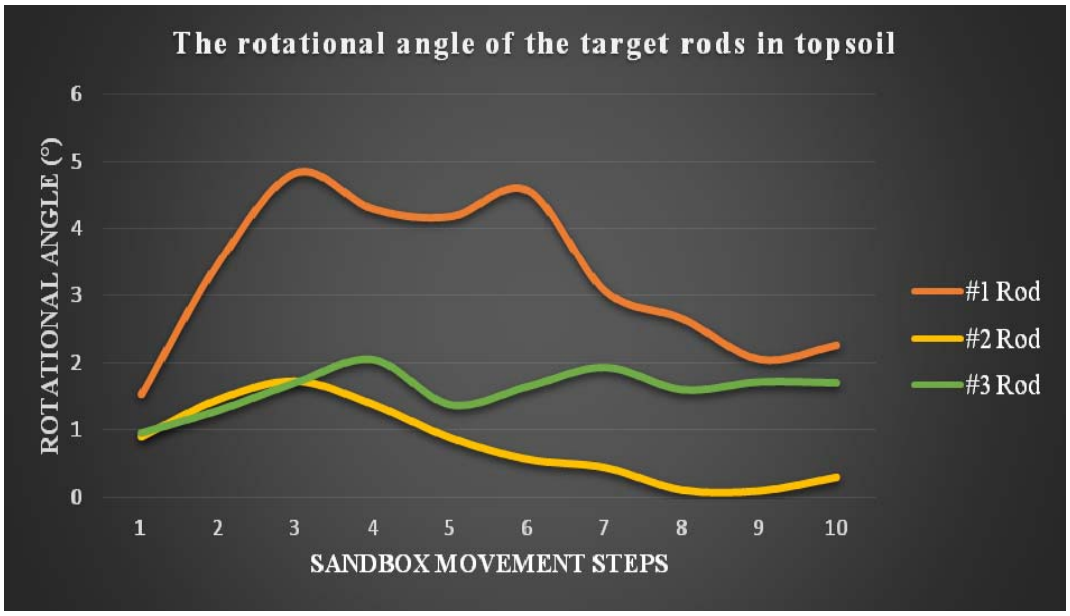

Figure 5.34 The change tendency of the rotational angle of three scanning target rods in the topsoil. Each sandbox movement step is 5.08mm (0.2 inch)

The Figure 5.35, 5.36 and 5.37 explain the reason of the scanning results of the sandbox test 2 (Figure 5.33 and 5.34). Three rods in the sandbox test 2 have different rotational angles because of their positions and bottom conditions. According to the scanning results and the figures shown:

$$\theta_1 > \theta_3 > \theta_2$$

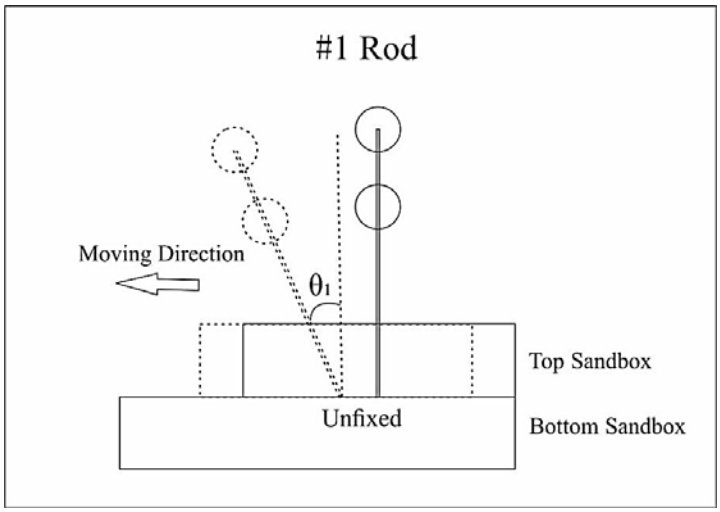

Figure 5.35 The rotational angle of the #1 rod

The #1 target rod has the largest rotational angle, and the rotational angle of the #3 target rod is larger than the #2 because of the different bottom conditions. In natural environment, the common research situation should be the same as the #1 and #3 rods in which the rod position is above or through the failure or displacement difference boundary between soil layers, and the bottom can move freely.

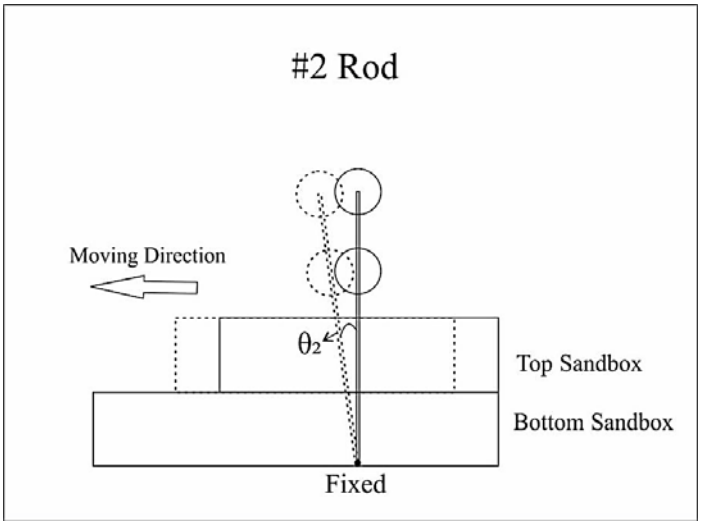

Figure 5.36 The rotational angle of the #2 rod

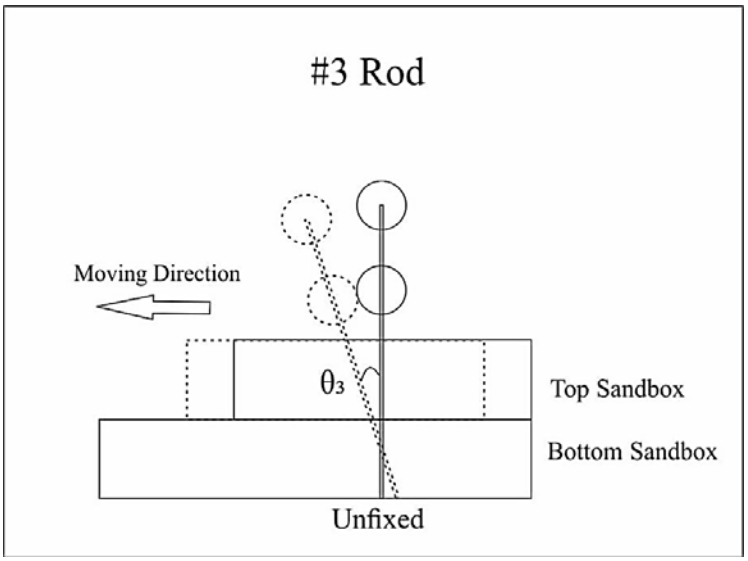

Figure 5.37 The rotational angle of the #3 rod

Through the sandbox test 2, the LiDAR scanning method proves that it can be used to measure the displacement difference between soil layers through the displacement of the scanning targets and the rotational angle of the scanning target rod.

6. THE BENCH MODEL TEST

In accordance with results from the error test, the sandbox test and the computer simulation, the theoretical foundation and feasibility of the new LiDAR measurement method have been verified. Furthermore, the interaction between the soil and scanning target rod has been analyzed by the computer simulation methods. Depending on the application in Section 4 and 5, Section 6 uses a designed bench model test which is a small-scale landslide one to prove the applicability of the new LiDAR monitoring method.

The test objective of this small-scale landslide simulation model is to combine the LiDAR technology with the designed artificial scanning targets(Figure 6.1) to monitor an artificial landslide and explain the scanning results to see if the new measurement method could be used to obtain the surface and subsurface movement or displacement difference of soil layers in landslide.

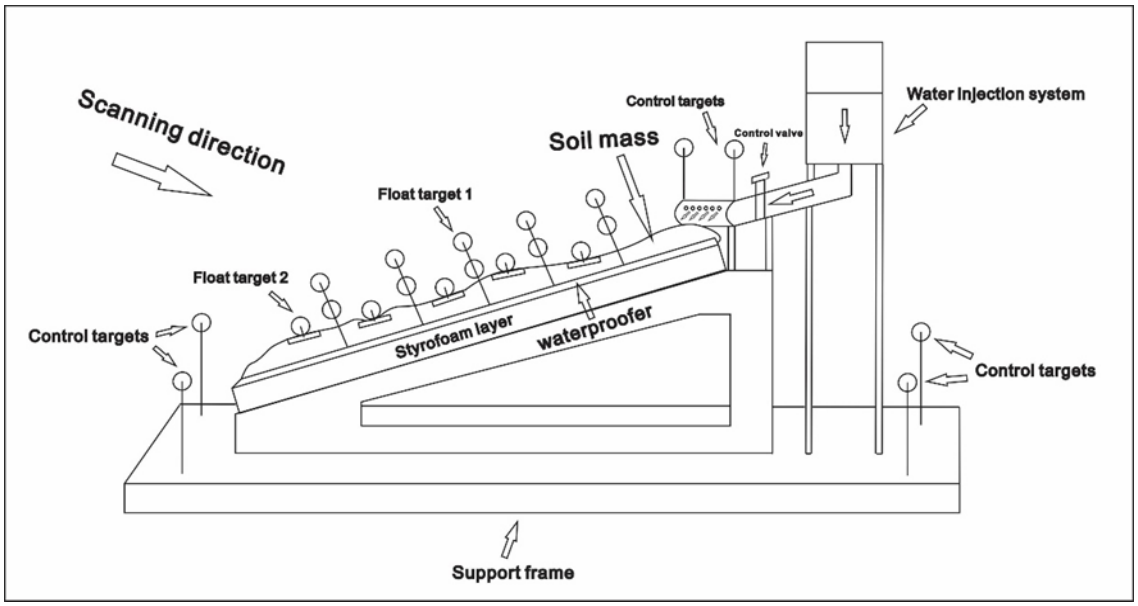

Figure 6.1 The bench model for landslide simulation

The model consists of five main parts: support frame, soil mass, water infiltration system, water proofing layer and artificial scanning targets and target rods. The support frame is made of wood, whose main function is to support the model. The soil mass is the key component which is used to simulate the movement of landslide. According to previous research results (Iverson, R.M., 2000; Wartman, J. et al., 2016), the rain infiltration is the most important trigger of landslide. In this landslide model, the water is used as the trigger for the landslide and the water injection system is designed to inject water to simulate the rain on the top part of soil mass which result in soil mass slide along the support frame. To keep the water from leading out the bottom of the model, a Styrofoam board and water proofing layer are used in the bench model, as is shown in the Figure 6.1. As is described in the research principle in Section 3 and the test results in Section 4 and 5, there are two types of scanning targets which are the same as in the sandbox test: controlling targets and floating targets. In the meantime, there are two types of the floating targets (Figure 6.1): the floating target 1's, which is composed of an aluminum rod and two spheres, driven to the base of the soil layer, is used to monitor the subsurface soil movement; and the floating target 2's is composed of a single sphere fixed on piece of wood floating on the soil surface.

The parameters of each part of bench model are shown in Table 6.1:

Table 6.1 The Bench Model Parameters

Bench Model Parameters	
Length of Structure Frame:	185.42cm (73 inch)
Width of Structure Frame:	179.83cm (70.8 inch)
Soil Type:	Topsoil
Slope Angle:	20 degree

Table 6.1 The Bench Model Parameters(Cont.)

Bench Model Parameters	
Thickness of Soil Slope:	10.16cm (4 inch)
Number of the Floating Target:	30
Diameter of the Floating Target:	6.35cm (2.5 inch)
Number of the Control Target:	5
Diameter of the Control Target:	10.16cm (4 inch)
Position of the Top Target in Rod:	0-6.35cm (0-2.5 inch)
Position of the Bottom Target in Rod:	12.7-19.05cm (5-7.5inch)
Length of Scanning Target Rods:	45.72cm (18 inch)
Diameter of Scanning Target Rods:	0.635cm (1/4 inch)
Burial Depth of Target Rods (Failure Depth):	10.16cm (4 inch)

The soil used in this test is the topsoil, inducing the soil mass to slide along the slope, a water infiltration system being necessary. The experiment uses perforated pipes to simulate rain on the top of the soil body. The water infiltration system is positioned on the upper end of the slope and as is shown in Figure 6.1, and the water infiltration method is using a pressure head which generated by raising the water reservoir, which is different from the elevation required to produce the desired discharge (Figure 6.1). The water injection speed is controlled by a control valve. The injection water volume is shown in Test 6-1, 3 gallons water every 30 minutes and Test 6-2, 6 gallons water every 5 minutes.

6.1. THE PROCESS OF TEST

As is explained in Section 3 and 4, the control targets are set around the scanning area for the registration of each scanning result to a single three-dimensional coordinate system. The floating scanning targets are similar with those in the sandbox test in Section 5; the floating target 1 is used to monitor the subsurface movement, and the floating target 2 is used to monitor the surface movement (Figure 6.2). The top and bottom sphere

of the floating target 1 can reflect the differential displacement of soil layers. To obtain the average scan result for the bench landslide model, two types of floating targets (type 1 and 2) are set up in four parallel lines along the slope (Figure 6.2).

The whole test processes are as follows:

1. Establish the support frame;

2. Fill the topsoil on the surface of the slope;

3. Set up the water infiltration system;

4. Fix the control targets around the bench frame and the floating targets in the soil body (Figure 6.2);

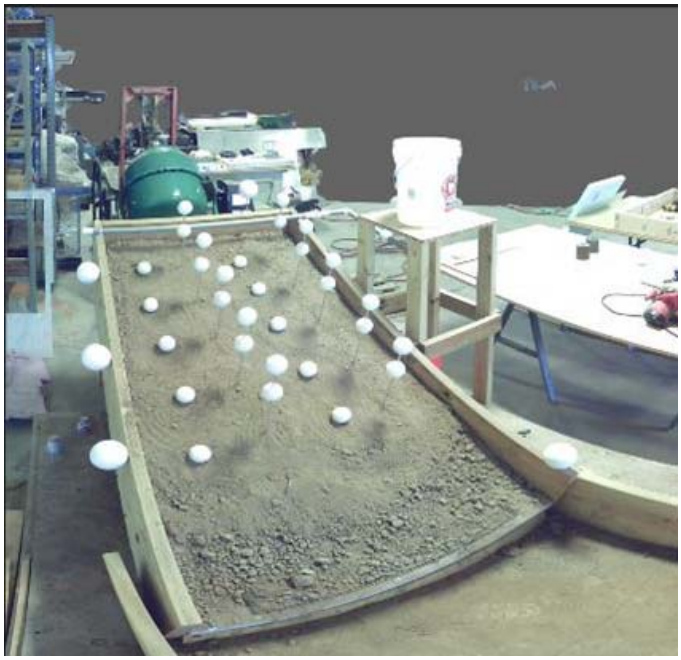

Figure 6.2 The bench model and the scanning targets. The spherical targets which are fixed around the support frame are the control targets; the spherical targets which are set up on the slope are the floating targets.

5. Use the Faro Focus^{3D} (LiDAR scanner) to finish the baseline scan for the bench model to obtain the original position for all floating and control targets;

6. Fill water into the water tank and regulate the injection water flow to three gallons every 30 mins, and scan the bench model before and after each watering;

7. Inject water 20 times (Test 6-1);

8. Change new soil for the Test 6-2;

9. Use Faro Focus^{3D} to accomplish the baseline scan for the bench model to obtain the original position for all floating targets;

10. Fill water into the water tank and control the injection water flow to six gallons every 5 minutes, and scan the bench model before each watering;

11. Inject water 20 times (Test 6-2);

12. Use FARO SCENE, Lidarsw and Surfer to process the scan data (Figure 6.3);

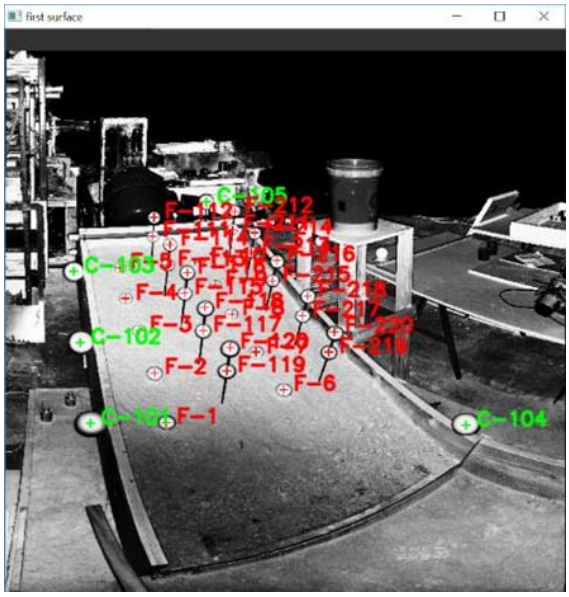

Figure 6.3 The scan result of the bench model by Lidarsw; the red targets are the floating targets and the green targets are the control targets.

13. Compare the LiDAR scanning results for the landslide behaviors under different water condition to see if the LiDAR technology and the new designed artificial scan targets can obtain both surface and subsurface movement of the landslide model.

The scanning result exported from Lidarsw can be divided into four types (Figure 6.3):

(1) The three-dimensional position change of the floating target 2 which can present the surface movement of soil mass;

(2) The three-dimensional position change of the top sphere of the floating target 1, presenting the subsurface movement or the displacement difference between surface and subsurface of soil;

(3) The three-dimensional position change of the bottom sphere of the floating target 1 that can present the superficial layer movement or the displacement difference between surface and subsurface of soil slope;

(4) The relative three-dimensional position change of the two spheres of floating target 2(the rotational angle of the target rod), indicating the relative subsurface movement of soil slope.

6.2. THE RESULT OF BENCH MODEL TEST

All scanning targets for each scan are of a three-dimensional position (X, Y, Z) in an arbitrary three-dimensional coordinate system subsequent to the LiDAR scan and data processing. To compare with the positions of different scans, each scan must be registered to a common coordinate system (Figure 6.4). Author of this research uses the

software “Surfer” to present the LiDAR scanning data so as to help visualize the displacement or the rotational angle of the scanning targets on the soil slope (Figure 6.5). In the data analysis results, the abscissa and ordinate are Y and X axis of the slope in the two-dimensional coordinate system, demonstrating the displacement of the floating target 1 and 2 (unit is mm) which obtained by LiDAR scanner and the rotational angle of the floating target 1 (unit is degree).

The difference of displacement and rotational angle between each scan step is not very obvious owing to the volume of injection water. In order to show the change of landslide clearly, the 2nd, the 5th, the 10th, the 15th and the 20th scanning results of test 6-1 are picked to be compared (Figure 6.5- 6.8).

The processes and results of test 6-1 are shown below:

a

b

c

d

e

Figure 6.4 (a-e) The scanning results of the bench model test 6-1; (a) the 2nd stage of test 6-1; (b) the 5th stage of test 6-1; (c) the 10th stage of test 6-1; (d) the 15th stage of test 6-1; (e) the 20th stage of test 6-1

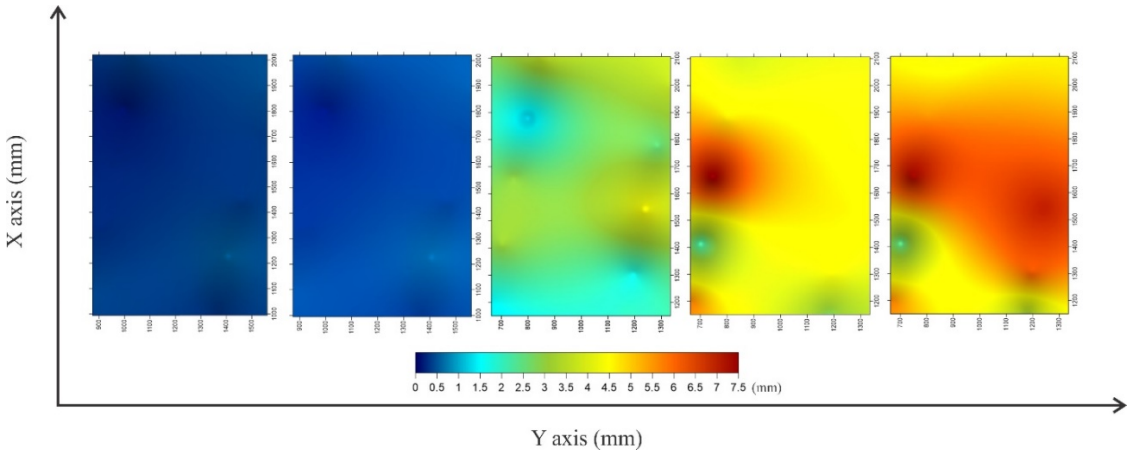

Figure 6.5 The scanning results of bench model test 6-1 illustrate the displacement of the surface scanning targets of the bench landslide model. According to the result in the sandbox test 1 in Section 4, the displacement of the surface target can present the surface soil movement. Abscissa and ordinate are Y and X position of the surface of the soil slope, and the color scale displays the value of displacement. From left to right, the figures show the 2nd, the 5th, the 10th, the 15th and the 20th scanning results. The apparent displacement of surface soil can be recognized from the 10th scan.

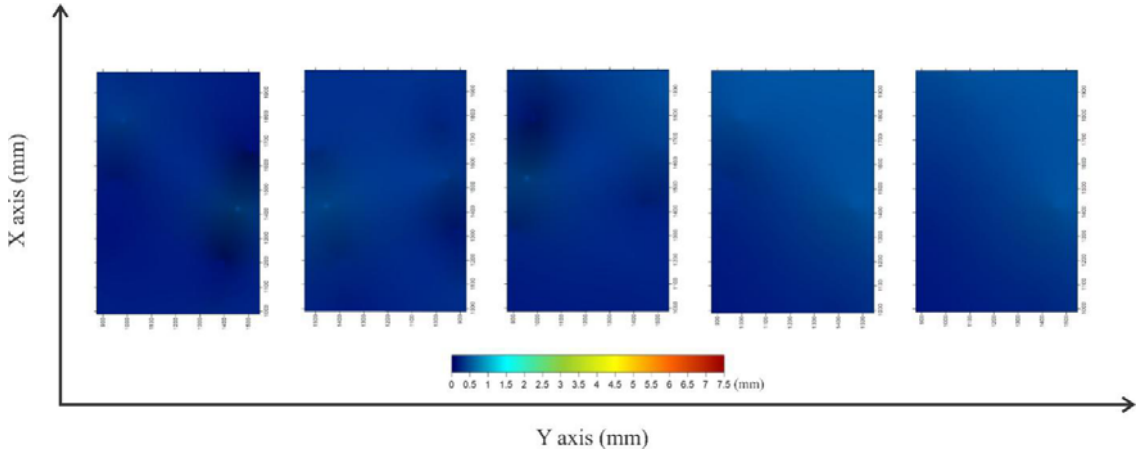

Figure 6.6 The scanning results of bench model test 6-1 illustrate the displacement of the top scanning targets on the target rods. According to the result of the sandbox test 1 in Section 4, the displacement of the top target on the target rod can present the subsurface soil movement. Abscissa and ordinate are Y and X position of the surface of the soil slope, and the color scale displays the value of displacement. From left to right, the figures show the 2nd, the 5th, the 10th, the 15th and the 20th scanning results. There is almost no movement in that the water only infiltrated the top of the soil and did not affect the target representing deep seated movement.

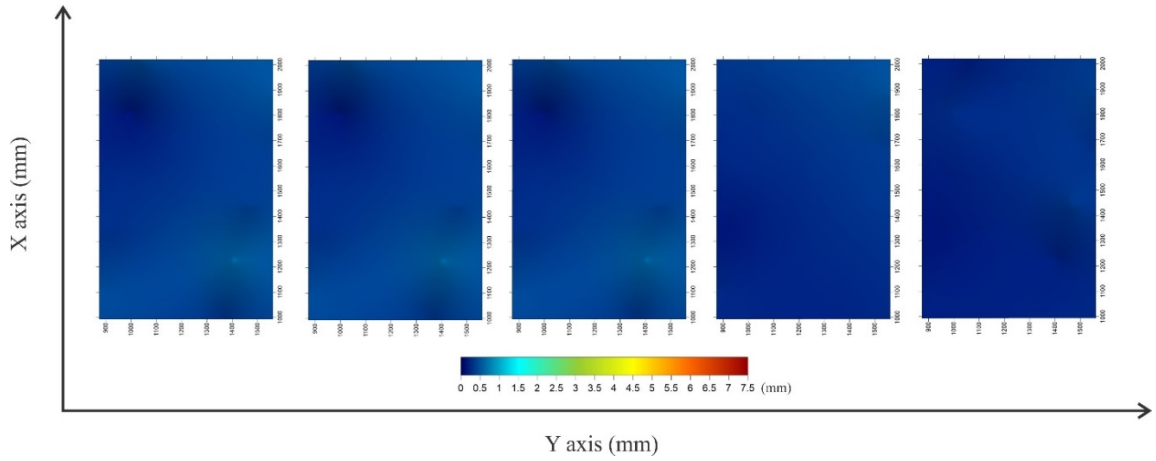

Figure 6.7 The scanning results of bench model test 6-1 illustrate the displacement of the bottom scanning targets on the target rods. According to the result of the sandbox test 1 in Section 4, the displacement of the bottom target on the target rod can present the movement of the shallow soil layer. Abscissa and ordinate are Y and X position of the surface of the soil slope, and the color scale displays the value of displacement. From left to right, the figures show the 2nd, the 5th, the 10th, the 15th and the 20th scanning results. There is almost no movement for the water only infiltrated the top of the soil and did not affect the target representing shallow soil movement.

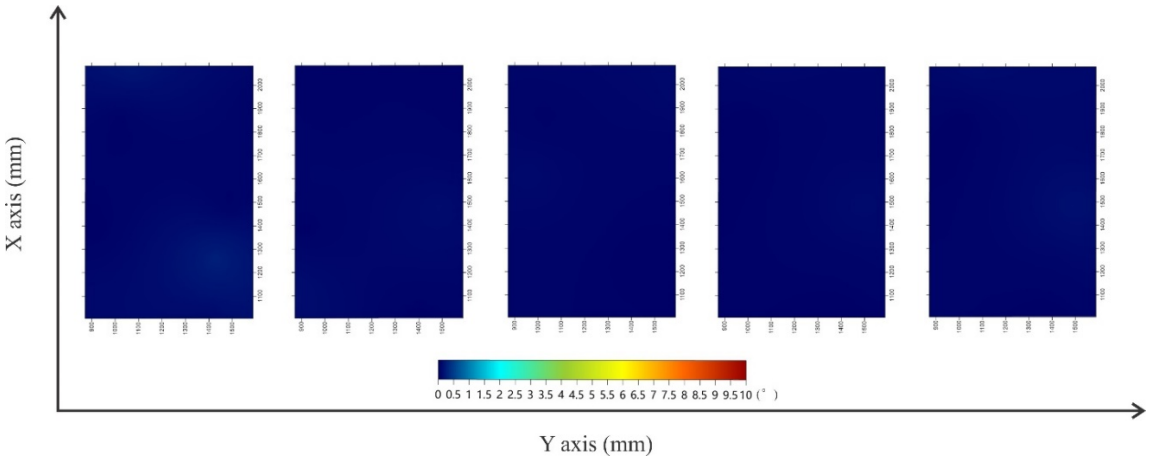

Figure 6.8 The scanning results of bench model test 6-1 illustrate the rotational angle of the target rods. According to the result of the sandbox test 1 in Section 4, the rotational angle of the target rod can present the displacement difference between soil layers. Abscissa and ordinate are Y and X position of the surface of the soil slope, and the color scale displays the value of rotational angle of the target rods. From left to right, the figures show the 2nd, the 5th, the 10th, the 15th and the 20th scanning results. There is almost no rotation of the target rods on account of the fact that the water only infiltrated the top of the soil and did not affect the target rod representing displacement difference of soil layers.

The bench model test 6-2 is of same procedure with the test 6-1 (Figure 6.9), but different water injection speed. The test 6-2 picked the 2nd, the 6th, the 11th, the 13th and the 16th scan result to analyze (Figure 6.10-6.13). The scan results from the 16th cannot be accepted in that the rill erosion occurred on the slope and some target rods fell down and some floating target 2 slide off the frame from the 17th scan, which lead the value of displacement and rotational angle to be abnormal data which need to be deleted.

The results of test 6-2 are shown below:

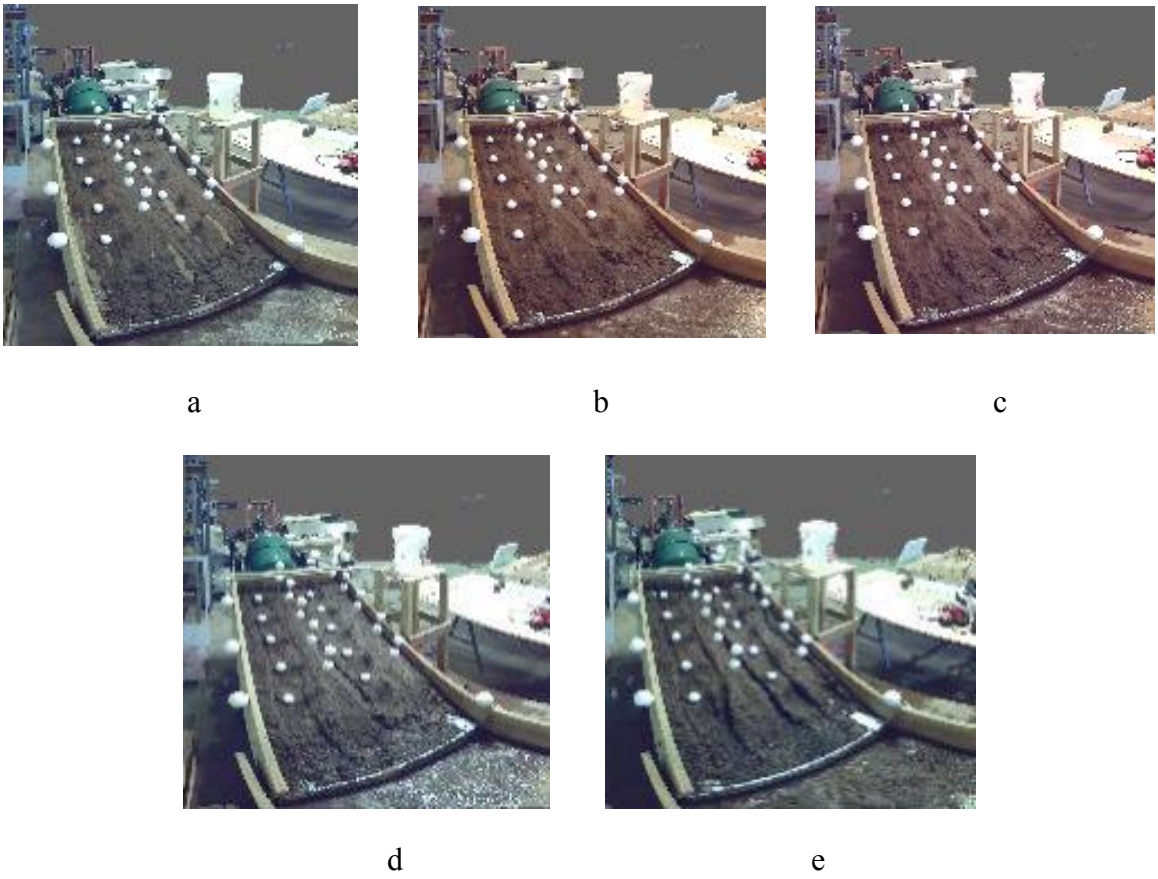

a b c

d e

Figure 6.9 (a-e) The scanning results of the bench model test 6-2; (a) the 2nd stage of test 6-2; (b) the 6th stage of test 6-2; (c) the 11th stage of test 6-2; (d) the 13th stage of test 6-2; (e) the 16th stage of test 6-2.

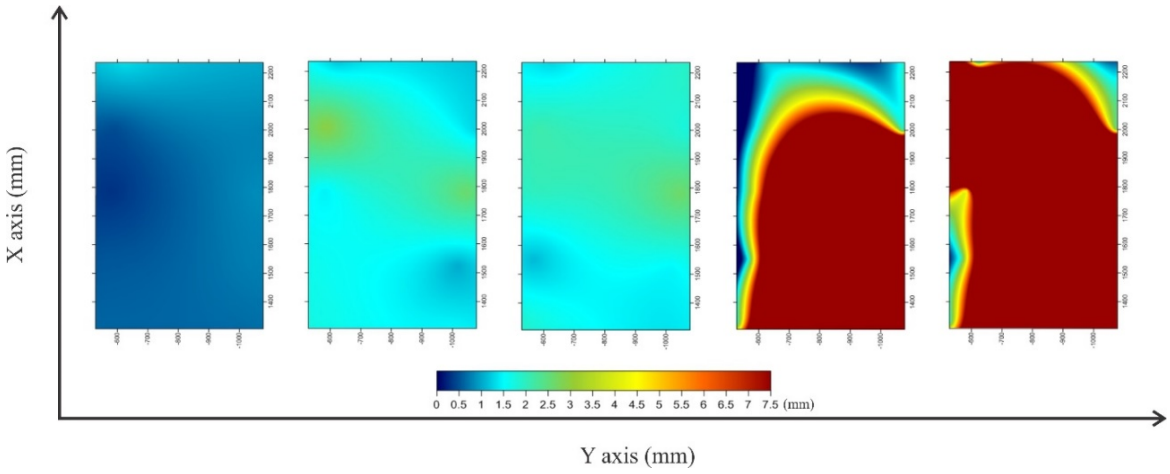

Figure 6.10 The scanning results of bench model test 6-2 illustrate the displacement of the surface scanning targets of the bench landslide model. According to the result from the sandbox test 1 in Section 4, the displacement of the surface target can present the surface soil movement. Abscissa and ordinate are Y and X position of the surface of the soil slope, and the color scale displays the value of displacement. From left to right, the figures show the 2nd, the 6th, the 11th, the 13th and the 16th scanning results. The apparent displacement of surface soil can be recognized from the 6th scan.

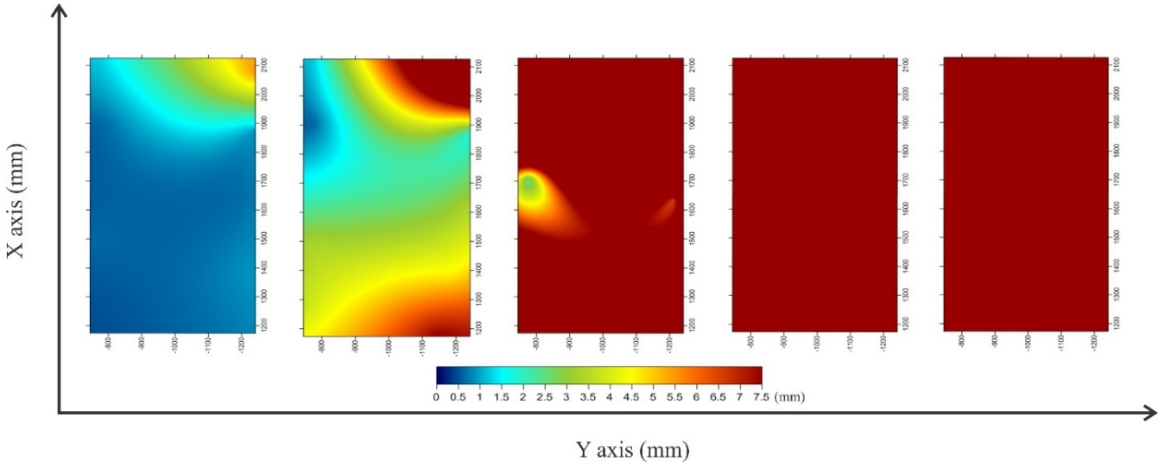

Figure 6.11 The scanning results of bench model test 6-2 illustrate the displacement of the top scanning targets on the target rods. According to the result from the sandbox test 1 in Section 4, the displacement of the top target on the target rod can present the subsurface soil movement or the displacement difference between soil layers. Abscissa and ordinate are Y and X position of the surface of the soil slope, and the color scale displays the value of displacement. From left to right, the figures show the 2nd, the 6th, the 11th, the 13th and the 16th scanning results. The apparent displacement difference between soil layers can be recognized from the 6th scan. The displacement difference between soil layers is due to the fact the water infiltrated from the surface of the soil slope which leads the displacement of the surface soil is larger than the bottom layers.

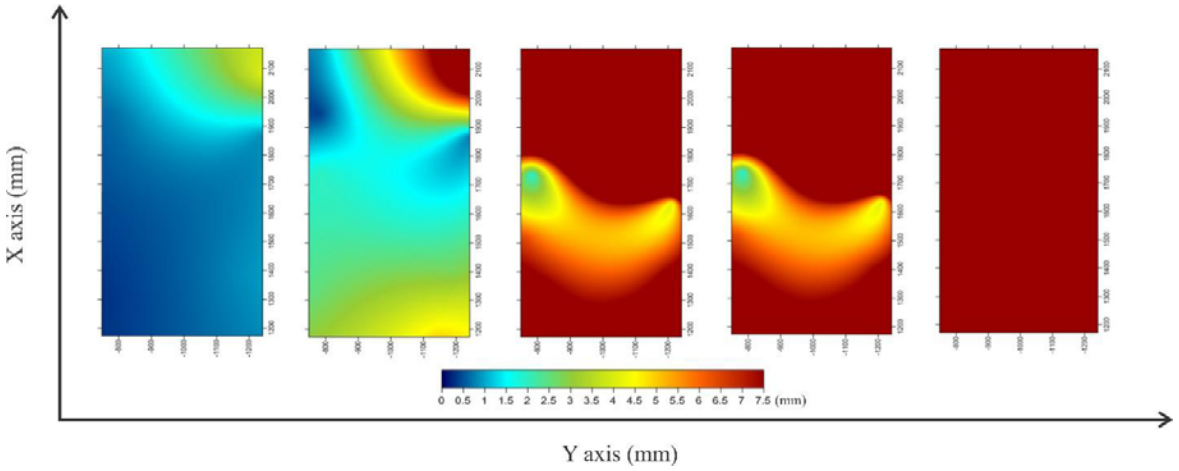

Figure 6.12 The scanning results of bench model test 6-2 illustrate the displacement of the bottom scanning targets on the target rods. According to the result from the sandbox test 1 in Section 4, the displacement of the bottom target on the target rod can present the movement of the shallow soil layer or the displacement difference between soil layers. Abscissa and ordinate are Y and X position of the surface of the soil slope, and the color scale displays the value of displacement. From left to right, the figures show the 2nd, the 6th, the 11th, the 13th and the 16th scanning results. The apparent displacement difference between soil layers can be recognized from the 6th scan.

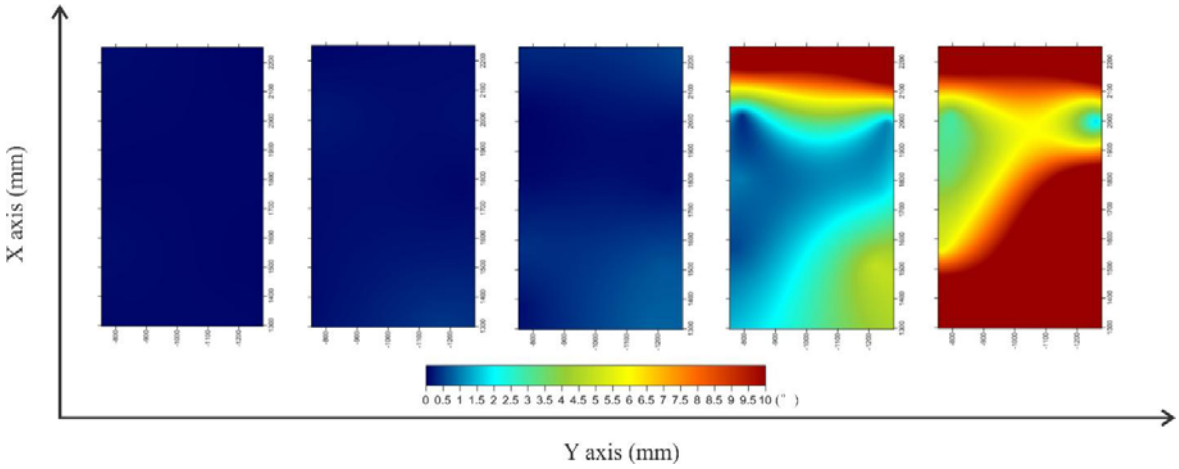

Figure 6.13 The scanning results of bench model test 6-2 illustrate the rotational angle of the target rods. According to the result from the sandbox test 1 in Section 4, the rotational angle of the target rod can present the displacement difference between soil layers. Abscissa and ordinate are Y and X position of the surface of the soil slope, and the color scale displays the value of rotational angle of the target rods. From left to right, the figures show the 2nd, the 6th, the 11th, the 13th and the 16th scanning results. The apparent rotational angle can be recognized from the 13th scan.

6.3. CONCLUSION

The LiDAR scanning result in the bench model test is negative influenced by gullying which has been generated by the water injection method (Figure 6.14). Most of the scanning results, especially those in the late stages of test 6-1 and 6-2, have various degrees of distortion in that the gullying leaves the target rods untimely incline which makes the displacement of the top and bottom spherical targets on the rods and the rotational angle abnormally increase. The abnormal data has been deleted from the database.

Figure 6.14 The gullying on the soil slope in bench model test. This is the scanning result from the late stage of the bench model test 6-2 and the gullying is generated by the water injection on the top of the slope. Therefore, the displacement of some scanning targets and the rotational angle of some scanning target rods are abnormal increasing. The abnormal scanning results have been deleted from the database.

A comparison between the test results is made, and some relevant conclusions are reached:

The scanning results of the floating target 2 indicate the surface soil have obvious displacement in both test 6-1 and 6-2 (Figure 6.5 and Figure 6.10). The difference between the scan results of the floating target 2 in test 6-1 (22.72 liters/hr) and 6-2 (283.88 liters/hr) is that the main displacement of the scan target in the test 6-1 occurs after the 10^{th} scan, but in test 6-2 it occurs after the 6^{th} scan. This phenomenon means the designed scan target can help the LiDAR technology to detect the surface displacement of landslide. Furthermore, the main influence of difference between the results of test 6-1 and 6-2 should be the watering velocity.

In test 6-1, except the result of the floating target 2, both the top and bottom sphere targets on the floating target 1 have no obvious displacement, and the rotational angle stays near 0°(Figure 6.5-6.8). This phenomenon indicates that in test 6-1 except the surface soil of the slope has displacement, all other parts of soil body having no obvious displacement.

In test 6-2, both the floating target 1 and 2 have obvious displacement, in the meantime, the rotational angle has notable change from the 13^{th} scan (Figure 6.10-6.13). The result shows that in test 6-2 the shallow soil layers have already had displacement and all scanning results are in that the displacement difference is generated in experiment process.

Both of the test 6-1 and 6-2 have some abrupt or nonuniform color change (Figure 6.5, 6.10, 6.11, 6.12 and 6.13). The reason of the target displacement or the rotational

angle distribution being asymmetric or nonuniform is that the parameters of soil material, such as penetrability and bulk density of the soil, is not unified distribution on the slope.

Compared with the surface target (the floating target 2 in Figure 6.1), the floating target 1 is a better choice to help the LiDAR scanner to obtain the displacement of whole soil body, and the floating target 2 sometimes can only detect the surface soil movement(Figure 6.5) instead of the soil layers slide. Meanwhile, the following assumptions can be made: if the scanning target rod can keep rigid and has no plastic deformation, the rotational angle of the floating target 1 is a reliable measurement equipment to help LiDAR scanning technology obtain the displacement difference or the bottom displacement of soil slide.

7. SUMMARY, CONCLUSION AND RECOMMENDATIONS

7.1. SUMMARY

Landsliding is a kind of geological hazard whose consequences are hard to predict because the geometries of the landslide are difficult to measure accurately even if most landslides do not happen instantly. Many geotechnical engineers have researched landslides using various methods, such as remote sensing and computer simulation. They found that to predict the consequence of landslides depends on knowing the geometry of the slip surface as well as the triggers of landslide, because most of displacement of landslide start along the failure surface of rock or soil (Maerz, N.H. et al., 2016).

LiDAR technology has been used in landslides research for several decades (Jaboyedoff, M. et al., 2012). Previous research used the LiDAR scanning method to measure the surface displacement and the volume change of landslides or monitor and describe the features of soil and rock slopes (Maerz, N.H. et al., 2016). But the main barrier of the using LiDAR technology in landsliding research is how to extend the function of LiDAR to measure the dynamic subsurface movement of landslides.

Based on the features of slow landslides (USGS, 2017) and the previous mentioned research results and tools, this dissertation studies the LiDAR technology to verifying new measurement methods to study both surface and subsurface soil movement to help further research of slow-moving landslides.

In this new method of researching slow moving landslides, the choice of equipment is very important. The use of LiDAR scanners is necessary to accurately measure the minute precursor movement of landslides. Because landslides do not have

many natural target features, and growing vegetation obscures actual landslide movement, artificial targets mounted inside and outside the landslide are must be used. The difficulty is that LiDAR scanning can nominally only detect the surface movement of the landslide, but landslides always start underground, and those underground dynamics are import for prediction purposes. Therefore, two types of new scanning targets are used in this dissertation to extend the function of the LiDAR scanner. The new scanning targets include the surface mounted scanning targets to measure the surface soil movement and the scanning target rods to measure the subsurface soil movement. Additionally, to prove the reliability of the new LiDAR measurement method, computer simulation software was used to simulate the landsliding process and help to study the interaction between the soil and the scanning target rods.

To prove the precision and principle of this new measurement method, this dissertation uses three steps: (1) Test the three-dimensional error of the LiDAR scanner measurements, the displacement error of the scanning spherical targets and the rotational angle error of the scanning target rod; (2) Test the new measurement method in different soil types in sandbox and compare the LiDAR scanning results with computer simulation results to study the interaction between the soil and the target rods; (3) Use a bench model to simulate the slow moving landslide to validate the new measurement method.

In this dissertation, the software “Lidarsw” and “SCENE” are used to process the LiDAR scanning data; the software “FLAC3D” and “PFC3D” are used to simulate the sandbox test to analyze the displacement and interaction between the soil and the scanning target rod.

7.2. CONCLUSION

To measure the movement of soil, the LiDAR scanning technology uses scanning targets to improve the precision of scanning, and extend its function to measure the displacement of subsurface soil. Three error tests were designed to prove the LiDAR scanner and the measurement method has sufficient precision to measure the tiny displacements of the targets or rotational angles of the target rods. Through these designed error tests, the following conclusions can be drawn:

1. The three-dimensional position error test results of the FARO Focus3D (the LiDAR scanner used in this research) reveal:

(1) The average three-dimensional position error in X-axis was 0.168 mm, in Y-axis was 0.185 mm and in Z-axis was 0.090 mm;

(2) The maximum three-dimensional position error in all the test completed X-axis was 0.471 mm, in Y-axis was 0.492 mm and in Z-axis was 0.191 mm;

(3) The average three-dimensional position error is 0.265 mm and the maximum three-dimensional position error is 0.707 mm.

2. The displacement error test results reveal:

(1) The FARO Focus3D can recognize the scanning target displacement greater than or equal to 0.508 mm (20 mil) in all cases;

(2) When the displacement of the scanning target is less than 0.4064 mm (16 mil), the FARO Focus3D, for a single measurement cannot differentiate the actual displacement from the scanner error because the scanner error is larger than or close to value of the displacement. However, when averaging multiple scans or increasing the

number of scanning points on the target, much smaller displacements can be accurately measured.

(3) The size of the scanning spherical target has no obvious influence to the displacement error, if the number of scanning points on the target is greater than 1000 (Maerz, N.H. et al., 2016).

3. The rotational angle error test results reveal:

(1) The FARO Focus3D can recognize the rotational angle of the designed scanning target rod. The average rotational angle error is 0.127°;

(2) The size of the scanning spherical target has no obvious influence to the rotational angle error, if the number of scanned points on the target is greater than 1000 (Maerz, N.H. et al., 2016).

A series of shear box tests and computer simulation programs were designed to study the interaction between the target rod and the soil so as to prove if the target rods can accurately reflect the subsurface movement of the soil. Through the sandbox tests and computer simulation results, following conclusions can be drawn:

(1) The LiDAR scanning method can obtain the subsurface displacement or the displacement difference between soil layers by the rotational angle change of the scanning target rods, whether the bottom of the rod is fixed or not;

(2) The soil type has direct influence on the rotational angle scanning result because of different mechanical behaviors of different soil types;

(3) FLAC3D and the PFC3D can be used to: (a) Simulate the sandbox experiments and use three-dimensional figures to display the test model; (b) Calculate the

displacement for all parts of the model; (c) Analyze the interaction between the soil and the target rod; (d)Prove if the target rod enters yield state in entire experiment procedure;

(4) The displacement and the stress simulation results show the FLAC3D is much better than the PFC3D to predict the movement and the stress conditions of the scanning target rod;

(5) The PFC3D is an efficient tool to simulate the movement process of the soil and the target rod; The simulation results of the PFC3D also can help to explain the mechanism of movement between the soil layers and the target rod in this experiment. However, it was not possible to run a satisfactory PFC3D simulation because of the limitation of the computing power of the computer. This computing power limited the initial speed of model and the particle size of the soil materials which input into the coding of the PFC3D simulation program and lead parameters distortion. If the program uses the actual parameters, the simulation process will crush or continue for thousands hour.

(6) The combination of FLAC3D and PFC3D cannot be an accurate forecasting tool in landslide research, but it is a highly effective tool to study the interaction and the behavior of the soil layers and the scanning target rods in monitoring and analyzing slow moving landslides.

The designed bench model test which is a small-scale landslide was used to prove the applicability of the new LiDAR monitoring method. There was a degree of distortion in the scanning results of the bench model test because the water injection method resulted in surface erosion as well as shear slippage.

7.3. RECOMMENDATIONS

Using LiDAR to measure the surface and subsurface displacement of landsliding, the use of the scanning target is very important. The scanning target is not only can improve the precision of the scanning result, but use of target rods driven into the ground can also make it possible for the LiDAR scanner to measure subsurface landslide movement. The shape of the scanning target also can influence the measurement result because difference shapes of scanning target need to use different algorithms to calculate the thee-dimensional position of the targets which can lead to a different outcome.

The LiDAR scanner capabilities are also crucial influence factors for this research. The higher the resolution of the scanning process means more scanning points would reflect back to the scanner, improving the precision of the scanning result.

Using the scanning targets in further landsliding research needs to consider the field conditions, such as the change in the height of vegetation and the subsurface changes in the landslide. These realistic conditions direct influence the specification of the designed scanning targets.

Different soil types can result in difference scanning results because of different mechanical behaviors. The different mechanical behaviors can influence the interaction between the soil and the target rod which needs to be considered in the research plan.

The computer simulation results can be improved by better computer power and more precise parameters.

The following future work and research are recommended:

(1) Using the experiment values of the soil parameters in the computer simulation programs, instead of published values;

(2) More experiments to find the relationship between difference soil types and the scanning targets movement;

(3) Change the water injection mode in the bench model test to avoid the outcome of the surface gullying to improve the reliability of the new LiDAR measurement method;

(4) Further field experiments to verify the validity of the designed scanning targets;

(5) Develop the automatic LiDAR measurement method and combine the LiDAR technology with UAV (unmanned aerial vehicle) system to improve the LiDAR measurement efficiency.

BIBLIOGRAPHY

1. HTTPS://pubs.usgs.gov/fs/2004/3072/fs-2004-3072.html. USGS, 2017.

2. Waltham, T., 2014. Foundations of engineering geology. CRC Press.

3. Maerz, N.H., Boyko, K.J., Hill, B.J., Herries, B.M., Hopkins, M. and Lu, C., 2016. Displacement Measurement of Slow Moving Landslides using Sub-mm LIDAR Scanning. In 67th Highway Geology SymposiumHighway Geology Symposium.

4. Cruden, D.M. and Varnes, D.J., 1996. Landslides investigation and mitigation, transportation research board. Landslide types and process, National Research Council, National Academy Press, Special Report, 247, pp.36-75.

5. de Vallejo, L.G., 2011. Geological engineering. CRC Press.

6. Varnes, D.J., 1978. Slope movement types and processes. Special report, 176, pp.11-33.

7. Jaboyedoff, M., Oppikofer, T., Abellán, A., Derron, M.H., Loye, A., Metzger, R. and Pedrazzini, A., 2012. Use of LIDAR in landslide investigations: a review. Natural hazards, 61(1), pp.5-28.

8. Shan, J. and Toth, C.K., 2008. Topographic laser ranging and scanning: principles and processing. CRC press.

9. Fruneau, B., Achache, J. and Delacourt, C., 1996. Observation and modelling of the Saint-Etienne-de-Tinée landslide using SAR interferometry. Tectonophysics, 265(3-4), pp.181-190.

10. Colesanti, C., Ferretti, A., Prati, C. and Rocca, F., 2003. Monitoring landslides and tectonic motions with the Permanent Scatterers Technique. Engineering geology, 68(1-2), pp.3-14.

11. Squarzoni, C., Delacourt, C. and Allemand, P., 2003. Nine years of spatial and temporal evolution of the La Valette landslide observed by SAR interferometry. Engineering Geology, 68(1-2), pp.53-66.

12. Mazzanti, P., Bozzano, F., Cipriani, I. and Prestininzi, A., 2015. New insights into the temporal prediction of landslides by a terrestrial SAR interferometry monitoring case study. Landslides, 12(1), pp.55-68.

13. Carter, W., Shrestha, R., Tuell, G., Bloomquist, D. and Sartori, M., 2001. Airborne laser swath mapping shines new light on Earth's topography. Eos, Transactions American Geophysical Union, 82(46), pp.549-555.

14. Haugerud, R.A., Harding, D.J., Johnson, S.Y., Harless, J.L., Weaver, C.S. and Sherrod, B.L., 2003. High-resolution lidar topography of the Puget Lowland, Washington. GSA Today, 13(6), pp.4-10.

15. Slob, S. and Hack, R., 2004. 3D terrestrial laser scanning as a new field measurement and monitoring technique. In Engineering geology for infrastructure planning in Europe (pp. 179-189). Springer, Berlin, Heidelberg.

16. Jaboyedoff, M., Metzger, R., Oppikofer, T., Couture, R., Derron, M.H., Locat, J. and Turmel, D., 2007, May. New insight techniques to analyze rock-slope relief using DEM and 3D-imaging cloud points: COLTOP-3D software. In Rock mechanics: Meeting Society's Challenges and demands (Vol. 1, pp. 61-68).

17. Duan, Y., Li, X., Maerz, N. and Otoo, J., 2011, January. Automatic 3D facet orientations estimation from LiDAR imaging. In Proceedings of 2011 NSF Engineering Research and Innovation Conference.

18. Abellán, A., Oppikofer, T., Jaboyedoff, M., Rosser, N.J., Lim, M. and Lato, M.J., 2014. Terrestrial laser scanning of rock slope instabilities. Earth surface processes and landforms, 39(1), pp.80-97.

19. Carrea, D., Abellan, A., Derron, M.H. and Jaboyedoff, M., 2015. Automatic rockfalls volume estimation based on terrestrial laser scanning data. In Engineering Geology for Society and Territory-Volume 2 (pp. 425-428). Springer, Cham.

20. Franz, M., Carrea, D., Abellán, A., Derron, M.H. and Jaboyedoff, M., 2016. Use of targets to track 3D displacements in highly vegetated areas affected by landslides. Landslides, 13(4), pp.821-831.

21. Jaboyedoff, M., Oppikofer, T., Abellán, A., Derron, M.H., Loye, A., Metzger, R. and Pedrazzini, A., 2012. Use of LIDAR in landslide investigations: a review. Natural hazards, 61(1), pp.5-28.

22. Woodbury,N., Brubacher, M., Woodbury, J.R., 1993. Noninvasive tank Gauging with frequency Modulated Laser Ranging sensors, pp 27-31, September, 2003.

23. Kassebaum, T.J., 2012. Using LiDAR as a monitoring device to calculate volume of rockfall over time.

24. https://www.itascacg.com/software/flac3d. Itasca Consulting Group, Inc., 2018.

25. Naji, A., Rehman, H., Emad, M. and Yoo, H., 2018. Impact of shear zone on rockburst in the deep neelum-jehlum hydropower tunnel: A numerical modeling approach. Energies, 11(8), p.1935.

26. Poisel, R. and Preh, A., 2008. 3D landslide run out modelling using the particle flow code PFC3D. na.

27. Heritage, G. and Large, A. eds., 2009. Laser scanning for the environmental sciences. John Wiley & Sons.

28. Lichti, D., Stewart, M.P., Tsakiri, M. and Snow, A.J., 2000. Calibration and testing of a terrestrial laser scanner. International archives of Photogrammetry and Remote sensing, 33(B5/2; PART 5), pp.485-492.

29. Buckley, S.J., Howell, J.A., Enge, H.D. and Kurz, T.H., 2008. Terrestrial laser scanning in geology: data acquisition, processing and accuracy considerations. Journal of the Geological Society, 165(3), pp.625-638.

30. Rowlands, K.A., Jones, L.D. and Whitworth, M., 2003. Landslide laser scanning: a new look at an old problem. Quarterly Journal of Engineering Geology and Hydrogeology, 36(2), pp.155-157.

31. Aryal, A., Brooks, B.A., Reid, M.E., Bawden, G.W. and Pawlak, G.R., 2012. Displacement fields from point cloud data: Application of particle imaging velocimetry to landslide geodesy. Journal of Geophysical Research: Earth Surface, 117(F1).

32. Barbarella, M. and Fiani, M., 2013. Monitoring of large landslides by Terrestrial Laser Scanning techniques: field data collection and processing. European Journal of remote sensing, 46(1), pp.126-151.

33. Carrea, D., Abellan, A., Derron, M.H. and Jaboyedoff, M., 2015. Automatic rockfalls volume estimation based on terrestrial laser scanning data. In Engineering Geology for Society and Territory-Volume 2 (pp. 425-428). Springer, Cham.

34. Corsini, A., Borgatti, L., Cervi, F., Dahne, A., Ronchetti, F. and Sterzai, P., 2009. Estimating mass-wasting processes in active earth slides–earth flows with time-series of High-Resolution DEMs from photogrammetry and airborne LiDAR. Natural Hazards and Earth System Sciences, 9(2), pp.433-439.

35. Dunning, S.A., Massey, C.I. and Rosser, N.J., 2009. Structural and geomorphological features of landslides in the Bhutan Himalaya derived from terrestrial laser scanning. Geomorphology, 103(1), pp.17-29.

36. Oppikofer, T., Jaboyedoff, M., Blikra, L., Derron, M.H. and Metzger, R., 2009. Characterization and monitoring of the Åknes rockslide using terrestrial laser scanning. Natural Hazards and Earth System Sciences, 9(3), pp.1003-1019.

37. Miller, P.E., Mills, J.P., Barr, S.L., Lim, M., Barber, D., Parkin, G., Clarke, B., Glendinning, S. and Hall, J., 2008. Terrestrial laser scanning for assessing the risk of slope instability along transport corridors. International Archives of Photogrammetry, Remote Sensing and Spatial Information Sciences, 37(B5), pp.495-500.

38. Akca, D., Gruen, A., Askarinejad, A. and Springman, S.M., 2011, May. Photogrammetric monitoring of an artificially generated landslide. In International Conference on Geo-information for Disaster Management (Gi4DM), Antalya, Turkey (pp. 3-8).

39. Barbarella, M. and Fiani, M., 2013. Monitoring of large landslides by Terrestrial Laser Scanning techniques: field data collection and processing. European Journal of remote sensing, 46(1), pp.126-151.

40. Maerz, N.H., Youssef, A.M., Otoo, J.N., Kassebaum, T.J. and Duan, Y.E., 2013. A simple method for measuring discontinuity orientations from terrestrial LiDAR data. Environmental & Engineering Geoscience, 19(2), pp.185-194.

41. Renslow, M.S. ed., 2012. Manual of airborne topographic lidar. American Society for Photogrammetry Remote Sensing, pp. 246.

42. Travelletti, J., Oppikofer, T., Delacourt, C., Malet, J.P. and Jaboyedoff, M., 2008. Monitoring landslide displacements during a controlled rain experiment using a long-range terrestrial laser scanning (TLS). International Archives of Photogrammetry and Remote Sensing, 37, pp.485-490.

43. Prokop, A. and Panholzer, H., 2009. Assessing the capability of terrestrial laser scanning for monitoring slow moving landslides. Natural Hazards and Earth System Sciences, 9(6), pp.1921-1928.

44. Kasperski, J., Delacourt, C., Allemand, P., Potherat, P., Jaud, M. and Varrel, E., 2010. Application of a terrestrial laser scanner (TLS) to the study of the Séchilienne Landslide (Isère, France). Remote Sensing, 2(12), pp.2785-2802.

45. Wang, D., Hollaus, M., Puttonen, E. and Pfeifer, N., 2016. Automatic and self-adaptive stem reconstruction in landslide-affected forests. Remote Sensing, 8(12), p.974.

46. Biasion, A., Bornaz, L. and Rinaudo, F., 2005. Laser scanning applications on disaster management. In Geo-information for Disaster Management (pp. 19-33). Springer, Berlin, Heidelberg.

47. Oppikofer, T., Jaboyedoff, M. and Keusen, H.R., 2008. Collapse at the eastern Eiger flank in the Swiss Alps. Nature Geoscience, 1(8), p.531.

48. Abellán, A., Calvet, J., Vilaplana, J.M. and Blanchard, J., 2010. Detection and spatial prediction of rockfalls by means of terrestrial laser scanner monitoring. Geomorphology, 119(3-4), pp.162-171.

49. Canli, E., Höfle, B., Hämmerle, M., Benni, T. and Glade, T., 2015, April. Permanent 3D laser scanning system for an active landslide in Gresten (Austria). In EGU General Assembly Conference Abstracts (Vol. 17).

50. Thiebes, B., Tomelleri, E., Mejia-Aguilar, A., Schlögel, R., Darvishi, M., Remondino, F., Toschi, I., Rutzinger, M. and Zieher, T., 2016, April. UAV-based landslide deformation monitoring-first results from Corvara landslide. In EGU General Assembly Conference Abstracts (Vol. 18, p. 12115).

51. Rosser, N., Lim, M., Petley, D., Dunning, S. and Allison, R., 2007. Patterns of precursory rockfall prior to slope failure. Journal of geophysical research: earth surface, 112(F4).

52. Conforti, D., 2014, May. Automating slope monitoring in mines with terrestrial lidar scanners. In EGU General Assembly Conference Abstracts (Vol. 16).

53. Agliardi, F., Crosta, G. and Zanchi, A., 2001. Structural constraints on deep-seated slope deformation kinematics. Engineering Geology, 59(1-2), pp.83-102.

54. Chen, C.Y. and Martin, G.R., 2002. Soil–structure interaction for landslide stabilizing piles. Computers and Geotechnics, 29 (5), pp.363-386.

55. Petley, D.N., Mantovani, F., Bulmer, M.H. and Zannoni, A., 2005. The use of surface monitoring data for the interpretation of landslide movement patterns. Geomorphology, 66(1-4), pp.133-147.

56. Poisel, R. and Preh, A., 2008. Modifications of PFC3D for rock mass fall modeling. na.

57. Conner, J.C. and Olsen, M.J., 2014. Automated quantification of distributed landslide movement using circular tree trunks extracted from terrestrial laser scan data. Computers & Geosciences, 67, pp.31-39.

58. Dong, M., Hu, H. and Song, J., 2018. Combined methodology for three-dimensional slope stability analysis coupled with time effect: a case study in Germany. Environmental Earth Sciences, 77(8), p.311.

59. FARO® Laser Scanner Focus^{3D} X 130 Manual, 2014. FARO Technologies Inc..

60. Richard G. Brown, 1996. Advanced Mathematics: Precalculus with Discrete Mathematics and Data Analysis. Houghton Mifflin School Press.

61. Kenneth J. Boyko, 2014. Missouri S&T Lidar Software Manual.

62. Maerz, N.H., Kassebaum, T., Boyko, K.J. and Otoo, J., 2015. Evaluation of Rock Fall Hazards using LiDAR Technology.

63. Cundall, P.A., 1971. A computer model for simulating progressive, large-scale movement in blocky rock system. In Proceedings of the International Symposium on Rock Mechanics, 1971.

64. American Society for Testing and Materials, 1985. Classification of Soils for Engineering Purposes: Annual Book of ASTM Standards, D 2487-83, 04.08, pp. 395–408.

65. Naval Facilities Engineering Command, 1986. NAVFAC Design Manual 7.2 - Foundations and Earth Structures, SN 0525-LP-300-7071.

66. Prat, M., Bisch, P.H., Millard, A., Mestat, P. and Pijaudier-Calot, G., 1995. La modélisation des ouvrages.

67. Swiss Standard, S.N., 1999. 670 010b. Characteristic Coefficients of soils, Association of Swiss Road and Traffic Engineers.

68. Minnesota Department of Transportation, 2007. Pavement Design Manual.

69. Das, B.M., 2008. Advanced Soil mechanics: Tylor & Frances.

70. Obrzud, R. and Truty, A., 2012. The hardening soil model-a practical guidebook z soil. PC100701 Report.

71. Yu Lipeng, 2014. Analysis of Soil's Elastic Modulus Values Based on FLAC3D Simulation. Journal of Water Resource and Architectural Engineering, 12 (2), pp: 162-166.

72. Handbook, ASM Metals. "Howard E." Boyer and Timothy L. Gall, Eds., American Society for Metals, Materials Park, OH (1985).

73. Handbook, Metals. "Vol. 2." Properties and Selection: Nonferrous Alloys and Special-Purpose Materials (1990): 180.

74. Structural Alloys Handbook, 1996 edition, John M. (Tim) Holt, Technical Ed; C. Y. Ho, Ed., CINDAS/Purdue University, West Lafayette, IN, 1996.

75. Information provided by The Aluminum Association, Inc. from Aluminum Standards and Data 2000 and/or International Alloy Designations and Chemical Composition Limits for Wrought Aluminum and Wrought Aluminum Alloys (Revised 2001).

76. Iverson, R.M., 2000. Landslide triggering by rain infiltration. Water resources research, 36(7), pp.1897-1910.

77. Wartman, J., Montgomery, D.R., Anderson, S.A., Keaton, J.R., Benoît, J., dela Chapelle, J. and Gilbert, R., 2016. The 22 March 2014 Oso landslide, Washington, USA. Geomorphology, 253, pp.275-288.

VITA

Chengxun Lu was born in Beijing, China. He attended the Department of the Earth Sciences and Resources at China University of Geosciences (Beijing) in Beijing, China in 2005. He received the bachelor degree of Geology in July, 2009.

After graduation, Chengxun Lu started his research career in China University of Geosciences (Beijing). His research topic was Structural Geology. He received his Master degree of Structural Geology in July, 2012. He participated in an internship at the Institute of Geological Mechanics, in the Chinese Academy of Geological Science (CAGS), as a research assistant. Also, he worked for the Institute of Minerals Resources, in CAGS, as coordinator and research assistant from 2012 to 2015.

In September 2011, Chengxun Lu started his Ph.D. program at Missouri University of Science and Technology, in Rolla. During his studies at Missouri University of Science and Technology, he participated in multiple research projects about LiDAR technology and Structural Geology. He published three papers in the Journal of "Geotectonica et Metallogenia" and "Earth Science Frontiers" as the first author.

He received his Doctor of Philosophy in Geological Engineering from Missouri University of Science and Technology in July 2019.